

Problems and Solutions in Sintering Science and Technology

Suk-Joong L. Kang

About the author...

Suk-Joong L. Kang has been with the Department of Materials Science and Engineering at KAIST as Professor, Distinguished Professor and Professor Emeritus since 1980. (e-mail: sjkang@kaist.ac.kr)

Dr. Kang has published over 300 papers on sintering and microstructural evolution, and authored the textbook *Sintering: Densification, Grain Growth and Microstructure* (2005). He developed the "Pore Filling Theory" of liquid phase sintering. He introduced the concept of the mixed control mechanism of boundary migration and developed the mixed mechanism principle of grain growth and microstructural evolution. Since 2000, he presented over 120 invited talks at international conferences and symposia. Dr. Kang is a fellow of the American Ceramic Society, an honorary fellow of the European Ceramic Society, and a member of both the World Academy of Ceramics and the Korean Academy of Science and Technology. Suk-Joong L. Kang received a Dr.-Ing degree from the Ecole Centrale de Paris (1980), and a Doctorate of Science (Dr. d'Etat) degree from the University of Paris VI (1985).

To my former students

Korea Advanced Institute of Science and Technology
Yuseong-gu, Daehak-ro 291,
Daejeon 34141, Republic of Korea

First published 2024

Copyright © 2024, Suk-Joong L. Kang. All rights reserved

No part of this work may be reproduced or translated, and no derivative work is allowed for commercial use in any material form (including photocopying or storing any medium by electronic means) without the written permission of the copyright holder (CC-BY-NC-SA).

ISBN 979-1192990-19-4 (95570)



- CONTENTS -

Preface	v
<u>Problems</u>	1
PART I. Basis of Sintering Science	1
PART II. Bonding and Densification	6
II-1. Solid state sintering	6
II-2. Liquid phase sintering	13
PART III. Grain Growth and Microstructural Evolution	16
III-1. Solid state sintering	16
III-2. Liquid phase sintering	22
PART IV. Supplementary Subjects	26
IV-1. Sintering of ionic compounds	26
IV-2. Diffusion induced interface migration	27
<u>Solutions</u>	30
PART I. Basis of Sintering Science	30
PART II. Bonding and Densification	39
II-1. Solid state sintering	39
II-2. Liquid phase sintering	49
PART III. Grain Growth and Microstructural Evolution	56
III-1. Solid state sintering	56
III-2. Liquid phase sintering	74
PART IV. Supplementary Subjects	83
IV-1. Sintering of ionic compounds	83
IV-2. Diffusion induced interface migration	89
Subject Index	93

Preface

This book collects the problems and questions that have been offered to students in my sintering course at the Korea Advanced Institute of Science and Technology (KAIST) from 1984 to 2019. Many of them are from the book “Sintering: densification, grain growth and microstructure” (ISBN 07506 63855), published by Elsevier Butterworth-Heinemann in 2005. Most of the problems and questions were originally developed to test the students’ knowledge and to enhance their understanding of sintering fundamentals and processes. I believe most of them and their solutions are correct and appropriate. Some of them, however, may be incorrect and inappropriate. In such cases, I hope the readers can find the correct solutions and answers. Some others may be unrealistic; they are included to emphasize the physical meaning behind them.

I classified the problems and questions into four parts: (i) Basis of Sintering Science, (ii) Bonding and Densification, (iii) Grain Growth and Microstructural Evolution, and (iv) Supplementary Subjects. Part 1 collects problems and questions about general sintering processes, thermodynamics of the interface, and polycrystalline microstructures. In Parts 2 and 3, the problems concerning solid-state sintering and liquid-phase sintering are listed separately. Part 4 contains problems concerning sintering of ionic compounds and diffusion-induced interface migration. The scheme of this book is a modification of that of the book “Sintering: densification, grain growth and microstructure”. After the publication of the sintering book, I felt that the modified scheme was better than the original one for understanding not only the general but also detailed aspects of sintering fundamentals and processes.

For several solutions and answers, I added a few references that provide more details on the subject. Readers may consult these references for further understanding. For convenience, this book utilizes some figures and equations from my sintering book (“Sintering: densification, grain growth and microstructure”) without specific indication. For example, Fig. 13.1 and Eq. (6.12) are from the sintering book.

I hope this solution book can help readers further their understanding of sintering science and technology.

Suk-Joong L. Kang
Daejeon
August 2024

PROBLEMS

PART I. Basis of Sintering Science: Sintering Processes, Thermodynamics of the Interface, and Polycrystalline Microstructure

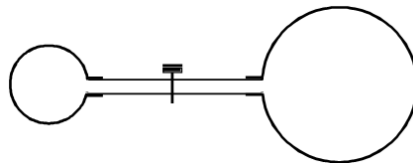
1-1. Derive the energy change when a cube-shaped powder of edge l is densified without grain growth. From the calculated energy change, discuss conditions to improve sinterability. The specific surface energy of the powder is γ_s and the specific grain boundary energy γ_b .

1-2. Derive Eq. (2-15) in the book "Sintering" $\left(\sigma_{ij} = \delta_{ij} \gamma + \frac{d\gamma}{d\varepsilon_{ij}} \right)$.

1-3. In a solid, why can the surface specific energy be different from the surface tension force?

1-4. When a tube is inserted into a liquid, the liquid level in the tube varies with the wetting angle θ , the tube radius r , liquid density ρ , and surface tension of the liquid γ_l . Derive the equation of the liquid level height using two different concepts: the capillary pressure of the liquid in the tube and the surface tension of the liquid.

1-5. Two elastic balloons that contain different amounts of air are separated by a valve in a glass tube, as shown in Fig. P1-5. When the valve is opened, what will happen?



<Fig. P1-5>

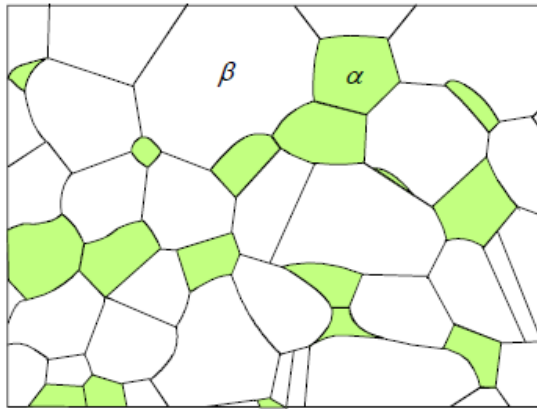
1-6. What is the equilibrium gas pressure in a spherical pore with a radius of r_1 entrapped within a spherical crystal with a radius of r_2 ? The pressure in the crystal is assumed to be hydrostatic.

1-7. Pores with a radius of $5 \mu\text{m}$ containing insoluble gases of 1 atm pressure are entrapped within a glass with a relative density of 0.90. What are the equilibrium size of the pores and the final density of the glass? γ_s is assumed to be 0.5 J/m^2 .

1-8. Consider an isolated spherical pore with a radius of $3 \mu\text{m}$ that was entrapped within a Cu powder compact during pressing at 20°C . Does the pore expand or shrink at 1000°C ? Assume the initial pressure of insoluble gases entrapped within the pore to be 10^5 N/m^2 and the surface energy of Cu at 1000°C to be 1.4 J/m^2 .

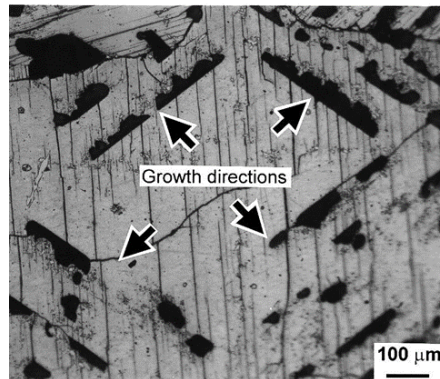
1-9. A gas bubble of $1 \mu\text{m}$ diameter is formed in water below 10 m from the surface. Calculate the pressure in the gas bubble. Assume $\gamma_l = 0.1 \text{ J/m}^2$.

- 1-10. Prove that the energy increase caused by the formation of a particle with a radius of r from the bulk state is $4\pi r^2 \gamma_s$. Assume that the material is incompressible.
- 1-11. Calculate the size of a Cu sphere where the surface energy is equal to the elastic strain energy due to its curvature. Assume that the surface energy γ_s of Cu is 1.4 J/m^2 and its compressibility $\kappa = 7.1 \times 10^{-12} \text{ m}^2/\text{N}$. Discuss the result.
- 1-12. When ten water drops of $1 \text{ }\mu\text{m}$ radius stick together and form a large drop, what is the energy change? The compressibility of water is $4.5 \times 10^{-10} \text{ m}^2/\text{N}$ and the surface energy $7.3 \times 10^{-2} \text{ J/m}^2$.
- 1-13. Draw a figure showing the change in equilibrium vapor pressure with the radius of curvature of a material (from $0.01 \text{ }\mu\text{m}$ to $10 \text{ }\mu\text{m}$) at $1000 \text{ }^\circ\text{C}$. Assume the molar volume and the surface energy of the material to be $1 \times 10^{-5} \text{ m}^3$ and 1 J/m^2 , respectively.
- 1-14. Estimate the difference in equilibrium vapor pressure at $500 \text{ }^\circ\text{C}$ for two spherical particles, one with a diameter of $0.1 \text{ }\mu\text{m}$ and the other with a diameter of $10 \text{ }\mu\text{m}$. Assume that the atoms are in cubic close packing, the atomic radius is 10^{-10} m and the surface energy is 1 J/m^2 .
- 1-15. When the molar volumes of α and β phases are the same, Eq. (2-28) in the book “Sintering” suggests that the pressure P^α in an α particle with a radius of r embedded in β becomes infinite. Is this consequence reasonable? Discuss.
- 1-16. What is the equilibrium shape of an entrapped pore within a single crystal whose equilibrium shape is a cube in air?
- 1-17. A rectangular cuboid-shaped small pore is entrapped within a single crystal of which the equilibrium shape is a cube. Do you expect the pore shape to change when you anneal this crystal at a high temperature? If so, describe the change in the pore shape and its cause. Assume that the atom diffusion is reasonably fast.
- 1-18. What is the equilibrium shape of grains in a 2-dimensional polycrystal with isotropic grain boundary energy? Justify your answer. Here, the equilibrium shape means the shape with the minimum grain boundary energy for grains of the same size.
- 1-19. You have two polycrystalline samples of the same composition but with different grain size distribution: one with a unimodal distribution as a result of normal grain growth (NGG) and the other with a bimodal distribution as a result of abnormal grain growth (AGG). Do you think the microstructure (shape) of the matrix grains in the sample with AGG is the same as that in the sample with NGG? Explain.
- 1-20. The microstructure in Fig. P1-20 consists of α (green area) and β (white area) phases. Explain a possible method for measuring the ratio of the grain boundary energies between α/α and β/β phases, $\gamma_{\alpha/\alpha}/\gamma_{\beta/\beta}$, and describe the assumptions made for the measurement. Which grain boundary has a higher energy?



<Fig. P1-20 >

- 1-21. Draw schematically and also explain the variation in groove angle ϕ formed at a symmetric tilt grain boundary with tilt angle θ . As the temperature increases, how does the relationship between ϕ and θ change approximately? Assume invariable surface energy
- 1-22. Let γ_b be the grain boundary energy of α and γ_{st} be the interfacial energy between an α grain and a matrix. Draw schematically and also explain the variation of γ_{st}/γ_b with dihedral angle ϕ .
- 1-23. Calculate the differences in total interfacial energy when a spherical second-phase particle with a radius of r is located at a 2-grain boundary, a 3-grain edge and a 4-grain corner. Assume that the dihedral angle is 180 degrees although the grain boundary energy γ_b is finite.
- 1-24. The microstructures of powder compacts being sintered often show that isolated pores are mostly located at triple junctions rather than at grain boundaries. Why?
- 1-25. To prepare a bulk $\text{YBa}_2\text{Cu}_3\text{O}_{7-x}$ (123) superconductor with high critical current density, a melt-texturing technique, which consists of a peritectic reaction between Y_2BaCuO_5 (211) and an oxide melt, is often utilized. The 123 grains, which are formed through the peritectic reaction between the 211 phase and the oxide melt, grow preferentially in the $\langle 100 \rangle$ direction and often trap isolated pores in the melt. In a system containing BaCeO_3 , the shape of the entrapped pores within the 123 grains is peculiar, as shown in Fig. P1-25. (Kim CJ, et al., *J. Mater. Res.*, 14, 1707-10 (1999)). Explain possible causes of the formation of the crystallographically aligned pores with an elongated shape.
- 1-26. A liquid phase sintered body has, in general, a microstructure with well-distributed grains in a matrix. For a liquid phase sintered body containing gas bubbles, draw schematically the shape of a gas bubble on a grain for a wetting angle θ larger and smaller than 90 degrees, respectively. For both cases, do you expect a difference in mechanical properties, for example, the tensile strength? Explain.



<Fig. P1-25>

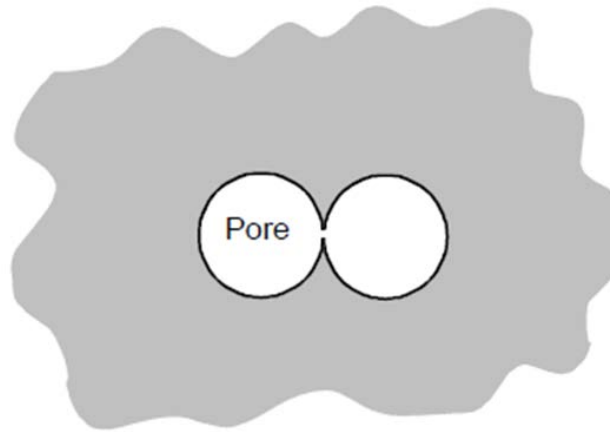
- 1-27. Consider a polycrystal with a uniform microstructure. If the polycrystal is disintegrated into isotropic rounded grains in liquid A and faceted angular grains in liquid B, what would be the variation of γ_b and γ_{sl} with the tilt angle of symmetric grain boundaries for the two cases? Show this as schematic figures and explain.
- 1-28. Consider two polycrystals with and without a small amount of liquid, say 1 vol%, with a dihedral angle of zero degrees. Describe the difference in shape of a boundary, if any, between a large and a small grain for both of the polycrystals. The grain boundary energy and solid/liquid interfacial energy are assumed to be invariable with grain boundary orientation.
- 1-29. When a Ti-excess BaTiO_3 powder compact is sintered above the eutectic temperature, Ti-rich liquid pockets form at triple junctions of grains and no liquid film is present at grain boundaries unless abnormal grain growth (AGG) occurs. As AGG occurs, however, a liquid film forms at grain boundaries between an abnormal grain and fine matrix grains, and its thickness increases with the growth of the abnormal grain.
- Explain how a liquid film forms at the boundary between an abnormal grain and matrix grains.
 - Explain possible causes of film thickening with AGG.
 - When the sample is fully covered with abnormal grains and no more grain growth takes place at the sintering temperature for a long time, what will happen microstructurally?
 - Does the formation of a liquid film mean that the dihedral angle between grains is zero degrees? If yes, is a dry boundary without a liquid film not an equilibrium configuration? Explain.
- 1-30. Park and Yoon (Park HH, Yoon DN, *Metall. Trans. A.*, 16A, 923-28 (1985)) calculated the total interfacial energy of two-phase systems, as shown in Fig. 3-13 in the book "Sintering". According to their calculation, for a system with a dihedral angle ϕ , $0^\circ < \phi < 90^\circ$, the interfacial energy is a minimum at a finite volume fraction of the matrix phase.
- If the matrix volume fraction in a powder compact is larger than that for the minimum interfacial energy, what will happen during sintering of the compact?
 - Under what condition is the total interfacial energy calculated for the liquid volume fraction larger than that for the minimum interfacial energy?
 - What does the right end of the calculated curves mean?

- 1-31. Describe possible microstructural changes with annealing time (from 0 h to a very long time, say 1000 h) of an oxide polycrystal that was fully densified by hot pressing in a vacuum. Assume that the dihedral angle is 75 degrees.

PART II. Bonding and Densification

II-1. Solid state sintering

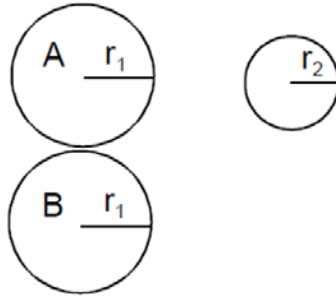
- 2-1. (a) Consider two identical glass spheres of the same size in contact several tens of degrees below their melting point. Draw schematically the change in shape of the two spheres with sintering time and explain. Assume no gravity effect.
- (b) Consider two identical single-crystalline spheres in contact at a sintering temperature. Draw schematically and explain the shape change with sintering time. Assume isotropic interfacial energies and no gravity effect.
- 2-2. Consider that two inert gas-containing spherical pores of the same size are in contact within a single crystal, as shown in Fig. P2-2. Describe the microstructural changes and their processes during annealing of this crystal. Assume that the pore volume does not change during annealing and that the equilibrium shape of the pores is a sphere.



<Fig. P2-2>

- 2-3. Which process governs the neck growth controlled by the evaporation-condensation mechanism?
- 2-4. If the capillary pressure at the neck region between two particles can cause a plastic deformation of the region, the capillary pressure must be larger than the yield strength. What condition (an equation) should be provided for the generation of dislocations by the capillary pressure? Discuss the possibility of dislocation generation by capillary pressure in real systems.
- 2-5. A powder compact with a particle size of $1\ \mu\text{m}$ is known to be sintered in one hour at $1600\ ^\circ\text{C}$. Assuming that densification occurs by lattice diffusion with an activation energy of $500\ \text{kJ/mol}$, plot the dependence of the required sintering temperature against powder size for one hour sintering. Assume negligible grain growth.
- 2-6. In sintering of glass spheres with a radius of $15\ \mu\text{m}$, it took 200min at $627\ ^\circ\text{C}$ and 10 min at $677\ ^\circ\text{C}$ to obtain a shrinkage of 5%. Calculate the viscosity of the glass and the activation energy of sintering. The surface energy of the glass is $0.3\ \text{J/m}^2$.

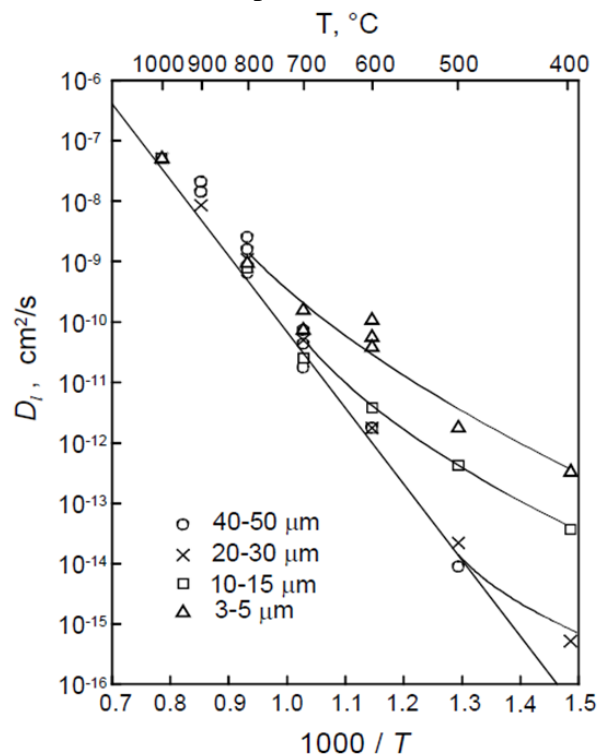
- 2-7. The system Cu-Ag ($T_{m,Cu} > T_{m,Ag}$) is a eutectic with the eutectic temperature of 780 °C. What will happen microstructurally when two 95Cu-5Ag(at.%) spherical particles of a solid solution are sintered below the eutectic temperature, say 750 °C. The solubility limit of Ag in Cu is known to be 8 at.% at the sintering temperature.
- 2-8. Consider three separate particles, as shown in Fig. P2-8. Draw schematically and explain the change in their shape with annealing time if material transport occurs via a gas phase. Assume that all of the evaporated material is transported between particles and that the distance between particles A and B is very small.



<Fig. P2-8>

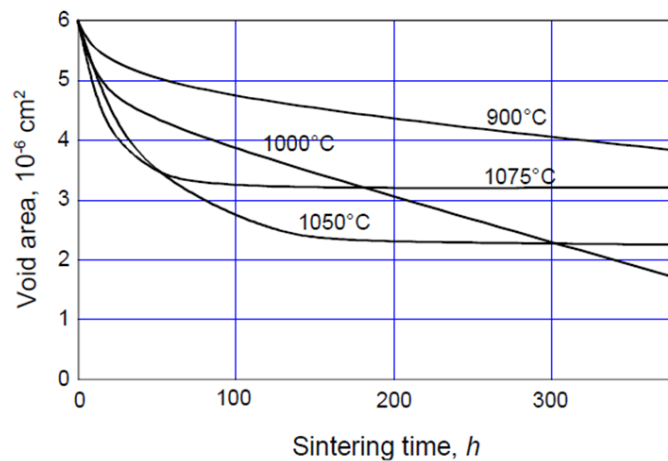
- 2-9. Consider a two-particle system where the neck growth occurs through gas phase transport. Explain the dependence of sintering time on temperature for (i) gas diffusion and (ii) evaporation/condensation. Assume that the gas pressure in the system is the vapor pressure of the material at the temperature concerned and all of the evaporated material is deposited on the particles.
- 2-10. Consider a system where the sintering occurs by gas phase transport.
- Explain the change in neck growth rate (dx/dt) with sintering temperature by the evaporation/condensation mechanism in vacuum sintering.
 - Draw schematically and explain the change in neck radius with external Ar gas pressure (from zero to several thousand atm) for the same temperature and the same period of time ($\log x$ vs. $\log P_{Ar}$).
- 2-11. With a decreased particle size, what sintering mechanisms become relatively more important? Why?
- 2-12. Explain Herring's scaling law in solid state sintering and describe important points to be considered in its application to real systems.
- 2-13. Consider a system where neck growth occurs via Langmuir-type adsorption of material at the neck.
- What is the relationship between the weight of the material deposited on a unit area of the neck and the vapor pressure?
 - Deduce the scaling law for the evaporation/condensation mechanism.
- 2-14. Derive the scaling laws for the neck growth of particles by grain boundary diffusion with and without a high external pressure, say 1000 atm.
- 2-15. The scale exponent in Herring's scaling law is one for viscous flow sintering. Explain physically why the scale exponent is one.

- 2-16. In the two particle model of initial stage sintering, the neck growth is expressed as $(x/a)^n = F(T) \cdot a^{m-n} \cdot t$ (Eq. (4-28) in the book “Sintering”), where x is the neck radius and a the particle radius. The equation is, in general, acceptable for $x/a < 0.2$. With increasing values of x/a above 0.2, would the exponent n become smaller or larger? Explain.
- 2-17. From a sintering experiment of Cu spheres on Cu plates, Kuczynski deduced Cu diffusivity data, as shown in Fig. P2-17 (Kuczynski GC, *Metall. Trans. AIME*, 185, 169-78 (1949)). What would be the cause of the deviation of some data points from a straight line in the figure? Note that the deviation starts to occur at different temperatures for different sizes of spheres.

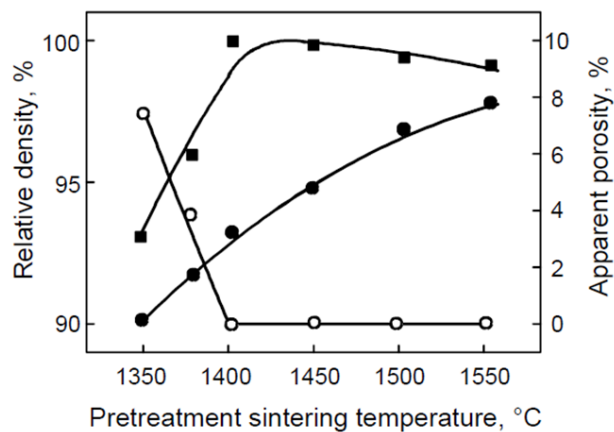


<Fig. P2-17>

- 2-18. In a sintering experiment using a Cu-wire wound Cu spool, Alexander and Balluffi obtained the result shown in Fig. P2-18 (Alexander BH, Balluffi RW, *Acta Metall.*, 5, 666-77 (1957)). Explain why the variation in void area differs among the samples annealed at different temperatures.
- 2-19. Figure P2-19 (Fig. 5.8 in the book “Sintering”) (Kwon ST, et al., *J. Am. Ceram. Soc.*, 70, C69-70 (1987)) shows the relative density (●) and apparent porosity (interconnected porosity, ○) of Al_2O_3 compacts after sintering for 2h at the respective sintering temperatures. It also shows the relative density (■) obtained after hot isostatic pressing (HIP) of the sintered compacts at 1450 °C under 150 MPa Ar.
- Explain why the effect of HIP on the final density is different for samples sintered at different temperatures.
 - Describe the phenomenon that may occur and its cause when you anneal the 1375°C-sintered and HIPed sample at 1375 °C in air.



<Fig. P2-18>



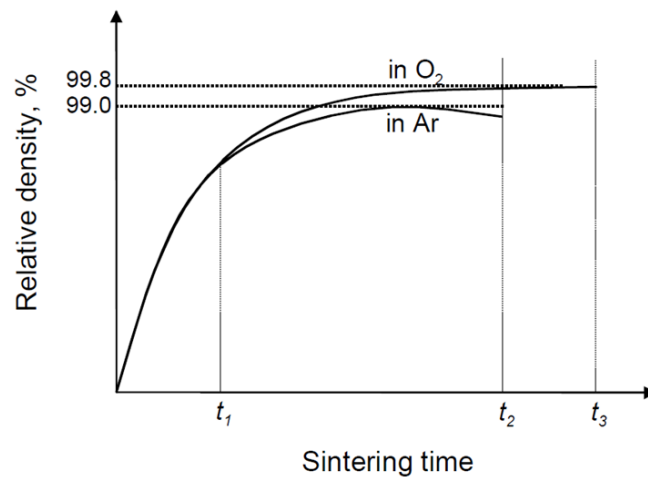
<Fig. P2-19>

- 2-20. During solid state sintering of crystalline materials, densification and grain growth occur concurrently.
- What are the driving forces of these two phenomena? Are they different or not?
 - What are the possible mechanisms of densification? Are they operative in parallel or serially?
- 2-21. Explain the possible change in sintering kinetics of an openly porous powder compact with application of hydrostatic pressure P of an inert gas. Assume that the sintering occurs by lattice diffusion.
- 2-22. Why is gas pressure sintering effective for sintering of material, in particular, with a high vapor pressure at the sintering temperature?
- 2-23. Draw schematically and explain the changes in the driving force of densification with relative density of (i) close-packed mono-size powder compact and (ii) a powder compact with a particle size distribution and hence grain growth during sintering? Assume the same average pore size for the two different compacts.
- 2-24. Consider a powder compact in which the neck growth at the initial stage sintering occurs by lattice as well as surface diffusion. Discuss the relative importance of the two mechanisms according to sintering time.

- 2-25. Using appropriate data in reference 27 in Part II of the book “Sintering”(Ashby MF, *Acta Metall.*, 22, 275-89 (1974)), construct sintering diagrams of Cu under the following ranges of experimental conditions.
- Sintering diagram of $\log a$ vs. $1/T$, showing the regions of dominant mechanisms for a shrinkage of 5% in the ranges of $10^{-6} \sim 10^{-3}$ m in particle size and 600~1300 K in temperature.
 - Sintering diagram of $\log (x/a)$ vs. T/T_m showing the regions of dominant mechanisms and the contours of constant time for a particle size of 10^{-3} m.
- 2-26. Consider an ideally close-packed mono-size powder compact. To explain the densification rate at a given moment an engineer assumed the driving force for densification to be the difference in total interfacial energy between the powder compact at that moment and a fully dense powder compact. Is this assumption acceptable? Explain. Assume no grain growth during densification.
- 2-27. Explain why the shrinkage and densification equations derived from simple geometrical models (such as two-particle model and other geometrical models) cannot be directly applicable to the prediction of the shrinkage and densification of a real powder compact with a particle size distribution.
- 2-28. Why is Herring’s scaling law not applicable to the densification at the final stage of sintering?
- 2-29. Describe the fundamental difference between Coble’s model (Coble RL, *J. Appl. Phys.*, 32, 789-92 (1961)), and Kang and Jung’s model (Kang SJL, Jung YI, *Acta Mater.*, 52, 4373-78 (2004)) for the final stage of sintering. Discuss the validity of the two models.
- 2-30. At the final stage of sintering, the densification of a powder compact occurs by both lattice and grain boundary diffusion. With an increased sintering time, which mechanism is more important for densification? Is it possible to obtain an answer from Herring’s scaling law? Assume negligible grain growth.
- 2-31. Lattice diffusion and grain boundary diffusion are known to be operative in sintering of a powder compact. Discuss the relative contribution of the two mechanisms to densification (a) with increasing temperature and (b) with reducing the initial particle size.
- 2-32. From a sintering experiment of powder compacts of the same material but with different particle sizes (fine and coarse), a researcher obtained different activation energies for densification. What could be the reason for the difference in activation energy? Which one is smaller?
- 2-33. Figure 5.3 (Kang SJL, Jung YI, *Acta Mater.*, 52, 4373-78 (2004)) in the book “Sintering” is a sintering diagram of alumina at final stage sintering. Explain why the dominant sintering mechanism can change from lattice diffusion to boundary diffusion and again to lattice diffusion at a constant sintering temperature.
- 2-34. Consider pressureless sintering of an Al_2O_3 compact that contains isolated pores of 4 μm size at 1400 °C. You want to increase the densification kinetics of this sample by

20 times by (i) applying an external pressure, and (ii) by increasing temperature. What should be the applied pressure and sintering temperature? Assume no grain growth, and boundary diffusion as the densification mechanism under any experimental conditions studied. Note that $D_b \delta_b = 8.6 \times 10^{-10} \exp(-418\text{kJ}/RT)\text{m}^3/\text{s}$, and $\gamma_s = 0.7 \text{ J}/\text{m}^2$.

- 2-35. At final stage sintering, the densification rate decreases with increasing sintering time. Explain possible causes (at least two) of this phenomenon.
- 2-36. In vacuum sintering, does the pore size decrease continuously? Answer the question and explain.
- 2-37. Figure P2-37 shows densification curves of an oxide during sintering in oxygen and in argon.
- Assuming no difference in grain size for the different sintering atmospheres, explain a possible cause for the similar density up to the period of sintering time t_1 in the two different atmospheres.
 - At t_2 , do you expect a difference in grain size between the oxygen and argon-sintered samples? Explain.
 - What is a possible cause of essentially no change in the sintered density of the oxygen-sintered sample between t_2 and t_3 ?
 - What is the cause of dedensification of the Ar-sintered sample?
 - Is it possible to quantitatively calculate the dedensification of the Ar-sintered sample?
 - Describe possible directions for obtaining fully dense sintered parts.



<Fig. P2-37>

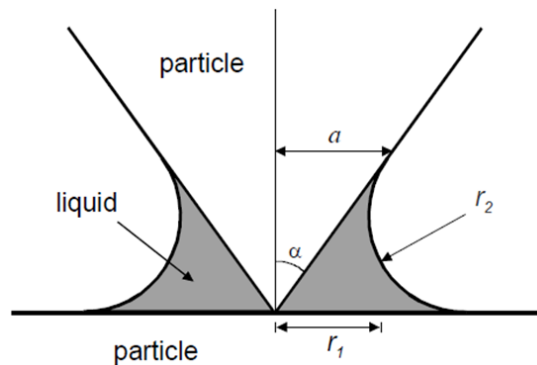
- 2-38. During extended sintering of a sintered sample with a 98% density, the average grain size is doubled. What will then be the relative density of the sample if the number of pores per grain remains constant? Assume that the capillary pressure of pores is balanced with the pressure of insoluble gases within them and all the pores are located at grain boundaries. Assume $P_{ext} = 0 \text{ atm}$.
- 2-39. Assuming γ_s to be constant, what will be the change in densification rate with the dihedral angle of a compact containing insoluble gases in isolated pores?

- 2-40. Kang and Yoon (Kang SJL, Yoon KJ, *J. Eur. Ceram Soc.*, 5, 135-39 (1989)) calculated the maximum attainable density of a powder compact containing insoluble gases within isolated pores with no coalescence, as shown in Fig. 5-5 in the book "Sintering". Assuming that the number of pores per grain is constant, explain quantitatively how you can use this figure to predict the maximum attainable density of the same compact with a grain growth of S times.
- 2-41. Consider a powder compact which consists of two kinds of agglomerates with different densities, ρ_h and ρ_l ($\rho_h > \rho_l$). If the relative densification rates of these agglomerates, $(d\rho/dt)/\rho$, are the same, what would happen? Discuss whether this assumption is satisfied in real sintering.
- 2-42. During sintering of powder compacts, pore opening can occur. What are possible causes (at least two) of pore opening? State and explain possible measures (at least two) to suppress pore opening.
- 2-43. The diffusional material transport from grain boundary to neck during hot pressing is similar to the diffusional creep of polycrystalline materials.
- (a) During hot pressing of a powder compact at T_1 , densification is reported to occur by Nabarro-Herring creep. If you increase the hot pressing temperature, is it possible that the powder compact will be densified by Coble creep?
 - (b) In the case of hot pressing, derive the equations showing the dependence of the densification rate on grain size for the mechanisms of grain boundary diffusion and lattice diffusion.
 - (c) Plot schematically the dependence of the apparent densification rate on the grain size of Al_2O_3 during hot pressing. Assume that both grain boundary diffusion and lattice diffusion are operative. Assume also that $D_{Al}^l > D_O^l$ and $D_O^b > D_{Al}^b$.
- 2-44. Derive Eqs (5-27) and (5-28) in the book "Sintering".
- 2-45. Describe possible techniques that can enhance the sintering of a nitride with a high vapor pressure and explain why these techniques work.
- 2-46. The grain boundary (also surface) structure (morphology) can be categorized into two types: atomically disordered (macroscopically rounded) and ordered (faceted). Do you think the grain boundary (surface) type affects the densification behavior during solid state sintering? Explain. What will be the effect of powder size (between very fine and coarse) on densification if densification occurs via boundary diffusion?
- 2-47. Kingery and Francois (Kingery WD, Francois B, The sintering of crystalline oxides, I. Interactions between grain boundaries and pores, in *Sintering and Related Phenomena*, Kuczynski GC, et al. (eds) Gordon and Breach, NY, 471-98 (1967)) suggested that the stability of a pore in a polycrystal is governed by the relative size of the pore to the grain size and the relative ratio of surface energy to grain boundary energy. In a glass with no grain boundaries, can a pore be stable?
- 2-48. What measures (at least three) can be taken to enhance the densification during sintering? What are the grounds for these measures?

II-2. Liquid phase sintering

- 2L-1. (a) Given that the wetting angle is zero degrees, the particle radius a , the two principal radii of the liquid meniscus r and x , and the contact angle of liquid ψ (see Fig. 14-2 in the book “Sintering”), what is the compressive force between particles of an equal size?
- (b) For the model system described in (a), if grain growth does not occur and contact flattening is the only mechanism of densification, how does the densification rate $d\rho/dt$ of a compact vary with particle size?

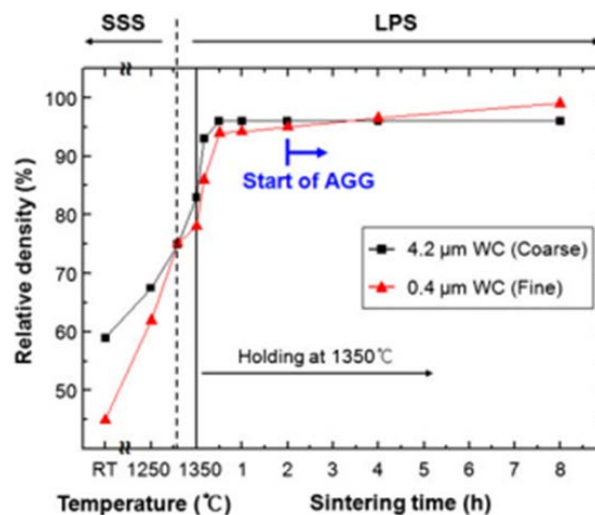
- 2L-2. (a) Calculate the force between the cone-shaped particle and the plate shown in Fig. P2L-2. For this system, $r_1 = a[1 - \frac{1 - \cos \alpha}{\tan \alpha(1 + \sin \alpha)}]$ and $r_2 = \frac{a}{\tan \alpha(1 + \sin \alpha)}$. Assume that the wetting angle is zero degrees.
- (b) What is the dependency of the force calculated in (a) on the liquid volume V_l ?



<Fig. P2L-2>

- 2L-3. Consider three different liquid phase sintered compacts with the same chemical composition, same grain size and distribution, and same liquid volume fraction, say 5 vol%. One is fully densified, another is partially densified with a number of pores having a size similar to the grain size, and another contains only a few pores that are more than ten times larger than the grain size. Describe and compare the microstructures of these compacts in view of the shapes of the grains within the liquid and in contact with the pores.
- 2L-4. Explain the densification and shrinkage processes in the pore-filling model and theory of liquid phase sintering (LPS). What are the fundamental differences between this model and Kingery's contact flattening model?
- 2L-5. Explain the mechanism of the pore filling during liquid phase sintering.
- 2L-6. If Kingery's contact flattening mechanism is the only mechanism of densification during LPS, what is the expected variation of the pore size distribution with respect to the sintering time? What is the expected variation of the pore size distribution in the case of the pore filling mechanism? Compare.
- 2L-7. Discuss the effects of the wetting angle and dihedral angle on densification and grain growth in liquid phase sintering. Assume that all other parameters are invariable.

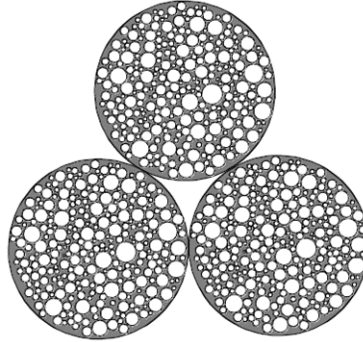
- 2L-8. In liquid phase sintering, pore filling was found to be the essential process of densification. What is the dependence of densification on scale?
- 2L-9. Explain why densification is, in general, faster in liquid phase sintering than in solid state sintering.
- 2L-10. (a) Describe a possible method to estimate the activation energy of densification during liquid phase sintering.
 (b) What are the assumptions you made for the estimation?
 (c) What is the activation energy of densification in the pore filling theory?
- 2L-11. The pore filling theory of liquid phase sintering describes that the densification of powder compacts is determined by grain growth. Assuming that the grain growth occurs by diffusion control and all other parameters are invariable,
 (a) discuss the effect of grain growth rate on densification time in quantitative terms.
 (b) plot schematically sintered density vs. average grain size trajectories for different grain growth rates with a ratio of 1:2:3.
- 2L-12. Figure P2L-12 (Yang DY, et al., *J. Mater. Sci.*, 47, 7056-63 (2012)) shows the densification curves of 95WC-5Co(wt%) powder compacts that contained large (4.2 μm size) and small particles (0.4 μm size). The densification of the sample containing coarse WC powder is faster than that of the sample containing fine WC powder at the beginning of liquid phase sintering. After 30min, however, no further densification occurred in the coarse WC powder sample while densification occurred continuously in the fine WC powder sample after 2h when abnormal grain growth took place. Explain these observations in view of the pore filling theory.



<Fig. P2L-12>

- 2L-13. According to the pore filling theory, the shrinkage of a compact occurs by successive accommodation/recovery of grain shape and microstructural homogenization. Explain the process of sample shrinkage in detail and its related driving force.
- 2L-14. Observations suggest that, in general, a solid-state sintered compact contains more pores entrapped within grains than a liquid-phase sintered compact. Why?

2L-15. When you crush a liquid-phase sintered compact into coarse powders, as shown in Fig. P2L-15, make a compact and resinter it, what do you expect the microstructural evolution will be during resintering? Will the microstructural evolution be different depending on the liquid volume fraction?



<Fig. P2L-15>

2L-16. The improvement of densification by an external gas pressure after pore isolation is far more pronounced in liquid phase sintering than in solid state sintering. Application of even a few atm pressure is very effective in liquid phase sintering, in contrast to the case of solid state sintering. Explain why the external pressure effect differs between solid state sintering and liquid phase sintering. What is the implication of your answer?

2L-17. Discuss the effect of mixedness of two elemental powders on densification during liquid phase sintering.

2L-18. What is the fundamental difference in densification between solid state sintering and liquid phase sintering?

PART III. Grain Growth and Microstructural Evolution

III-1. Solid state sintering

- 3-1. Compare and explain normal grain growth (NGG) in a polycrystalline pure material and a pure material with second phase particles, and the classically explained abnormal grain growth (AGG).
- 3-2. The average grain size of a dense ceramic after annealing for 120min. at 1200 °C was found to be 5 μm. Annealing for 60min at 1400 °C gave an average size of 11 μm. If the average grain size at time=0 was 2 μm at any temperature, estimate what the average grain size will be after 30min annealing at 1600 °C. Assume that normal grain growth occurs at the temperatures concerned.
- 3-3. Consider two cases of spherical particles in contact with the same radius. In one case, both of the particles are single crystalline. In the other case, one particle is polycrystalline while the other is single crystalline. Compare the microstructural changes during annealing for the two cases. The system is known to exhibit normal grain growth at the annealing condition. The surface energy is assumed to be isotropic.
- 3-4. For ionic compounds, what should the values of D_b^\perp and V_m be in Eq. (6.1) of grain growth?
- 3-5. Prove Eq. (6-7) in the book “Sintering”.
- 3-6. The original Smith-Zener equation overestimates the drag effect of second phase particles. Why?
- 3-7. Consider a polycrystal with uniformly distributed second-phase particles of a fine size. What will be the variation of grain size with annealing time of the polycrystal for the following cases? (a) no growth of the second-phase particles, (b) growth of the second-phase particles by lattice diffusion and (c) growth of the second-phase particles by grain boundary diffusion. Draw schematic figures and explain. Assume that all the particles are located at grain boundaries.
- 3-8. Consider two sintering powder compacts of the same relative density and same average grain size, but with and without uniformly distributed small second-phase particles. Discuss the densification rates of the compacts and state your assumption(s) for your conclusion.
- 3-9. Calculate the degree of Ca^{2+} segregation at an MgO grain boundary assuming that the elastic strain energy is the only driving force of the segregation. Assume that the Young’s modulus and the Poisson’s ratio of MgO are $2.1 \times 10^{11} \text{ N/m}^2$ and 0.3, respectively. The ionic radii of Mg^{2+} and Ca^{2+} are 0.72 and 1.0 Å, respectively.
- 3-10. Derive the solute concentration at a grain boundary, C_b ,

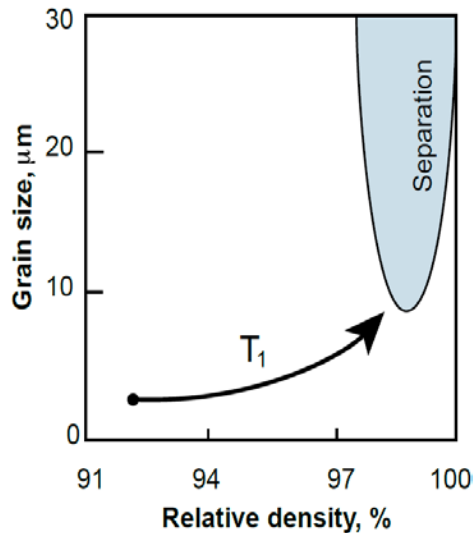
$$C_b = \frac{C \exp(-\Delta E/RT)}{1 - C + C \exp(-\Delta E/RT)},$$

where C is the solute concentration in the bulk and ΔE the energy of solute segregation at the grain boundary.

- 3-11. Consider three samples without and with second phase particles/solutes. Assuming that the initial capillary driving force for grain growth is the same and very high, schematically draw the G vs. t plot and explain their curves. For the three samples, the classical grain growth theory, Smith-Zener theory and Cahn-Lücke theory are assumed to be valid.
- 3-12. Draw a schematic figure and explain the boundary migration velocity as a function of grain size from 0.01 to 100 μm for a single-phase system with high solute segregation at the grain boundary. Assume diffusion-controlled migration at any grain size.
- 3-13. Consider a solid solution containing two kinds of solutes with fast and slow diffusivities perpendicular to the grain boundary. Assuming a high solute segregation at the grain boundary and the same interaction potential of the grain boundary for the two kinds of solutes, draw schematically and explain the variation of solute drag force with grain size.
- 3-14. (a) Explain the variation of solute segregation at grain boundaries with increasing temperature.
(b) Draw schematically and explain the variation in grain boundary velocity with temperature for pure, slightly impure and highly impure materials. Assume that the driving force for boundary migration is the same.
- 3-15. Do you expect to observe intensive abnormal grain growth (AGG) in an alloy with solute segregation at grain boundaries? Explain. Assume that the boundary migration follows the Cahn-Lücke theory.
- 3-16. The grain boundary mobility of a pure material is D_b^\dagger/kT . Derive the grain boundary mobility for the low velocity limit of an impure material with high grain boundary segregation. Assume the grain boundary segregation follows the McLean model.
- 3-17. After a grain growth experiment using two kinds of fully dense polycrystals with 99.8 and 99.999% purity, an engineer found that the activation energy for grain growth was different between the two polycrystals. Which one has a higher activation energy? Answer with the species and process that affect the activation energy in both cases.
- 3-18. Consider isolated pore-containing polycrystal samples with different grain sizes but with a similar microstructure.
(a) How does the number of pores per unit area vary with grain size?
(b) How does the drag force per unit area of the grain boundary vary with the grain size?
- 3-19. Consider isolated pores that move along grain boundaries by lattice and surface diffusion of atoms. Draw a schematic figure that shows the variation of the pore migration velocity with pore size, and explain. Assume that the driving force of grain boundary migration is constant.

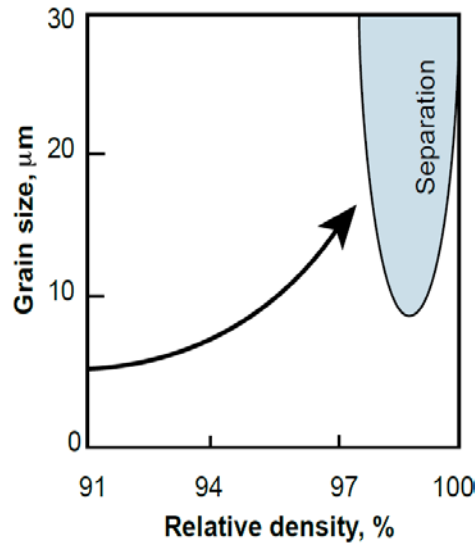
- 3-20. (a) What is the maximum drag force of a spherical pore with a radius of r against grain boundary movement? Assume a non-zero and constant grain boundary energy.
 (b) If the dihedral angle decreases by a reduction of the solid/vapor interfacial energy, how does the drag force of the pore change with the dihedral angle? The pore volume is assumed to be invariable.
 (c) For pore migration by surface diffusion, explain the change in pore migration rate (velocity) with a decreasing dihedral angle. Assume a constant driving force for grain boundary migration.
- 3-21. For pore migration (movement) by gas diffusion, what is the effect of pore size on pore migration velocity? The gas pressure in the pore is assumed to be in equilibrium with the pore capillary pressure.
- 3-22. When a pore at a grain boundary moves by the evaporation/condensation mechanism, the pore mobility is inversely proportional to the square of the pore radius. What is the velocity ratio of pores with a radius of r_1 and a radius of r_2 in two different samples with the same porosity? Assume that the driving force of boundary migration is the same for the two samples.
- 3-23. If grain growth is governed by the movement of pores by gas diffusion, what is the activation energy of grain growth? Assume a constant gas pressure in the pores.
- 3-24. The migration of grain boundary in a sample that contains isolated pores is known to be controlled either by the atom diffusion across the boundary or the movement of the isolated pores at the boundary via surface diffusion. Draw a schematic figure that shows the variation of the pore migration velocity (boundary migration velocity) with pore size, and explain. Assume that the driving force of boundary migration is constant.
- 3-25. (a) What are general directions for suppressing pore/boundary separation during sintering?
 (b) What are possible techniques (as many as possible) to suppress pore/boundary separation?
- 3-26. Consider a system where densification is governed by grain boundary diffusion and grain growth by the migration of pores under the mechanism of evaporation/condensation. There are two powder compacts of different grain sizes but with similar microstructures except the scale. When the samples were fully densified by sintering, which sample exhibits less grain growth compared with its initial grain size? Explain.
- 3-27. Consider a system where densification occurs by lattice diffusion and grain growth by surface diffusion. How can you determine the optimum size of the starting powder in view of sintering and powder production cost? If you adopt hot pressing to produce sintered compacts, do you expect the optimum powder size will change? If so, how?
- 3-28. Under which conditions is the microstructure development map in Fig. 11-2 in the book "Sintering" constructed? To enhance densification while suppressing grain growth at the beginning of the final stage of sintering, what conditions should be provided?

- 3-29. At the final stage of sintering of a powder compact, densification is known to occur by lattice diffusion and grain growth by surface diffusion. When you raise the sintering temperature from T_1 to T_2 ,
- how will the sintered density vs. grain size trajectory in Fig. P3-29 change?
 - how does the pore/boundary separation region change?
 - will the critical grain size where the relative densification rate is equal to the relative grain growth rate change?



<Fig. P3-29>

- 3-30. Figure P3-30 shows the microstructural development trajectory of an Al_2O_3 powder compact with an initial particle size of $5 \mu\text{m}$.
- Show and explain the microstructural development trajectory of another Al_2O_3 powder compact with an initial particle size of $0.5 \mu\text{m}$. Assume that the densification occurs by grain boundary diffusion (D_b) and the grain growth by the movement of pores via surface diffusion (D_s).
 - If a dopant addition enhances D_s by ten times, what will be the trajectories of compacts with $5 \mu\text{m}$ and $0.5 \mu\text{m}$ particle sizes. How about the separation region?
 - If densification occurs by lattice diffusion (D_l) and the grain growth by surface diffusion (D_s), what will the trajectories of the two different compacts be? Compare the result with that of (a).
- 3-31. Draw schematically and explain the $G - \rho$ trajectories for two sintering bodies (a) with different relative densities (low and high) but with the same grain size, and (b) with the same relative density, same pore number and same grain size, but with different pore size distributions (narrow and broad). Assume that the sintering bodies were made from the same starting powder and that densification occurs by lattice diffusion and grain growth by surface diffusion
- 3-32. Consider a system at final stage sintering where densification occurs via lattice and grain boundary diffusion, and grain growth by the movement of pores via surface diffusion. Show schematically and explain the variations of the relative densification rate and relative grain growth rate with respect to grain size.



- 3-33. Discuss whether Herring's scaling law is applicable to a system where densification occurs by lattice diffusion and grain growth by surface diffusion. Assume that all the pores are at the grain boundary and that the number of pores per grain is invariable during sintering.
- 3-34. Consider a system where densification occurs by lattice diffusion and grain growth by the movement of pores via surface diffusion.
- Describe how the activation energy of diffusion can be obtained from diffusivity data.
 - Discuss a desirable sintering cycle (T vs. t) to enhance densification while minimizing grain growth.

- 3-35. At the final stage of sintering of alumina powder compacts, densification and grain growth are reported to follow the equations

$$\frac{d\rho}{dt} = \frac{735D_b\delta_b\gamma_sV_m}{G^4RT}$$

and

$$\frac{dG}{dt} = \frac{110D_s\delta_s\gamma_bV_m}{G^3(1-\rho)^{4/3}RT}$$

respectively. Draw a microstructural development map (G vs. ρ) for an alumina compact with a grain size of 1 μm and a relative density of 0.9 during sintering at 1500°C. Note that $D_b\delta_b = 8.6 \times 10^{-10} \exp(-418\text{kJ}/RT)\text{m}^3/\text{s}$, $D_s\delta_s = 1.26 \times 10^{-7} \exp(-493\text{kJ}/RT)\text{m}^3/\text{s}$, $\gamma_s = 0.71 \text{ J}/\text{m}^2$, $\gamma_b = 0.34 \text{ J}/\text{m}^2$, and $V_m = 2.56 \times 10^{-5} \text{ m}^3$. 35-38 in Part IV of the book "Sintering"

- 3-36. What is the thermodynamic background of fast firing?
- 3-37. Describe possible processes for preparing sintered compacts with the following microstructures.
- Fully densified compacts with different grain sizes (at least 10 times difference in size)

- (b) Compacts with the same grain and pore sizes but with different porosities, say 1~5 vol%.
 - (c) Compacts with the same grain size and porosity but with different pore sizes, say 1~10 μm .
- 3-38. Consider powder compacts consisting of two kinds of powders with very low (A) and very high (B) sinterability. What do you expect the change in densification rate will be with decreasing size of the powder with a low volume fraction for the two kinds of powder compacts: (i) with a high volume fraction, say over 90%, of powder A and a low volume fraction of powder B, and (ii) a high volume fraction of powder B and a low volume fraction of powder A.
- 3-39. For some systems, irrespective of the heating rate, the sintered density shows approximately the same value upon reaching a fixed sintering temperature. Explain the possible cause of this phenomenon.
- 3-40. Unconventional sintering techniques with an external field, such as microwave sintering, spark plasma sintering, and flash sintering, are known to be effective in promoting densification and suppressing grain growth. What can be the major mechanism of these unconventional sintering?
- 3-41. In sintering, we usually aim at obtaining a fully dense body with a fine microstructure. Describe potential directions, at least four, to achieve the goal and briefly discuss their validities.
- 3-42. What are the differences in migration mechanism and behavior between rough (atomically disordered) and faceted (atomically ordered) boundary?
- 3-43. Why is the migration of a faceted boundary nonlinear with respect to the driving force?
- 3-44. Consider fine and coarse powders of the same chemical composition. During sintering, a fine powder compact showed abnormal grain growth while a coarse powder compact did not and its microstructure appeared to be fairly normal. Explain why the grain growth behavior was different between the two powders.
- 3-45. Based on the mixed control mechanism of boundary migration, explain the mixed mechanism principle of grain growth (microstructural evolution).
- 3-46. For a system where abnormal grain growth takes place during sintering, what possible measures can be taken to suppress abnormal grain growth in view of the mixed control mechanism of boundary migration?
- 3-47. Consider annealing of single crystal/polycrystal bi-layer samples. The average size of grains in each polycrystal is assumed to be unchanged during annealing.
- (a) Express and plot the driving force for the growth of the single crystal into a polycrystal as a function of the average grain size in the polycrystal.
 - (b) In the case where a critical driving force is needed for the growth of a single crystal, plot the migration distance of the single crystal as a function of the average grain size in a polycrystal with no impurity for a fixed period of annealing time.
 - (c) Prepare the same plot as in (b) but with an impure polycrystal. Compare with the graph for (b).

- (d) You have annealed the samples in (b) and (c) at a higher temperature. What do the graphs look like in comparison with those for (b) and (c)?
- 3-48. To make a single crystal from a sintered part, it is common to prepare a bilayer sample of a seed crystal and a sintered part, and anneal the bilayer sample. During growth of the seed crystal, it is essential to suppress grain growth in the polycrystal to maintain enough driving force for the growth of the seed crystal.
- (a) Describe and discuss general directions and possible means for suppressing grain growth in the polycrystal.
- (b) If the sample is annealed above the eutectic temperature, a liquid film can form and thicken with the growth of the seed crystal. With an increase in film thickness, can the growth kinetics of the seed crystal vary?
- 3-49. When we sinter for a fixed period of sintering time a fine powder compact of a material with well faceted boundaries at low temperature, stagnant grain growth and abnormal grain growth can occur in repetition with increasing the sintering temperature. Explain this repetitive grain growth behavior in view of the mixed mechanism principle of microstructural evolution.
- 3-50. What can be the effects of second phase particles, segregated impurities (or solutes) and liquid films at grain boundaries on grain growth behavior in the context of the mixed mechanism principle of microstructural evolution? Assume that the driving force for boundary migration and boundary energy anisotropy are invariable.

Note added in proof: for all problems in this part, except those from P3-42 to P3-50, grain growth is assumed to be governed solely by diffusion of atoms. (Here, the word diffusion means the thermal jumping and position change of atoms across the boundary, following the conventional understanding.)

III-2. Liquid phase sintering

- 3L-1. Describe the basic assumptions of the Lifshitz-Slyozov-Wagner (LSW) theory and its results, and discuss their implications.
- 3L-2. Consider a liquid phase sintering material containing inert second-phase spheres. Sketch and explain the growth shapes of a grain around a sphere for a dihedral angle between them of 0, 90 and 160 degrees, respectively.
- 3L-3. Consider two liquid phase sintered compacts with the same liquid volume fraction but with very different grain sizes. If you bond these two compacts and anneal at the liquid phase sintering temperature, how will the microstructure evolve? Assume that the compacts are fully dense and the grain shape is rounded.
- 3L-4. Consider a system where $\alpha - \beta - \text{liquid}$ are in equilibrium at a certain temperature, and the dihedral angles of α and β are 50 and 5 degrees, respectively. When a dense α -liquid compact and a dense β -liquid compact with 5 vol% of liquid each are in contact at the temperature, what will be the change in microstructure directly after contact and during annealing? Assume that the wetting angle is zero degrees, the molar volumes of

α and β are the same and the diffusivities of different atoms in the liquid are the same.

- 3L-5. Discuss the similarities and differences between the diffusional dissolution/precipitation mechanism in liquid phase sintering and the evaporation/condensation mechanism in solid state sintering.
- 3L-6. Consider a liquid-phase sintered compact with a small amount of liquid which forms an interconnected channel along the grain edges (dihedral angle smaller than 60 degrees). Explain a possible method of measuring the activation energy of grain growth and discuss the effect, if any, of grain boundaries on grain growth.
- 3L-7. Consider a two-dimensional crystal with $\{10\}$ and $\{11\}$ surface energies of 0.5 and 0.45 J/m², respectively. Assuming that the surface energies of the other planes are much higher than these values, delineate the exact equilibrium shape of this crystal.
- 3L-8. The equilibrium shape of an oxide in a melt is reported to be a cube. When you immerse for a long time a rectangular cuboid-shaped single crystal of the oxide in the melt, what will happen? Explain the process in detail in terms of solubility.
- 3L-9. (a) Write the equation for a change in Gibbs free energy with the formation of a disk-shaped nucleus with a step height h on a crystal surface as a function of radius r and show this graphically.
(b) How will the schematic graph change as temperature increases? Explain why. Assume that the driving force for the nucleation is unchanged.
- 3L-10. Consider two separate particles with a radius of r_1 and r_2 in a liquid. Draw schematically and explain the solute distributions in the liquid between the particles for diffusion- and precipitation-controlled (reaction-controlled) growth, respectively.
- 3L-11. In a liquid-phase sintered NbC-Co sample, large growing grains are mostly well faceted while small dissolving grains are mostly rounded. Explain why.
- 3L-12. The solid/liquid interfacial energy and its anisotropy of a grain can vary with the dopant and oxygen partial pressure. Knowing that two liquid phase sintered compacts with the same initial composition and the same initial grain size and distribution showed normal and abnormal grain growth under different atmospheres, respectively, explain the cause of the difference in grain growth mode between the two compacts.
- 3L-13. Describe the mixed mechanism principle and theory of grain growth (microstructural evolution) for two-phase systems (Jung YI, et al., *J. Mater. Res.*, 24, 2949-59 (2009); Kang SJJ, et al., *J. Am. Ceram. Soc.*, 92, 1464-71 (2009)).
- 3L-14. Consider a liquid phase sintering compact in which the equilibrium shape of the grains at the sintering condition changes but all the other parameters are invariable.
(a) The critical size of grains in the compact is the size where the grain is neither growing nor dissolving. How can you determine the critical grain size mathematically?
(b) When the shape of solid grains changes as a result of a change in step free energy, do you think the critical grain size also changes? Explain.

- (c) When the grain shape changes from spherical to well faceted (a step free energy change from zero to a large value), what types of growth behavior will the sample exhibit? Explain.
- 3L-15. Consider Ostwald ripening of faceted grains.
- Discuss the effect of the liquid volume fraction on the grain growth behavior. Assume that the maximum driving force is slightly larger than the critical driving force for growth.
 - At temperature T_1 , stagnant grain growth was observed to occur. When you raise the temperature, does the grain growth behavior change? Explain. Assume that the sintering time is the same.
- 3L-16. When a WC-Co powder compact is sintered at a liquid phase sintering temperature, abnormal grain growth often takes place, in particular, in a compact with fine powder.
- Explain the cause of the abnormal grain growth in this alloy.
 - What are possible strategies and measures (at least two) to suppress abnormal grain growth?
- 3L-17. It was reported that compared with conventional liquid phase sintering, two-step liquid phase sintering can retard abnormal grain growth (AGG) in WC-Co. What could be the reason for the retardation of AGG in two-step sintering?
- 3L-18. Consider two two-phase systems, one with faceted grains and the other with rounded grains in a liquid matrix.
- What is the cause of the difference in grain shape between the two systems?
 - What is the fundamental difference in growth behavior between a faceted grain and a rounded grain from a liquid?
 - Explain the grain growth behavior with annealing time from zero to 1000h for a faceted system where the maximum driving force for growth is very high.
- 3L-19. In a liquid phase sintering system of WC-TiC-Co, WC grains exhibited a well faceted shape while TiC grains a rounded (spherical) shape in the same Co liquid matrix. In the same sample, the growth behavior of TiC grains was normal while WC grains was abnormal or stagnant depending on their initial particle size. Explain why the growth behavior was different for WC and TiC grains. What is the implication of the result in view of grain growth behavior during liquid phase sintering?
- 3L-20. When a compact of NbC-Co powder without ball-milling was liquid-phase sintered at 1450 °C for 1h, abnormally large grains formed. In contrast, a ball-milled powder compact did not exhibit abnormal grain growth behavior after the same thermal treatment as that for the un-milled powder compact. Explain why the grain growth behavior in the two powder compacts with and without ball-milling was different.
- 3L-21. Consider three different liquid phase sintering compacts with (partially) faceted grains. Starting with the same initial average grain size and initial grain size distribution, what would be the difference in microstructural evolution between the three compacts with different critical driving forces, Δg_c , for grain growth, very small, small and large? Assume that the compacts are fully dense.

- 3L-22. The grain shape of NbC in a Co liquid varies between a well-faceted cube and a sphere depending on annealing temperature and the addition of dopants, such as B.
- (a) What do you expect the shape of NbC grains will be in Co without B at a low temperature?
 - (b) Explain the growth mechanisms of spherical and faceted NbC grains in Co. What are the kinetic equations of grain growth in compacts containing the two extreme types of grains?
 - (c) Which mechanism do you expect to be operative in the growth of round-edged (partially rounded) cubic NbC grains. Do you think the growth behavior varies with the fraction of round-edged area? Explain.
- 3L-23. What is the fundamental difference in the grain growth process between solid state sintering and liquid phase sintering?

PART IV. Supplementary Subjects

IV-I. Sintering of ionic compounds

4I-1. Using a statistical treatment, show that the vacancy concentration, n/N_A , in a pure compound with Frenkel defects is expressed as

$$\frac{n}{N_A} = \exp\left(-\frac{\Delta g_F}{2kT}\right),$$

where n is the number of vacancies per mole, N_A the Avogadro number and Δg_F the formation free energy of a Frenkel defect.

4I-2. When the oxygen concentration of an air-sintered pure oxide is decreased by annealing in a reducing atmosphere, by how much is the Fermi level of this oxide changed?

4I-3. In AgBr, the major ionic defect is a Schottky type and the minor is a Frenkel type. Show the variation of ionic defect concentrations with the concentration of CdBr₂.

4I-4. Consider the addition of an acceptor dopant MO to L₂O₃ oxide. Show the change in defect concentrations with the dopant amount. Assume that the major and minor defects in L₂O₃ are the Schottky disorder and the electronic disorder, respectively, and that all M cations go into L sites.

4I-5. Show the change in defect concentrations in Al₂O₃ with an increased addition of ZrO₂. Assume that the major and minor defects in Al₂O₃ are Schottky and Frenkel disorder, respectively, and that all Zr cations go into Al sites.

4I-6. In ZrO₂-doped Al₂O₃ (refer to Prob. 4I-5), how do you expect the effective diffusion coefficient of Al to vary by increasing the amount of ZrO₂ under conditions where the activation energy of Al interstitial diffusion is much smaller than that of Al lattice diffusion (a), and *vice versa* (b)?

4I-7. The major point defects in NaCl are Schottky defects. When CaCl₂ is added to NaCl, Ca ions replace Na ions. For a CaCl₂-doped NaCl, plot and explain the variation in $[V'_{Na}]$ with temperature in a $\ln[V'_{Na}]$ vs. $1/T$ plane.

4I-8. L₂O₃ dopant is added to an MO oxide with Schottky defects as the major defects. Assuming that all the L ions go into M sites,

(a) plot the variation of $[V''_M]$, $[V''_O]$ and $[L^\bullet_M]$ with temperature on a $\log[\text{concentration}]$ vs. $1/T$ plane, and

(b) plot the effective diffusion coefficient \bar{D} in MO with temperature. Assume that \bar{D} is governed by the diffusion of V''_M .

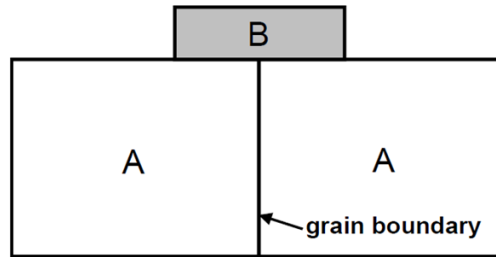
4I-9. (a) Write the effective diffusion coefficient in an M_aX_b compound.

(b) Sketch the variation of the effective diffusion coefficient with grain size for an M_aX_b compound where both lattice and grain boundary diffusions are operative. Assume $D^l_M > D^l_X$ and $D^b_M > D^b_X$.

- 4I-10. The densification rate is inversely proportional to the time required to obtain a constant change. An oxide MO is known to sinter by lattice diffusion as well as grain boundary diffusion at the rates, $(Rate)_l \propto \frac{D_l \gamma_s V_m}{RTG^3}$ and $(Rate)_b \propto \frac{D_b \delta_b \gamma_s V_m}{RTG^4}$, respectively. Given that $D_M^l > D_O^l$ and $D_O^b \delta_b > D_M^b \delta_b$, show schematically the variation of the sintering rate with changing particle size from very fine to very coarse.
- 4I-11. Consider an MO oxide where the dominant defects are Schottky type and ions move by the vacancy mechanism. Assume that the activation energy of metal ion diffusion, ΔH_m^M is higher than that of oxygen ion diffusion, ΔH_m^O . ($\Delta H_m^M > \Delta H_m^O$).
- (a) Sketch the variations of $[V_O^{\bullet\bullet}]$ and $[V_M^{\prime\prime}]$, and also those of the diffusion coefficients of the two different ions with oxygen nonstoichiometry.
- (b) In the sintering of this compound, what are the effective diffusion coefficient \bar{D} and the molar volume V_m that govern the sintering kinetics in the equation $t \propto 1/(JAV_m)$?
- 4I-12. In an MO metal oxide, the dominant defects are known to be Schottky-type. Assuming that $K_s=10^{-10}$ and $D_M=100D_O$, what kind of dopant and how much of it must be added to the oxide to obtain the maximum rate of densification in sintering if the densification occurs by lattice diffusion?
- 4I-13. The major defects in KCl are known to be Schottky-type and the formation free energy of the cation vacancy is lower than that of the anion vacancy. Sketch the surface charge and surface defect concentration in pure KCl and in highly CaCl₂-doped KCl.
- 4I-14. Express the mobility of an oxide grain boundary in which the migration is governed by the diffusion of segregated aliovalent dopant atoms. Assume that the dopant segregation follows the McLean model, where segregation occurs in a monatomic layer. (See problem P3-16.)

IV-2. Diffusion induced interface migration

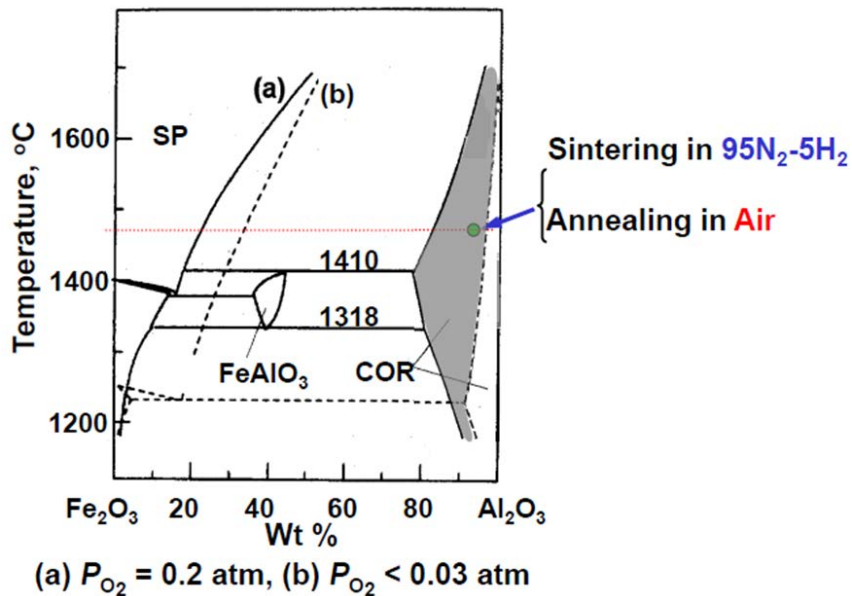
- 4D-1. When solute atoms diffuse into or diffuse out from grain boundaries, diffusion induced grain-boundary migration (DIGM) can occur. Explain how the migration direction is determined in DIGM.
- 4D-2. Is the driving force for DIGM with a thick migration thickness different from that for its initiation?
- 4D-3. Consider a heat-treatment of metal A in contact with metal B, as shown in Fig. P4D-3, below their melting points. Assuming a finite solubility of B in A, explain the variation in the concentration of B in A with heat-treatment temperature and time.



<Fig. P4D-3>

- 4D-4. Liquid film migration (LFM) occurred when solute atoms were added to a liquid phase sintering body. If the migration direction of some liquid films was reversed and the films went back to their original position during annealing, what would be the cause of this migration reversal? Knowing that the radius of the curvature of a liquid film was r just before its migration reversal, estimate the driving force of the observed liquid film migration.
- 4D-5. Consider a perfectly coherent diffusion layer on a large single crystal surface. Assuming that the lattice parameter of the layer is the same as that of the crystal with $d_{(100)} = a$,
- explain the state of the elastic stress in the diffusion layer, and
 - calculate the elastic stress and strain, as well as the elastic strain energy in the layer for a cubic crystal system.
- 4D-6. Consider a partially coherent thin β layer on an α single crystal. Given the distance between the misfit dislocations formed at the α/β interface to be d and the intrinsic (stress-free) lattice parameters of α and β to be a^α and a^β , respectively, derive the coherency strain ε in the β layer.
- 4D-7. Figure 8.6 in the book “Sintering” is a coherency strain energy map (in MJ/m^3) of $\text{Al}_2\text{O}_3/\text{Al}_2\text{O}_3(\text{Fe}_2\text{O}_3)$ for an Fe_2O_3 concentration of 5 mol% (with $\varepsilon_c/\varepsilon_a$ of 0.94) in a coherent diffusion zone.
- When you supply Fe_2O_3 to an Al_2O_3 bi-crystal sample with (0001) and $(\bar{2}110)$ planes, what do you expect to observe?
 - Compare the migration velocities of the boundaries between bi-crystals with (0001)/(01 $\bar{1}$ 0) and (0 $\bar{1}$ 12)/(01 $\bar{1}$ 0) planes.
- 4D-8. Figure P4D-8 shown below is the system $\text{Al}_2\text{O}_3\text{-Fe}_2\text{O}_3$.
- Describe the microstructure you will observe of a sample with the composition shown in the phase diagram when you sinter it in $95\text{N}_2\text{-}5\text{H}_2$ at 1470°C .
 - Describe the microstructural change, if any, when you anneal the sintered sample in air at 1470°C .
- 4D-9. Discuss whether the grain boundary migration during discontinuous precipitation or dissolution is basically different from DIGM.
- 4D-10. Explain how abnormal grains can form under chemical inequilibrium in terms of a DIIM (diffusion-induced interface migration) process.

Phase Diagram of Al_2O_3 - Fe_2O_3



<Fig. P4D-8>

4D-11. What is diffusion induced recrystallization (DIR)? Describe the process of DIR.

4D-12. The grain boundary structure of polycrystalline BaTiO_3 varies with the oxygen partial pressure, p_{O_2} : faceted and rough under a high and a low p_{O_2} , respectively. Assuming the same lattice and grain boundary diffusivities of solute ions in BaTiO_3 polycrystals with different grain boundary structures, do you expect the same degree of DIGM in two different BaTiO_3 samples with faceted and rough grain boundaries? Explain.

SOLUTIONS

PART I. Basis of Sintering Science: Sintering Processes, Thermodynamics of the Interface, and Polycrystalline Microstructure

1-1. Energy change ΔE = (grain boundary energy – surface energy) of a cube-shaped particle per unit volume

$$\begin{aligned}\therefore \Delta E &= \left(\frac{6}{2} l^2 \gamma_b - 6 l^2 \gamma_s \right) / l^3 \\ &= \frac{6}{l} \left(\frac{\gamma_b}{2} - \gamma_s \right) < 0.\end{aligned}$$

An increase in γ_s and a reduction in γ_b enhance the driving force for sintering and hence the sinterability. Note that the energy change (driving force) is inversely proportional to the particle size.

1-2. For a unit cube, two processes can be considered to have two halves: (i) stretch (or shear) + split and (ii) split + stretch (or shear). The work done in process (i) must be the same as that in process (ii).

For tension,

$$\begin{aligned}W_I &= \text{work to stretch} + \text{work to split} \\ &= W_o + 2(\gamma + d\gamma)(1 + d\varepsilon_{xx})\end{aligned}$$

$$\begin{aligned}W_{II} &= \text{work to split} + \text{work to stretch} \\ &= 2\gamma + W_I\end{aligned}$$

$$\text{Here, } W_I - W_o = 2\sigma_{xx}d\varepsilon_{xx}$$

$$\therefore 2\sigma_{xx}d\varepsilon_{xx} = 2\gamma d\varepsilon_{xx} + 2d\gamma$$

$$\therefore \sigma_{xx} = \gamma + d\gamma/d\varepsilon_{xx}$$

For shear,

$$W_I' = \text{shearing} + \text{splitting} = W_o' + 2(\gamma + d\gamma) \cdot 1$$

$$W_{II}' = \text{splitting} + \text{shearing} = 2\gamma + W_I'$$

$$W_I' - W_o' = 2\sigma_{xy}d\varepsilon_{xy} = 2d\gamma$$

$$\therefore \sigma_{xy} = d\gamma/d\varepsilon_{xy}$$

In general, we obtain Eq. (2-15) in the book “Sintering”..

$$\sigma_{ij} = \delta_{ij}\gamma + \frac{\partial\gamma}{\partial\varepsilon_{ij}}, \quad (2-15)$$

where $\partial\varepsilon_{ij}$ is the amount of strain per unit length and δ_{ij} is the Kronecker delta ($\delta_{ij} = 1$ for $i = j$ and $\delta_{ij} = 0$ for $i \neq j$)

Cf: Mullins WW, "Solid surface morphologies governed by capillarity," in *Metal Surfaces: Structure, Energetics and Kinetics*, ASM, Metals Park, Ohio, 17-66 (1963).

1-3. This is because unlike a liquid, a solid can sustain shear stresses. As a result, the atomic structure at the surface can vary with shear stress. The low atom mobility in the solid is in question.

1-4. In terms of surface tension:

$\gamma_1 \cdot 2\pi r \cdot \cos\theta = \rho\pi r^2 h \cdot g$, where g is the gravitational acceleration.

$$\therefore h = 2\gamma_1 \cdot \cos\theta / \rho g r$$

In terms of capillary pressure:

The pressure at the liquid meniscus is lower by the pressure of the liquid in the tube above the surface level. The radius of liquid meniscus R in the tube is $r/\cos\theta$.

The capillary pressure ΔP is $2\gamma_1/R = 2\gamma_1 \cdot \cos\theta/r$. This pressure is compensated by the pressure $\rho g h$ of the liquid in the tube above the surface level.

$$\therefore h = 2\gamma_1 \cdot \cos\theta / \rho g r$$

1-5. The gas pressure in a balloon = the external pressure + $2\gamma/r$, where r is the radius of the balloon. As the gas pressure in a small balloon is higher than that in a large one, gas flow occurs from the small balloon to the large one. The radii of the two balloons become the same after the gas flow.

$$1-6. P_{\text{pore}} = P_{\text{ext}} + 2\gamma/r_2 + 2\gamma/r_1$$

The pressure in the single crystal is assumed to be hydrostatic.

1-7. No gravity effect is assumed.

(i) With an external gas pressure of 1 atm

$$P_f = 2\gamma / r_f + 10^5,$$

where P_f is the gas pressure in the pore at the final state and r_f the final radius of the pore.

$$P_f V_f = \left(\frac{2\gamma}{r_f} + 10^5 \right) \frac{4}{3} \pi r_f^3 = P_i V_i = 10^5 \cdot \frac{4}{3} \pi r_i^3$$

where V_f and V_i are, respectively, the final and initial volume of the pore.

$$\therefore 10^5 r_f^3 + r_f^2 = 10^5 r_i^3 = 10^5 (5 \times 10^{-6})^3$$

$$r_f \approx 3.1 \times 10^{-6} \text{ m} = 3.1 \mu\text{m}$$

$$\text{Relative density} = \frac{0.9}{0.9 + 0.1 \times (r_f / r_i)^3} \times 100 \approx 97.4\%$$

(ii) Without an external gas pressure (in vacuum)

$$P_f V_f = \frac{2\gamma}{r_f} \left(\frac{4}{3} \pi r_f^3 \right) = P_i V_i = 10^5 \cdot \frac{4}{3} \pi r_i^3$$

$$r_f^2 = 10^5 (5 \times 10^{-6})^3$$

$$\therefore r_f \approx 3.54 \times 10^{-6} \text{ m} = 3.54 \mu\text{m}$$

$$\text{Relative density} \approx 96.2\%$$

1-8. The gas pressure in the isolated pore at 1000°C is $(1273/293) \times 10^5$ Pa.

The capillary pressure of the pore is $2\gamma/r = 9.3 \times 10^5$ Pa. In addition, the external atmospheric pressure of 1 atm ($\sim 10^5$ Pa) is also applied to the pore.

\therefore The pore shrinks at 1000 °C.

- 1-9. $\Delta P = 2\gamma/r = 2(0.1)/(0.5 \times 10^{-6}) = 4 \times 10^5 \text{ Pa} \sim 4 \text{ atm}$
 The pressure in the water below 10 m from the surface is 1 atm.
 The atmospheric pressure is 1 atm.
 Therefore, the pressure in the gas bubble is 6 atm.

- 1-10. The work required to increase an infinitesimal volume of a spherical particle with a radius of r is expressed as $PdV = (2\gamma/r)(4\pi r^2 dr) = 8\pi r \gamma dr$, where P is the pressure in the particle and V the volume.
 The work, W , done by an increase in size from 0 to r is:

$$W = \int_0^r 8\pi r \gamma dr = 4\pi r^2 \gamma$$

\equiv surface energy

The total work done with the creation of a particle with a radius of r is the same as the surface energy for an incompressible condensed phase. The excess energy in a particle over the energy of the same volume in the bulk of an infinite size is the total surface energy.

- 1-11. $E_{\text{surface}} = 4\pi r^2 \gamma$
 $E_{\text{elastic}} = [(4/3)\pi r^3 / V_m](1/2)V_m \kappa (2\gamma/r)^2 = (8/3)\pi \kappa r \gamma^2$
 For $E_s/E_e = 1$, $r = (2/3)\kappa \gamma = 6.6 \times 10^{-12} \text{ m}$

The calculated value is unrealistic, as the size is even much smaller than the atom size. This result indicates, in turn, that the elastic energy in a particle even with a range of nanometer size is negligible compared with the surface energy.

- 1-12. Calculation of the radius of one large drop:

$$(4/3)\pi(1)^3 \times 10 = (4/3)\pi r^3, \quad \therefore r = \sqrt[3]{10} \mu\text{m}.$$

Surface energy E_s of 10 drops of 1 μm size: $E_s = 4\pi(1)^2 \gamma \times 10 = 9.17 \times 10^{-12} \text{ J}$

Surface energy of the large drop: $E_s = 4\pi r^2 \gamma = 4.24 \times 10^{-12}$

The elastic strain energy E_e in 10 small drops: $E_e = (8/3)\pi(1)\kappa \gamma^2 \times 10 = 2.0 \times 10^{-16} \text{ J}$

The elastic strain energy in the large drop: $E_e = 4.3 \times 10^{-17}$

\therefore The energy decreased with the formation of one large drop $\Delta E = (9.17 - 4.24) \times 10^{-12} + (2.0 - 0.4) \times 10^{-16} \text{ J}$

- 1-13. $p_r = p_\infty \left(1 + \frac{2\gamma_s V_m}{RT r} \right)$

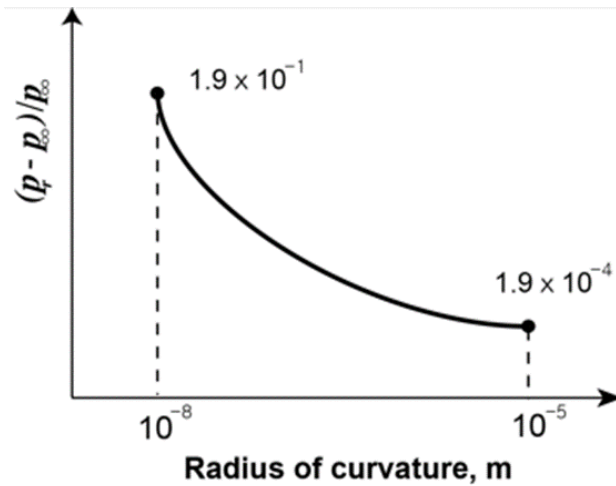
$$p_r - p_\infty = \frac{2\gamma_s V_m}{RT r} p_\infty$$

$$(p_r - p_\infty) / p_\infty = \frac{2\gamma_s V_m}{RT r} \quad (\text{Fig. S1-13(a)})$$

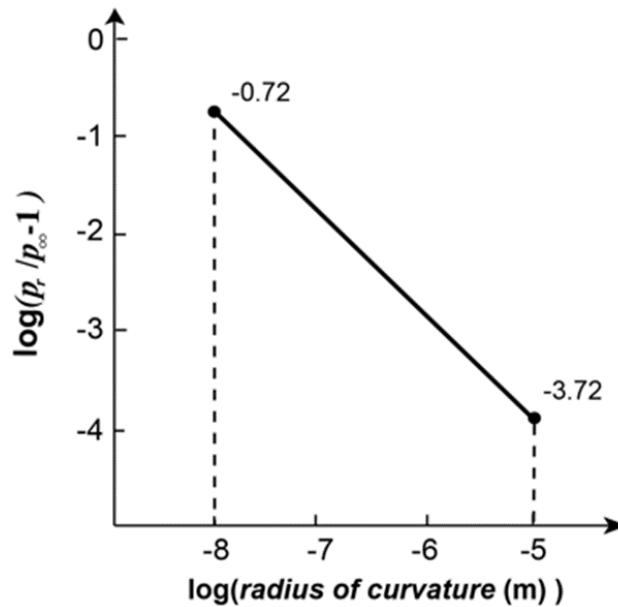
Taking logarithms gives

$$\log \left(\frac{p_r}{p_\infty} - 1 \right) = \log \left(\frac{2\gamma_s V_m}{RT} \right) - \log r$$

$$= -8.72 - \log r \quad (\text{Fig. S1-13(b)})$$



In log scale,



<Fig. S1-13>

1-14. We first need to know the molar volume of the material.

$$\text{The volume of the unit cell} = (2\sqrt{2})^3 = 16\sqrt{2} \times 10^{-30} \text{ m}^3$$

$$\text{The molar volume} = [(16\sqrt{2} \times 10^{-30})/4] \times (6.02 \times 10^{23}) = 3.4 \times 10^{-6} \text{ m}^3$$

Putting this value and other values into the equation $p_r = p_\infty \left(1 + \frac{2\gamma_s V_m}{RT r} \right)$ for the two particles gives the value of $\sim 0.021 p_\infty$.

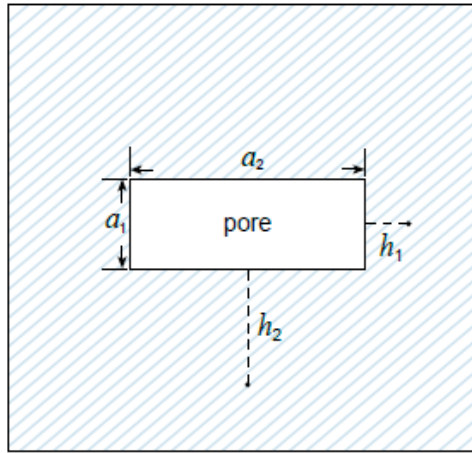
1-15. Yes. Refer also to the Clausius-Clapeyron equation. The temperature variation of pressure is infinity for a system with the same molar volume of α and β . The system remains in equilibrium coexistence (across a flat interface) with changing pressure at constant temperature.

1-16. Cube (a negative crystal). For a given volume, the equilibrium shape has the minimum total surface energy.

1-17. Shape change from a rectangular cuboid to a regular cube.

The capillary pressure on a facet plane is expressed as $2\gamma/h$ (Wulff theorem), where h is the distance from the facet to the center of an imaginary crystal with the same facet, as schematically shown in Fig. S1-17. Therefore, the value h increases as the size of the facet increases. The chemical potential of atoms on a facet surface is expressed as Eq. (15.27) in the book “Sintering”. As a pore is a negative crystal, the value of h is negative. The chemical potential of atoms on a large facet is less negative than that on a small facet. Atom transport will occur via surface diffusion, lattice diffusion and vapor phase transport at the same time from large facets to small facets, leading to the formation of a regular cube-shaped pore.

$$\Delta P \text{ between the two different planes, } a_2 \text{ and } a_1, = \gamma \left(\frac{1}{-h_2} - \frac{1}{-h_1} \right) > 0$$



<Fig. S1-17>

1-18. The equilibrium shape of grains in a polycrystal must satisfy the following conditions: (i) complete filling of the space, (ii) boundary tension balance of grain boundaries among adjacent grains, and (iii) minimum grain boundary area for a given volume (minimum boundary length for a given area in 2-dim. microstructure). It is hexagon.

1-19. The microstructures (grain shapes) are different from each other. According to the result of the application of Euler’s law for 2-dimensional microstructure, the average number of sides (edges) of grains is 6 for any sample. As the number of sides of abnormal grains is much larger than 6, the average number of sides of matrix grains in AGG sample is smaller than 6, unlike that in NGG sample, which is 6.

1-20. From the relations between interfacial tensions

$$2\gamma_{\alpha\beta} \cdot \cos \frac{\phi_{\alpha}}{2} = \gamma_{\alpha\alpha} \quad \text{and}$$

$$2\gamma_{\alpha\beta} \cdot \cos \frac{\phi_{\beta}}{2} = \gamma_{\beta\beta}$$

where ϕ_{α} and ϕ_{β} are the dihedral angles of α and β grains, respectively.

$$\therefore \gamma_{\alpha\alpha} / \gamma_{\beta\beta} = \cos \frac{\phi_{\alpha}}{2} / \cos \frac{\phi_{\beta}}{2}$$

Measurement of dihedral angles ϕ_{α} and ϕ_{β} gives the $\gamma_{\alpha\alpha} / \gamma_{\beta\beta}$ ratio.

From Figure P1-20,

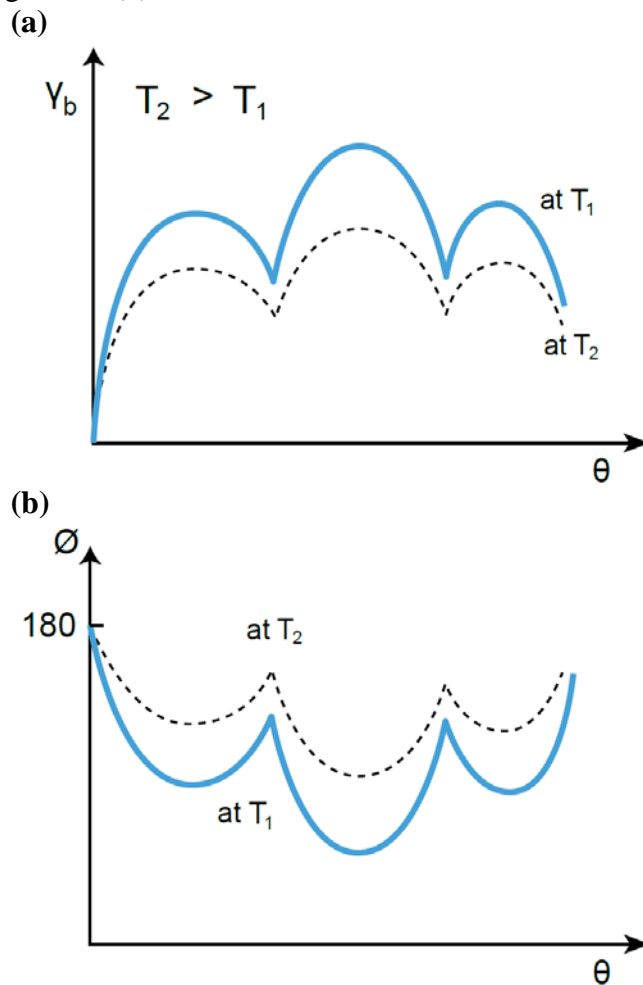
$$\phi_\alpha > \phi_\beta.$$

$$\therefore \gamma_{\beta\beta} > \gamma_{\alpha\alpha}.$$

Assumptions:

- (i) Interfacial energies are invariable.
- (ii) Random distribution of grain boundaries in space.

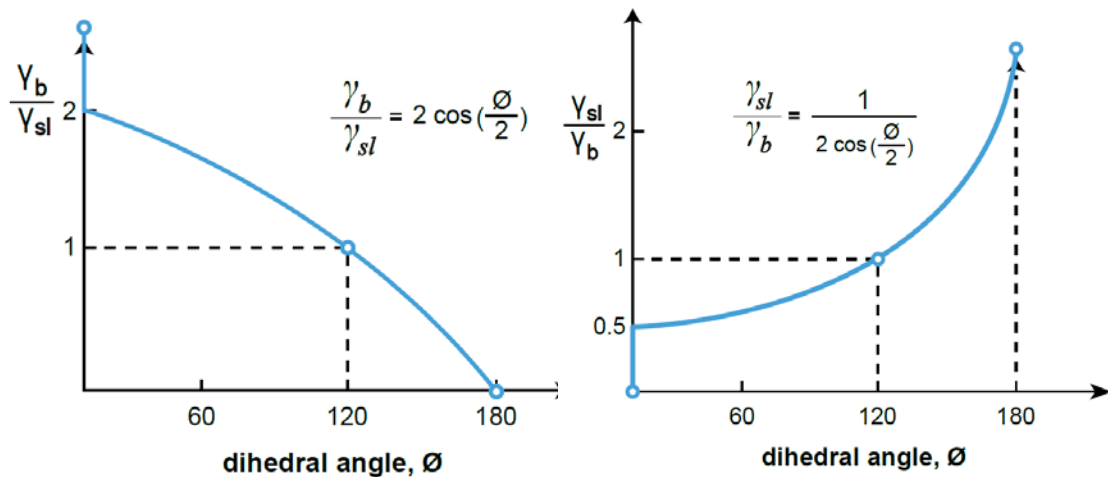
1-21. The energy of a tilt grain boundary varies with the tilt angle, as schematically shown in Fig. 3.4 in the book “Sintering”. Assuming that the boundary energy decreases with increasing temperature, the variation of γ_b with respect to θ can be drawn schematically as in Fig. S1-21(a) as the boundary energy anisotropy is reduced with increasing temperature. Using the equation $\gamma_b = 2\gamma_s \cdot \cos(\phi/2)$, the variation of ϕ with θ can be drawn as in Fig. S1-21(b)



<Fig. S1-21>

1-22. $\gamma_b = 2\gamma_{sl} \cdot \cos(\phi/2)$, $\gamma_{sl}/\gamma_b = 1/2\cos(\phi/2)$

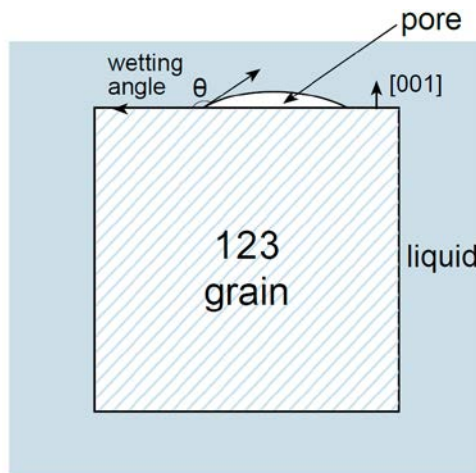
As γ_{sl} and γ_b have non-zero finite values, there must be discontinuities in the plot shown in Fig. S1-22. In reality, systems with $\gamma_{sl}/\gamma_b \gg 1$ or $\gamma_{sl}/\gamma_b \ll 1$ should be unavailable. It is also unrealistic that γ_{sl} equals γ_b .



<Fig. S1-22>

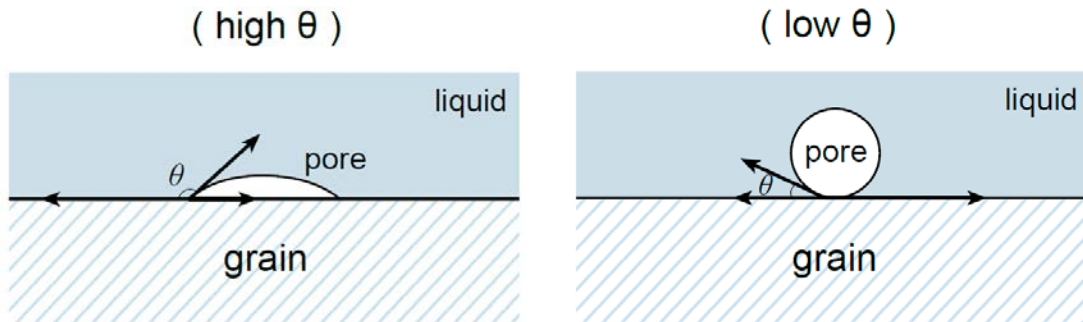
- 1-23. As the shape of a second phase particle is assumed to be spherical, the reduction of the total interfacial energy is the energy of the grain boundary that is covered by the particle: πr^2 , $1.5(\pi r^2)$, and $[(109.47 \times 6) \div 360] \pi r^2$ for a particle located at grain boundary, 3-grain edge, and 4-grain corner, respectively.
- 1-24. The area covered by a pore is larger at the triple junction than at the grain boundary. The total energy reduction is larger with the placement of a pore at a triple junction. (See Prob. 1-23.) There can be a kinetic factor that induces the preferential location of pores at triple junctions. With disappearance of small grains during grain growth, the pores present between the growing grains and small shrinking grains can coalesce and place at triple junctions among growing grains.
- 1-25. When a pore in a liquid comes in contact with a growing crystal, the shape of the pore will be determined by the contact angle θ' of the pore on the crystal. Here, $\theta' = 180^\circ - \text{wetting angle}$. As the wetting angle increases, the shape of the pore changes from rounded to elongated. The micrograph shows that the contact angle is around 90° and the shape of the entrapped pores is quite elongated, indicating that the wetting angle is fairly large in this system. The entrapment of crystallographically aligned and elongated pores suggests that the growth of 123 grains is fast.

Cf: Kim CJ, et al., *J. Mater. Res.*, 14, 1707-10 (1999)



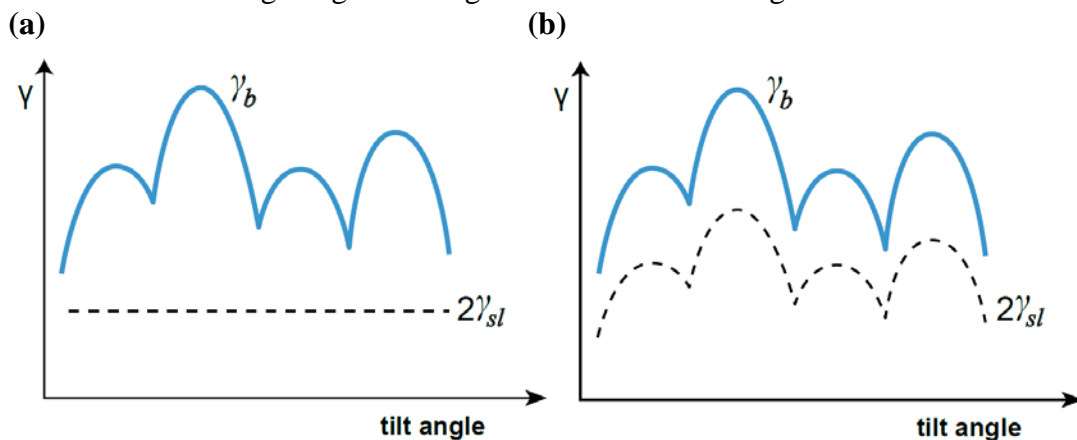
<Fig. S1-25>

1-26. Depending on the wetting angle, the shape of a pore on a grain is quite different, as schematically shown in Fig. S1-26. With increasing the wetting angle, the area of the pore on the grain increases and the circumference of the pore can act as a notch under tensile stress. The tensile strength of a sample must decrease with increasing the wetting angle, if all other parameters are the same. Note that in reality, the wetting angle for most of liquid phase sintering systems is low. Liquid phase sintering of a system with a high wetting angle is improbable. (Cf: Section 14.2 in the book “Sintering”.)



<Fig. S1-26>

1-27. As the grains are disintegrated in both liquid A and B, the boundary energy is larger than $2\gamma_{sl}$. γ_{sl} is constant in liquid A as schematically shown in Fig. S1-27(a), but is variable in liquid B as shown in Fig. S1-27(b). For penetration of liquid B into all the grain boundaries, the condition shown in Fig. S1-27(b) must be satisfied, but γ_{sl} can be only a few low values during the growth of grains after their disintegration.



<Fig. S1-27>

1-28. - In the polycrystal without liquid, the grain boundaries are curved between small and large grains to meet the dihedral angle condition of 120° .

- In the polycrystal with a liquid film at grain boundaries, the boundaries must be flat irrespective of the size difference between large and small grains because no dihedral angle condition is applied to this system.

1-29. (a) With growth of an abnormal grain, excess solute atoms and impurities that were segregated at the boundary of matrix grains accumulate in front of the growing abnormal grain. When the composition at the boundary reaches that of a liquid, a liquid phase can form at the boundary.

(b) Once a liquid film forms, the liquid at triple junctions between abnormal and matrix grains can redistribute with film migration and contributes to the thickening of the

film. With film migration, dissolution of segregated solutes into the film can also contribute to the film thickening.

- (c) The thickness of the liquid film between abnormal grains decreases to an equilibrium value of less than a few nanometers. This result indicates that the increase in film thickness during abnormal grain growth is a kinetic result.
- (d) A theoretical analysis (Ackler HD, Chiang YM, *J. Am. Ceram Soc.*, 82, 183-89 (1999)) showed that there can be two energy minima in a plot of Gibbs free energy vs. intergranular distance, suggesting that the two different configurations of boundary are both equilibrium configurations.
Cf: Choi SY, et al., *Acta Mater.*, 52, 3721-26 (2004).

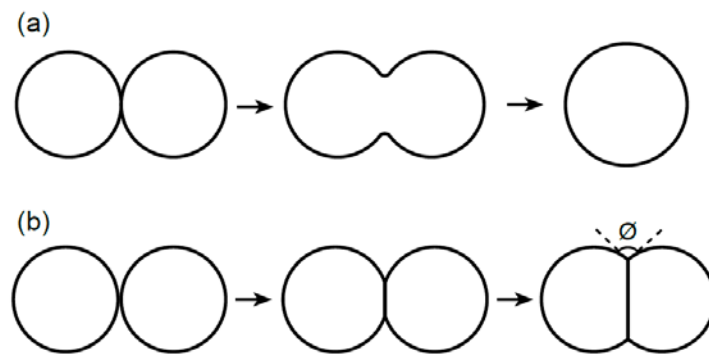
- 1-30. (a) If the matrix volume fraction is larger than that for the minimum interfacial energy, the excess liquid will sweat out from the compact.
- (b) The total interfacial energy is calculated for a uniform distribution of all the liquid within the compact
 - (c) The calculated value is for a compact with negligible grain boundary area. If the liquid volume fraction is larger than that for the calculated value, there will be no grain boundary for a compact with a uniform distribution of all the liquid in the compact. There is a discontinuity in terms of microstructure.

- 1-31. - Grooving of grain boundaries at the surface with a dihedral angle of 75° .
- Diffusion of oxygen into the sample, mostly along grain boundaries and the formation of pores at 4-grain corners with a dihedral angle of 75° .
 - There is an equilibrium value of the volume fraction of pores at 4-grain corners. (See Figure 3.13 in the book "Sintering").

PART II. Bonding and Densification

II-1. Solid state sintering

- 2-1. (a) Glass spheres: There is no grain boundary between particles. The difference in capillary pressure between regions, in particular, the neck region and particle surface induces viscous flow of the amorphous material. The final shape will be a single amorphous sphere, as shown in Fig. S2-1(a).
- (b) Crystalline spheres: A grain boundary forms and its area increases between the two particles as a result of material transport from the grain boundary and particle surface. A metastable state is reached when the two spherical surfaces meet the dihedral angle condition at the neck, as schematically shown in Fig. S2-1(b). Then, no further increase in contact area is expected unless there is a perturbation.



<Fig. S2-1>

- 2-2. The chemical potential of atoms at the contact region with a sharp circular shape is the highest and material transport from this region to other spherical surface region occurs. The pressure difference between the two regions is:

$$\Delta P = P_r - P_a = \gamma_s(1/r - 1/x + 2/a),$$

where r and x are the radii of curvature at the sharp circular region.

The final shape is one sphere. The change in shape of the pore will be similar to that of two glass spheres in Fig. S2-1(a), although the mechanisms of shape change are different from each other. The mechanisms that can be operative for the material transport for pore shape change are surface diffusion, evaporation/condensation (or gas diffusion) and lattice diffusion.

- 2-3. The evaporation/condensation mechanism adopts the Langmuir adsorption equation. Therefore, the deposition of material on the neck governs the neck growth kinetics, which is proportional to the difference in vapor pressure between the rounded surface and the neck,
- 2-4. If $\gamma/r > \sigma_y$, plastic deformation is possible during sintering. The yield stress $\sigma_y \sim 2Gb/l$, where l is the length of stressed region ($\sim r$), G is the shear modulus, and b the Burgers vector. Plastic deformation is then possible when $\gamma > 2Gb$. For a crystalline material at its usual sintering temperature, this condition is not satisfied. It is improbable that dislocation generation and plastic deformation occur at the usual sintering temperature of crystalline powder in pressureless sintering.

2-5. For the same degree of densification by lattice diffusion $\propto \frac{D_l}{T} a^{-3} t \approx D_l a^{-3} t$

For the same degree of densification for a given period of sintering time

$$a^3 \propto D_0 \exp\left(-\frac{Q_l}{RT}\right).$$

$$\ln a = \text{const} - \frac{Q_l}{3RT}$$

For 1 μm powder

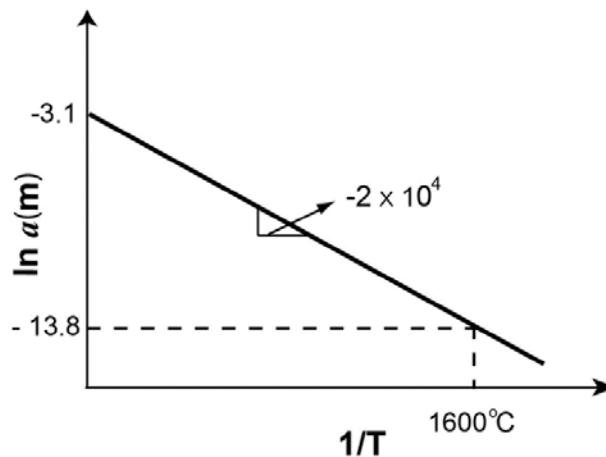
$$-13.8 = \text{const} - 10.7$$

$$\therefore \text{const} = -3.1$$

The equation is

$$\ln a \approx -3.1 - \frac{2 \times 10^4}{T}$$

The plot is then as shown in Fig. S2-5.



<Fig. S2-5>

2-6. $\Delta l/l = h/a = 3\gamma_{st}/8\eta a$ (Eq.1)

$$1/\eta \approx (1/\eta_0)\exp(-Q/RT) \quad (\text{Eq.2})$$

Insertion of data in (Eq.1) gives $\eta = 1.8 \times 10^9 \text{ Pa}\cdot\text{s}$ at 627°C (900 K) and $9 \times 10^7 \text{ Pa}\cdot\text{s}$ at 677°C (950 K).

Insertion of the viscosity data in (Eq.2) gives $Q = 426 \text{ kJ}$

2-7. Bonding and neck growth occur between the two particles. As the melting temperature of Ag is lower than that of Cu, diffusion of Ag towards the neck is expected to be faster than that of Cu. An Ag-rich solid solution forms in the neck.

Cf: Kuczynski GC, et al., *Acta Metall.*, 3, 209-15 (1960).

2-8. In this problem, it is assumed that the evaporated material does not disperse to the wall of the container. (This assumption is also applied to the problems related to gas phase transport of material, such as Problems 2-9 and 2-10.) Note that in reality, this assumption is not valid for model experiments.

Assume that evaporation/condensation is the dominant mechanism. Atoms evaporated from the particle with radius r_2 condensate uniformly on the surface of the particles with radius r_1 , if evaporation/condensation is the only mechanism. Since the gap between the two large particles is very small, the two particles come in contact with a size increase and

form a neck and a grain boundary. Material transport will further occur from the sphere surface to the neck that is formed. The final shape would be that of two identical spheres in contact, which satisfy the dihedral angle condition, unless there is a perturbation in the system. (See Fig. S2-1(b).) (In reality, as the stability of the two identical particles is low, the final shape can be one single sphere.)

If gas diffusion is the dominant mechanism, the growth of particle A will be faster than that of particle B. The spherical shape of particles would not be maintained during their growth. Uneven diffusion flux can affect the growth shape. With disappearance of the particle with radius r_2 , the two particles with radius r_1 come in contact, but the size of particle A must be larger than that of particle B. Atom transport occurs from particle B to A via gas diffusion, and finally particle B disappears and only particle A remains.

- 2-9. (i) $D_g = \lambda \bar{c}/3$, where λ is the mean free path of gas atoms, which is proportional to the temperature and inversely proportional to the gas pressure, and $\bar{c} = (8RT/\pi M)^{1/2}$ their mean velocity. Here, M is the molar weight of atoms.

From Eq. (4.25) in the book “Sintering”, $x^5 \propto (1/RT)^{1/2}t$.

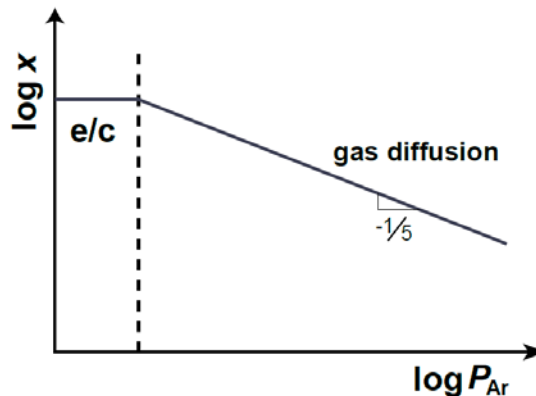
\therefore For constant x , $t \propto T^{1/2}$.

In gas diffusion, if the gas pressure is given by the vapor pressure, the neck growth rate is expected to decrease with increasing temperature. However, if the gas pressure is constant, the neck growth rate is expected to increase with increasing temperature. (See the case of evaporation/condensation.)

- (ii) From Eq. (4.24) in the book “Sintering” $P_\infty (1/T)^{3/2}t$ is constant. $t \propto \exp(-\Delta H_v/RT) \cdot T^{3/2}$, where ΔH_v is the heat of vaporization (vaporization enthalpy). In evaporation/condensation, the sintering time decreases considerably with increasing temperature as the exponential dependence of temperature is dominant.

- 2-10. (a) From Eq. (4.23) $dx/dt \propto \exp(-1/T)(1/T)^{3/2}$. In this expression, the term $(1/T)^{3/2}$ can be neglected. When we plot $\ln(dx/dt)$ vs $\ln(1/T)$, the slope is $-\Delta H_v/R$, where ΔH_v is the vaporization enthalpy.

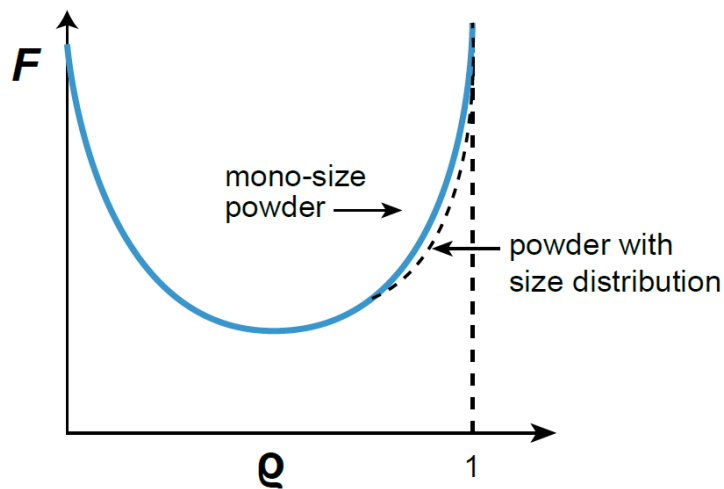
- (b) For the range where evaporation/condensation governs the neck growth kinetics, the neck size is independent of Ar pressure. As the Ar gas pressure increases, the mechanism should change from evaporation/condensation to gas diffusion. In the region where diffusion of gas controls the kinetics, $x^5 \propto D_g$, and hence the slope in a plot of $\log x$ vs $\log P_{Ar}$ will be $-1/5$. As an external hydrostatic pressure does not affect the driving force for neck growth in a compact with open pores, a high Ar pressure only reduces the kinetics of gas diffusion. Figure S2-10 plots the expected variation of x with P_{Ar} .



<Fig. S2-10>

- 2-11. As the particle size decreases, the surface to volume ratio increases. Therefore, the contribution of surface and grain boundary diffusion relative to lattice diffusion becomes more important. The same conclusion can be drawn from the comparison of the scale exponents in Herring's scaling law.
- 2-12. The scaling law is for powders of the same material and with similar shapes, but with different sizes. This law predicts the relative periods of sintering time required to obtain the same degree of sintering of the powders under the assumptions that the same experimental conditions are provided and the same sintering mechanism is operative. The required sintering times t_1 and t_2 for two different systems are interrelated as Eq. (4.26).
- 2-13. (a) $m \propto \Delta p$ (The weight is simply proportional to the vapor pressure.)
 (b) $V/JAV_m = (\text{area})(\text{deposition height})/(\text{driving force})(\text{area})V_m$
 $= (\text{constant})L/(1/L)(\text{constant})V_m \propto L^2$
 The neck area does not affect the kinetics because atom flux can come uniformly on the neck surface, irrespective of its area.
 Simple consideration of the system for the evaporation/condensation mechanism also allows us to obtain the scale exponent α of 2. The mass of material deposited on the neck is proportional to the material's vapor pressure (as in (a)), which is inversely proportional to the particle size, and the time needed to obtain a similar change in deposition height is also inversely proportional to the particle size.
- 2-14. In Eq. (4.27) ($t = V/JAV_m$), A is expressed as $L\delta_b$, where δ_b , the diffusion thickness of the grain boundary, is constant.
 Without high external pressure: $t = L^3/(D_b/RT)((\gamma/L) \cdot 1/L)L \delta_b \cdot V_m \propto L^4$
 With high external pressure: $t = L^3/(D_b/RT)((P_{ext} + \gamma/L) \cdot 1/L)L \delta_b \cdot V_m \propto L^3$
- 2-15. Stress is propagated everywhere in the volume element. The pressure difference between the neck and the surface induces uniform flow of material. Therefore, no scale is incorporated in matter transport except the driving force.
- 2-16. With an increase in x , as the driving force becomes smaller than that estimated from the initial geometry, the exponent n becomes larger. Consider a plot of $\log(x/a)$ vs. $\log t$
- 2-17. For a given particle size, the contribution of lattice diffusion relative to grain-boundary and surface diffusion increases with increasing temperature. The deviation in the figure is due to a change in the dominant mechanism of sintering, from grain boundary and surface diffusion to lattice diffusion with increasing temperature. The increase in the deviation temperature with decreasing particle size also supports this conclusion.
- 2-18. As temperature increases, the densification kinetics increases. The reduction of void area (densification) increases with a temperature increase at the early stage of sintering, up to a few tens of hours. With increasing temperature, grain growth kinetics also increases. During grain growth, pores can be entrapped within grains and the entrapped pores are stable and do not shrink. Densification stops with pore entrapment. As the pore entrapment is enhanced with increasing temperature, the limit of densification appears at earlier sintering time at higher temperature.

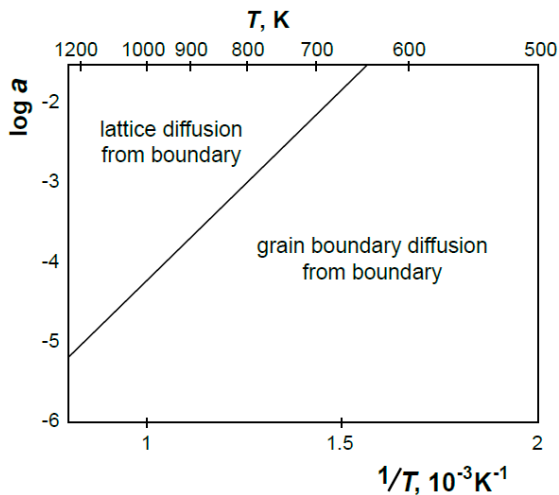
- 2-19. (a) Below 1400 °C, interconnected pores are present in the sample. HIP has no effect on the shrinkage of interconnected pores. At 1400 °C, where all the pores are isolated and located mostly at grain boundary, full densification can be achieved by HIP. Above 1400 °C, some of the isolated pores are entrapped within grains. HIP has practically no effect on the shrinkage of those entrapped pores.
- (b) During HIP, isolated pores shrink and disappear. According to the figure, a small fraction, less than 0.5%, of interconnected pores are isolated during HIP. Within those isolated pores, the gas used for HIP, which has a very high pressure, is entrapped. During annealing, the volume of those pores will increase dramatically. Bloating and cracking of the sample will result.
- 2-20. (a) The driving forces for densification and grain growth are different. The driving force for densification comes from the capillary pressure of pores while that for grain growth from capillary pressure between adjacent grains, which is caused by the curvature of the grain boundary (a difference in their size).
- (b) The mechanisms of densification for a crystalline material are grain boundary diffusion from grain boundaries to pores and lattice diffusion from grain boundaries to pores. The two mechanisms are operative in parallel.
- 2-21. Application of hydrostatic pressure does not affect the densification of an openly porous powder compact. At a very high external hydrostatic pressure, the activation volume for lattice diffusion is slightly reduced and lattice diffusion can also be slightly reduced. The effect, however, is negligible.
- 2-22. An external gas pressure increases the sintering pressure (driving force for densification) for a compact with isolated pores. In addition, the pressurized gas in the atmosphere suppresses volatilization of the material by decreasing the mean free path of gas atoms. The material loss due to its volatilization is reduced.
- 2-23. (i) In a sample with close-packed mono-size particles, no grain growth (or negligible grain growth) is assumed to occur. At the initial stage, the driving force is high, but decreases with neck growth. As the sintering proceeds, however, the driving force increases with pore size reduction and it increases considerably at final stage sintering, as shown in the schematic curve in Fig. S2-23.
- (ii) In a sample with a particle size distribution but with the same average pore size as that of a mono-size powder compact, grain growth can take place considerably at final stage sintering. At initial and intermediate stage sintering, where grain growth is negligible, the driving force would be similar to that of a mono-size powder compact. At the final stage with grain growth, however, the size of pores can increase due to pore coalescence and will be much larger than that in the mono-size powder compact. The driving force then becomes smaller than that in the mono-size powder sample. The schematic variation of the driving force can be that shown in Fig. S2-23.
- 2-24. As the sintering time and neck size increase, the contribution of lattice diffusion relative to surface diffusion increases. Compare Eq. (4.14) in the book "Sintering" for lattice diffusion and Eq. (4.20) for surface diffusion. Consider $\log(x/a)$ vs. $\log t$.



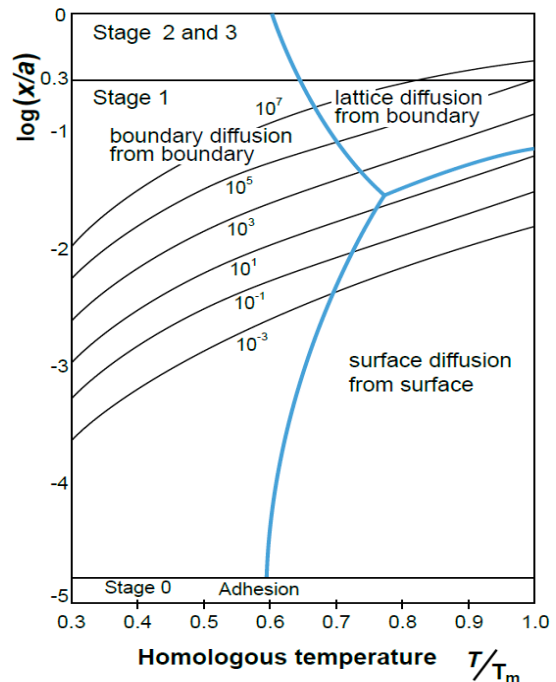
<Fig. S2-23>

2-25.

(a)



(b)



<Fig. S2-25>

2-26. No. In materials science and engineering, the term “driving force” has often been used with two different meanings, one for phenomena and one for kinetics. The driving force of sintering, which is described in section 1.3 in the book “Sintering” and also explained in solution 1-1 (S1-1), is an example of the former meaning. In this case, the driving force is the difference in (free) energy between the initial and the final state. The driving force of grain growth, on the other hand, is an example of the latter, which is the gradient of energy (thermodynamic force). (See Chap. 6 of the book “Sintering”.) In this regard, it may be worth to differentiate these two different meanings of “driving force”, the driving force of a phenomenon (may be called the thermodynamic driving force) and the driving force of kinetics (may be called the kinetic driving force). The kinetic driving force of densification is the gradient of the product of the capillary pressure of the pore

(or the variation of the total interfacial energy with respect to volume change (sintering pressure)) and the molar volume of the material, and can be understood as the capillary energy gradient.

- 2-27. Because of grain growth and local densification in the powder compact. When grain growth takes place, the pore size can change due to pore coalescence and pores can be entrapped within growing grains.
- 2-28. At the final stage of sintering, densification and grain growth interact with each other. The scale exponent of densification is, in general, not the same as that of grain growth.
- 2-29. Coble's final stage model adopts the concentric lattice diffusion assumption, where the material source for densification is considered to be the bulk material. On the other hand, Kang and Jung's model adopts the concept of the initial stage model. It considers the grain boundary to be the only atom source, and the surface area or grain boundary length on the pore to be the diffusional area of the atom sink. As densification is possible only when the material comes from the grain boundary, Kang and Jung's model appears to be appropriate to adequately describe the densification at the final stage.
- 2-30. – The contribution of grain boundary diffusion relative to lattice diffusion increases with decreasing pore size. (Note that the ratio of grain boundary length on the pore surface to pore area (L/A) increases as L decreases.)
 – For a system with negligible grain growth, it is possible to predict the pore size effect on the relative contribution following a similar derivation to that of the scaling law. The contribution of grain boundary diffusion relative to lattice diffusion is inversely proportional to the pore size. (According to the kinetic equations at the final stage of sintering, $J_{Db}/J_{Dl} \propto G^3/G^4 = 1/G$.)
- 2-31. $(d\rho/dt)_l \propto D_l \cdot a^{-3}$ and $(d\rho/dt)_b \propto D_b \cdot a^{-4}$.
 (a) The activation energy of lattice diffusion is, in general, larger than that of grain boundary diffusion. Therefore, as temperature increases, the contribution of D_l relative to D_b increases. (Consider a $\log D$ vs. $1/T$ plot.)
 (b) As the particle size decreases, the boundary area per unit volume increases in proportion. Therefore, the contribution of D_b relative to D_l increases with a reduction of particle size. $((d\rho/dt)_l/(d\rho/dt)_b \propto a)$. (Cf: P2-11.)
- 2-32. A change in the densification mechanism from lattice to grain boundary diffusion occurs with decreasing particle size (see S2-31). The activation energy obtained for the fine powder compact is lower than that obtained for the coarse powder compact.
- 2-33. With pore shrinkage, the reduction in pore surface area, which is proportional to the square of pore size, is more pronounced than the reduction in the length of the grain boundary on the pore, which is linearly proportional to the pore size. $((dV_p/dt)_l/(dV_p/dt)_b \propto (D_l/D_b)r)$. The sintering mechanism can change from lattice diffusion to grain boundary diffusion. As the pore size reduces considerably, grain growth is enhanced. Pore coalescence can occur considerably and pore size can increase during extended sintering for final densification although the sintered density increases with sintering time. Then, the contribution of D_l relative to D_b increases. At this stage, the contribution of D_l can be larger than that of D_b .

- 2-34. (i) Application of an external pressure means an increase in driving force of densification. (Note that the mobility of atoms is unchanged.) As the capillary pressure of pores of a 4 μm size is 7 atm, we need to apply 133 atm in order to increase the kinetics by 20 times. As the pore size decreases with densification, however, the pressure needed has to increase according to an increase of the capillary pressure of the pores. The effect of an external pressure relative to that of the capillary pressure of pores is dependent on the pore size, in contrast to the effect of temperature.
- (ii) Increase of sintering temperature means an increase of atom mobility, i.e. atom diffusivity. Using Eq. (5.10) we can estimate the sintering temperature for the enhancement of densification kinetics by 20 times. As the exponential dependence of temperature is much more pronounced than its linear dependence, we may neglect T in Eq. (5.10). Then,
- $$20 = \exp(-418000/8.3T)/\exp(-418000/(8.3 \times 1673))$$
- $$\therefore T = 1585^\circ\text{C}.$$
- 2-35. (i) $d\rho/dt = JAV_m = (D/RT)(\nabla\sigma)AV_m \propto (1/r)4\pi r^2 \propto r$. According to this equation, the densification rate decreases with shrinkage of pores.
- (ii) Pore size can increase due to pore coalescence as a result of grain growth. The number of pores and the driving force for their shrinkage can decrease.
- (iii) Pores are prone to be entrapped within grains with densification. Entrapped pores are stable and do not shrink.
- 2-36. If grain growth does not take place, the answer is Yes. If pore coalescence takes place as a result of grain growth, the answer is No.
- 2-37. (a) Densification at the initial and intermediate stage, where the pores are mostly interconnected to the surface (open pores), the sintering atmosphere does not affect densification. At the beginning of the final stage, where the pores are isolated, the capillary pressure of pores can be much higher than the pressure of the entrapped insoluble gas, Ar. The shrinkage of pores will be largely governed by the capillary pressure of pores until the pressure of entrapped gases becomes significant with the shrinkage of pores.
- (b) The grain size in the O_2 -sintered sample is expected to be larger than that in the Ar-sintered sample because of less drag of pores due to higher densification without any entrapped gas effect.
- (c) Entrapment of almost all the pores within growing grains.
- (d) Reduction of capillary pressure of pores due to pore coalescence, which is a result of grain growth.
- (e) Yes. Figure 5.5 in the book "Sintering" can be utilized to estimate the increase in pore volume with pore coalescence.
- (f) - Selection of a sintering atmosphere that does not contain insoluble gases.
 - Eliminate insoluble gases that can be generated during sintering by reactions between the powder and atmosphere before pore isolation.
 - Suppression of grain growth in order to avoid pore entrapment within grains.
- Cf: - Paek YK, et al., *J. Am. Ceram. Soc.*, 71, C380-82 (1988).
 - Kang SJL, Yoon KJ, *J. Eur. Ceram. Soc.*, 5, 135-39 (1989)
 - Kang SJL, *Materials*, 13, 3579 (2020)

2-38. This question is about dedensification that is due to grain growth in the sample with entrapped insoluble gases. As the grain size is doubled, eight pores coalesce to one. As the amount of gas is invariable, $PV = \text{constant}$. From this condition, we obtain the radius of a pore after coalescence of eight initial pores to be $\sqrt{8}$ times the initial pore radius. Therefore, the pore volume after coalescence is the $\sqrt{8}$ times the initial volume, i.e. $2\sqrt{8}\%$. A considerable dedensification can result from grain growth.

$$P_1 V_1 = 8 \times (4/3)\pi r_1^3 \times (2\gamma/r_1) = P_2 V_2 = (4/3)\pi r_2^3 \times (2\gamma/r_2) \quad \therefore r_2 = \sqrt{8}r_1$$

$$(4/3)\pi r_2^3 = 8\sqrt{8}\pi r_1^3 \quad \text{A volume increase by } \sqrt{8} \text{ times.}$$

2-39. As the dihedral angle decreases, the radius of curvature of the pore increases and the capillary pressure decreases. Therefore, a reduction in the dihedral angle results in a reduction in densification kinetics and limiting density. A quantitative calculation can be made as in reference 40 in Part II (Kang SJL, Yoon KJ, *J. Eur. Ceram. Soc.*, 5, 135-39 (1989)). A reduction of dihedral angle in a system with a constant γ_s means an increase of γ_b , implying a reduction of the driving force for densification. (Consider the meaning of surface and grain boundary energy in sintering, as discussed in Solution 1-1 (S1-1).)

2-40. As the number of pores per grain is assumed to be constant, an increase in grain size by S times corresponds to an increase in pore size by S times.

$$P_f r_f^3 = P_i (S r_i)^3 \quad \text{and} \quad P_i [(S r_i / r_f)^3 - 1] = 2\gamma_s / r_f$$

Scaling of the abscissa in Figure 5.5 by $S r_i$ should permit an estimation of the effect of grain growth.

2-41. From the assumption $(\dot{\rho}_h / \rho_h) = (\dot{\rho}_l / \rho_l)$, $\dot{\rho}_h = (\rho_h / \rho_l) \dot{\rho}_l$.

Since $\rho_h / \rho_l > 1$, the situation becomes worse as sintering proceeds. Flaws can form between the two kinds of agglomerates with high and low relative densities. In real sintering, there can be interactions between the two, and the situation may not be as bad as the assumed system.

2-42. Causes of pore opening: (i) locally enhanced densification due to non-uniform packing of particles, (ii) agglomerates with different densities, (iii) non-uniform growth of particles

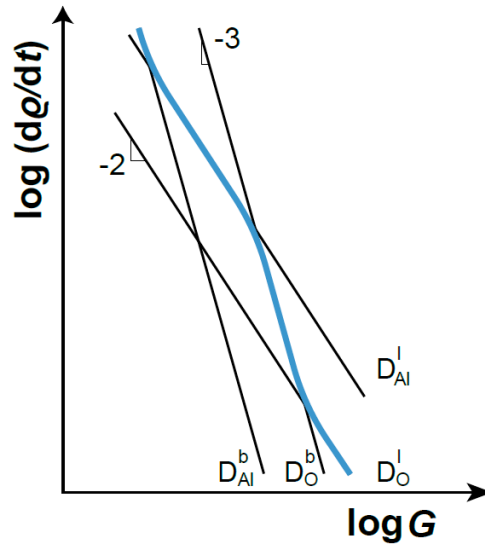
Possible measures: (i) use of powders with a narrow size distribution, or inversely use of powders with bi-modal or multi-modal distribution (ii) disintegration of hard agglomerates (use of softly agglomerated powder), (iii) application of an external pressure, such as in hot pressing.

2-43. (a) Nabarro-Herring creep occurs with transport of atoms via lattice diffusion and Coble creep via grain boundary diffusion. As temperature increases, the contribution of lattice diffusion relative to grain boundary diffusion increases. The answer is No.

(b) $t = V / J A V_m = L^3 / (D_l / RT) (P_{ext} + 2\gamma / r) (1/L) L^2 V_m \propto L^2$ for lattice diffusion.

$t \propto L^3$ for grain boundary diffusion. (Cf: P2-14.)

(c) $D_l: (d\rho/dt)_l \propto 1/G^2$. $D_b: (d\rho/dt)_b \propto 1/G^3$ in hot pressing. Plot $\log(\text{rate})$ vs. $\log G$ for the cases of boundary diffusion and lattice diffusion of Al and O, respectively. This can be schematically drawn as given in Fig. S2-43. As the slow moving species between Al and O controls the overall kinetics, the apparent densification rate is given by the thick blue line in the figure.



<Fig. S2-43>

2-44. Lattice diffusion

$$\text{With } 8\sqrt{2}l^3 = (\pi/6)G^3 \text{ and } 6\left(\frac{4}{3}\pi r^3\right) = (1-\rho)\frac{\pi}{6}G^3,$$

$$\begin{aligned} \frac{d\rho}{dt} &= -\frac{dV_p}{dt}/V_t = \frac{24}{4} \frac{D_l}{RT} P_{appl.} \frac{2}{l} 4\pi r^2 V_m / \frac{1}{6} \pi G^3 \\ &= 288 \frac{D_l V_m}{RTG^3} P_{appl.} \frac{r^2}{l} \\ &= 61 \frac{D_l V_m P_{appl.}}{RTG^2} (1-\rho)^{2/3} \end{aligned}$$

Grain Boundary Diffusion

$$\begin{aligned} \frac{d\rho}{dt} &= -\frac{dV_p}{dt}/V_t = \frac{24}{4} \frac{D_b}{RT} P_{appl.} \frac{2}{l} \frac{11}{6} \pi \delta_b r V_m / \frac{1}{6} \pi G^3 \\ &= 132 \frac{D_b \delta_b V_m}{RTG^3} P_{appl.} \frac{r}{l} \\ &= 101 \frac{D_b \delta_b V_m P_{appl.}}{RTG^3} (1-\rho)^{1/3} \end{aligned}$$

- 2-45. (i) Use of packing powder of a similar composition to that of the compact. Powder packing suppresses volatilization of the material.
- (ii) Application of external pressure. External pressure enhances densification. The techniques include gas pressure sintering, hot pressing and sinter+HIP. N₂ gas pressure sintering after pore isolation has an additional effect of suppressing volatilization.
- (iii) Application of electric field (current). An example is spark plasma sintering with an external pressure. Fast heating in field(current)-assisted sintering enhances densification while minimizing grain growth.
- (iv) Adoption of liquid phase sintering. Chemistry change and the presence of a liquid can enhance densification and suppress volatilization.

- 2-46. For a system with faceted boundaries and surfaces, recent studies suggest that there is a critical driving force for atom detachment from faceted boundaries or attachment on faceted pore surfaces. If the driving force for densification is below the critical driving force, essentially no densification can result. For a rounded boundary (surface), the kinetics is expected to be always linearly proportional to the driving force for densification. For a very fine powder with a high driving force for densification, the densification kinetics can be the same for both powders with a faceted and rounded boundary (surface). For a coarse powder with a moderate driving force, densification can be limited in the compact with a faceted boundary (surface).
 Cf: - Choi SY, Kang SJL, *Acta Mater.*, 52, 2937-43 (2004)
 - Lee MG, et al., *Acta Mater.*, 59, 692-98 (2011).
 - Dillon SJ, et al., *Acta Mater.*, 242, 118448 (2023).
- 2-47. Any pore in a glass is not stable if insoluble gases are not entrapped within the pore. According to Kingery and Francois, and Lange and Kellett (Lange FF, Kellett B, "Influence of particle arrangement on sintering", in *Science of Ceramic Chemical Processing*, L. L. Hench and D. R. Ulrich (eds), Wiley, New York, 561-74 (1986)) pores in a polycrystal can be stable (metastable). The size of metastable pore decreases with reduction of the dihedral angle.
- 2-48. (i) Reduction of particle size. The driving force for densification is inversely proportional to the particle size.
 (ii) Modification of particle size distribution for good packing. Packing is a critical factor for homogeneous densification of a compact.
 (iii) Application of an external pressure. An external pressure is an additional densification pressure to the capillary pressure of pores.
 (iv) Suppression of grain growth via modification of the thermal cycle, changing the sintering atmosphere, or adding dopants. With grain growth, in general, the driving force for densification decreases due to pore coalescence, and the tendency of pore entrapment increases.
 (v) Change in atmosphere or adding dopants to decrease the surface/boundary energy anisotropy, or to increase γ_s and decrease γ_b .

II-2. Liquid phase sintering

- 2L-1. (a) From Eq. (14.1) in the book "Sintering",

$$F = \gamma_l[\pi a^2 \sin^2 \psi (1/r - 1/a) + 2\pi a \sin^2 \psi] \propto a$$
- (b) If we assume that a thin liquid film transmits pressure between particles, as in Kingery's liquid phase sintering model (Kingery WD, *J. Appl. Phys.* 30, 301-306 (1959)), the pressure between particles $\propto F/a^2 \propto 1/L$
 From the scaling law,

$$t = V/JAV_m = L^3/(D/RT)(F/a^2)(1/L)L\delta_b V_m \propto L^4$$

$$\therefore d\rho/dt \propto 1/L^4$$
- This dependence of the densification rate on particle size is the same as that in Eq. (16.4), Kingery's contact flattening equation, which was indeed deduced from the compressive pressure between two particles.
 Note that the functional form of Eq. (16.4) in the book "Sintering" is the same as that of Eq.(4.17) for grain boundary diffusion in solid state sintering.

2L-2. (a) $F = \gamma_1[\pi a^2(1/r_2 - 1/r_1) + 2\pi a \cdot \cos\alpha] \propto a$

(b) Since $V_1 \propto a^3$, $F \propto V_1^{1/3}$

This result is opposite to the case of spherical particles, where F decreases with increasing the liquid volume fraction. (See Fig. 14.3.)

2L-3. (i) Fully dense sample: The shape of grains in the bulk is that of an equilibrium shape with the minimum interfacial energy for a given liquid volume fraction. (Refer to Fig. 3.13 in the book “Sintering”.) The shape of grains at the surface of the sample corresponds with that of grains in the bulk with a cutting plane.

(ii) Sample with big/small pores: The shape of grains in the bulk is similar to that in a fully dense sample, if the pore volume fraction is not very high. The shape of grains around a pore has a solid surface with part of the shape of the pore.

In summary, the shape of grains in the bulk is essentially the same irrespective of the presence of pores. The surface shape of grains towards a vapor phase is governed by the curvature radius of the pore, an infinite size (sample surface) and a finite size (pore). The surface is, in fact, a pore of an infinite size.

Cf: - Park HH, et al., *Metall. Trans. A*, 17A, 325-30 (1986).

- Kang SJL, “Liquid phase sintering: Fundamentals” in “*Encyclopedia of Materials: Technical Ceramics and Glasses*,” A. Leriche and F. Cambier (eds), Elsevier (2020).

2L-4. Contact Flattening Model

Densification occurs via material transport from the contact area to the surface of the neck. The driving force for this process is considered to be a compressive pressure exerted at the contact area. A thin liquid film was assumed to transmit the compressive pressure between particles. In principle, however, this pressure would usually not be present in the compact because the grains are mostly immersed in a liquid with a hydrostatic pressure. (This is a question of attaining an equilibrium shape of grains in a solid-liquid two-phase system. (See the solution of 2L-3 (S2L-3).) The result of contact flattening must be a continuous shrinkage of pores until their complete elimination. In terms of the pore size distribution, the maximum size of pores decreases continuously with densification. Such a change in the pore size distribution has hardly been observed in real systems. In this model, grain shape accommodation for densification is achieved only by atom transport from the contact area to pore surface, similar to the two particle model of solid state sintering.

Pore Filling Model

Densification occurs via liquid filling of pores when the liquid completely wets the pore surface with grain growth. The result of this process is an instantaneous disappearance of pores by liquid filling in temporal sequence: small pores earlier and large pores later. In terms of pore size distribution, the maximum pore size should not change during densification and small pores disappear with densification. This expected change in the pore size distribution is in agreement with experimental observations. In this model, densification is achieved by bulk flow of material (liquid) and shrinkage by shape change of grains around the liquid-filled pores during their growth and microstructural homogenization.

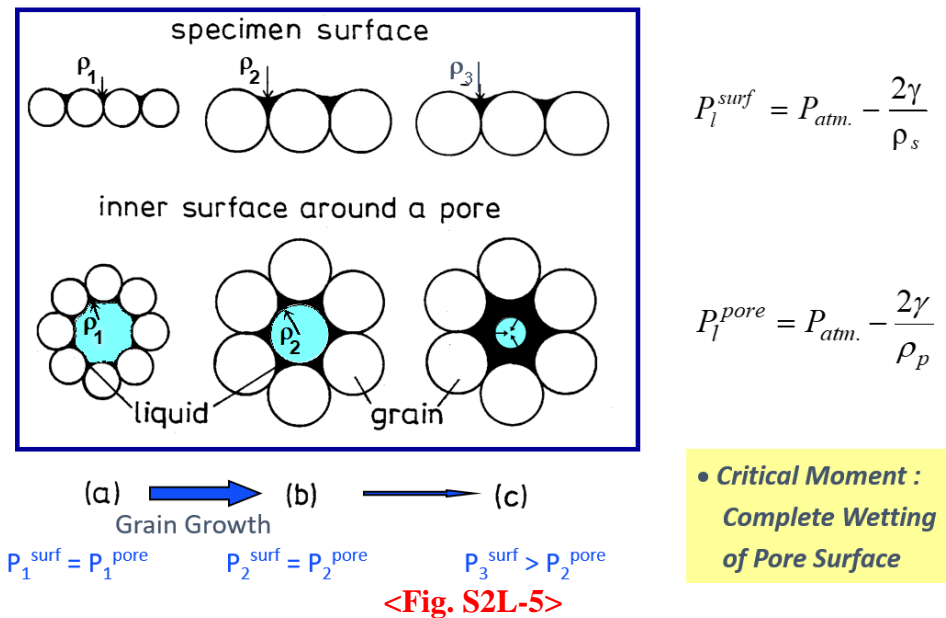
Unlike the contact flattening model, the pore filling model describes that densification is achieved by pore filling as a result of grain growth, while shrinkage occurs as a result of microstructural homogenization after pore filling.

Cf: - Kang SJL, et al., *J. Am. Ceram. Soc.*, 74, 425-427 (1991).

- Lee SM, Kang SJL, *Acta Mater.*, 46, 3191-202 (1998).
- Lee SM, Kang SJL, *Z. Metallkd.*, 92, 669-74 (2001).

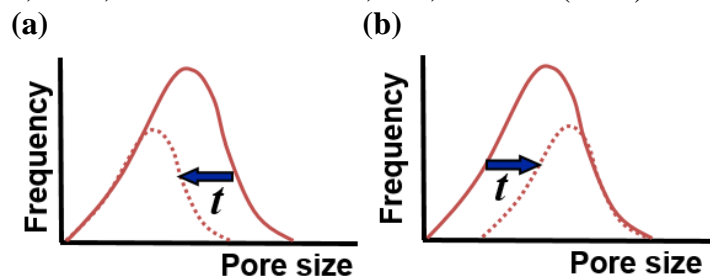
2L-5. When the surface of a pore is wetted by liquid, a pressure difference in the liquid arises between in the region around the pore and at the sample surface, including the intact pore surface, at the moment of wetting (for wetting angle $> 0^\circ$) or with further growth of grains (for wetting angle $= 0^\circ$). Liquid will then flow into the wetted pore. The driving force for pore filling is a pressure imbalance in the liquid. Figure S2L-5 illustrates the pore filling mechanism for the case with wetting angle of 0 degrees. (a) before pore filling, (b) complete wetting of pore surface (critical moment for pore filling), and (c) liquid flow into the pore right after the critical moment.). P is the pore and ρ is the curvature radius of liquid meniscus. (Kang SJL et al., *J. Am. Ceram. Soc.*, 72, 1166-69 (1989).)

Cf: Park HH, et al., *Metall. Trans. A*, 17A, 1915-19 (1986)



2L-6. In Kingery's model, as the size of all the pores decreases continuously with the transport of atoms from the contact area to the pore surface, the maximum size of pores should decrease with increasing the sintering time, as schematically shown in Fig. S2L-6(a). In the pore filling model, as the pores are filled with liquid in temporal sequence, small pores earlier and large pores later, the largest pore is intact until complete densification, as schematically shown in Fig. S2L-6(b).

Cf: - Kang SJL, "Sintering" (Chap. 6) in "*Ceramics Science and Technology*," R. Riedel and I.W. Chen (eds), Weinheim: Wiley-VCH Verlag & Co. KGaA, 141-69 (2012).
 - Bordia RK, et al., *J. Am. Ceram. Soc.*, 100, 2314-52 (2017)



2L-7. Grain Growth

- A change in wetting angle would not have any effect on grain growth because the shape of grains in a liquid is unaffected by the wetting angle.
- A change in dihedral angle, however, would affect the grain growth kinetics because the shape of grains changes with the dihedral angle. As the dihedral angle increases, the curvature radius of the solid/liquid interface increases and the maximum distance between grains increases. The grain growth rate would then decrease. This expectation, however, has not yet been theoretically supported.

Densification

- An increase in the wetting angle retards complete wetting of the pore surface for pore filling and hence densification. The effect of the wetting angle is more pronounced than that of the dihedral angle.
 - An increase in the dihedral angle increases the radius of the liquid meniscus for a given liquid volume fraction and thus enhances the pore filling and densification. However, the grain growth rate may decrease with an increase of the dihedral angle, as explained above, which retards the densification. This negative effect might not be very significant. Densification would be enhanced as the dihedral angle increases. The effect of the wetting angle was predicted to be more pronounced than that of the dihedral angle.
- Cf: - Park HH, et al., *Metall. Trans. A*, 17A, 325-30 (1986).
- Lee SM, Kang SJL, *Acta Mater.*, 46, 3191-202 (1998).
- Lee SM, Kang SJL, *Z. Metallkd.*, 96, 141-47 (2005)

2L-8. As pore filling occurs as a result of grain growth, grain growth kinetics governs the densification. If the grain growth kinetics follows the cubic law, which is valid for normal grain growth in LPS (see the diffusion-controlled LSW theory), the scale effect also follows the cubic law. The scale exponent is 3.

Cf: Lee SM, Kang SJL, *Acta Mater.*, 46, 3191-202 (1998).

2L-9. In liquid phase sintering, liquid can flow and fill the void space (pore filling, densification) with grain growth. Microstructural homogenization and grain shape change around the liquid pocket, which can result in shrinkage, can also occur during grain growth. In solid state sintering, on the other hand, densification occurs only via atom transport from grain boundaries to pores, which is a slow process. Grain growth in a solid-state does not contribute to shape accommodation and densification.

2L-10. (a) $t \propto V/J \propto RT/D \propto \exp(Q/RT)$. Plot $\ln t$ vs. $1/T$, where t is the time required to obtain a fixed relative density. On the plot, the slope is Q/R , where Q is the activation energy.

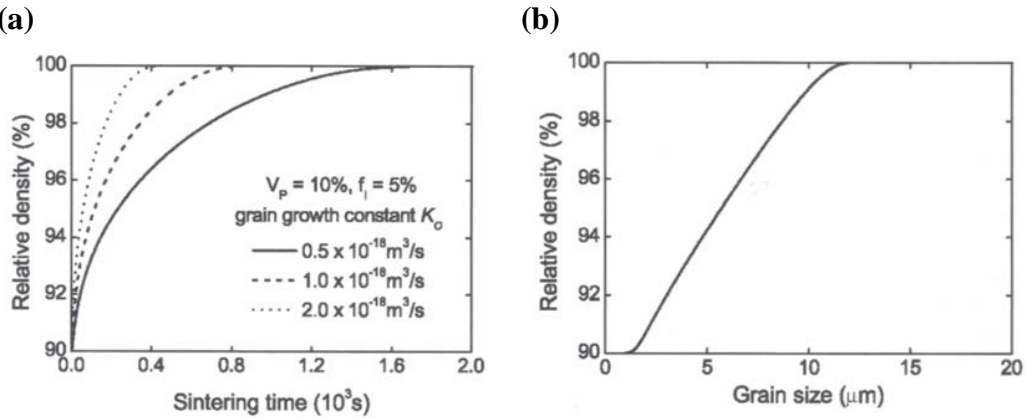
- (b) - Similar microstructural evolution at different temperatures.
- Invariable (insignificantly variable) liquid volume fraction at different temperatures.
 - Single mechanism (essentially diffusion control) of grain growth and densification at different temperatures.

(c) Activation energy of grain growth. (Activation energy of atom diffusion through the matrix.)

2L-11. (a) The equation of normal grain growth during LPS is expressed as $G^3 - G_o^3 = kt$, where G is the average grain size, k the grain growth rate constant, and t the annealing time.

As G is constant for the same degree of densification, $t \propto 1/k$. Schematic densification curves for different k values are shown in Fig. S2L-11(a).

- (b) As the attainable relative density is governed by the average grain size in the pore filling theory, the plot of sintered density vs. average grain size will be independent of the growth rate constant k , as shown in Fig. S2L-11(b) (Lee SM, Kang SJL, Z. Metallkd., 96, 141-47 (2005).)



<Fig. S2L-11>

2L-12. According to the “Pore Filling Theory”, the critical size of pores that can be filled with liquid is proportional to the average grain size. At the beginning of LPS, densification is enhanced in the coarse-grained sample compared with the fine-grained sample because of a larger liquid meniscus radius and hence, larger critical size of pores that can be filled with liquid. However, the size of grains is not large enough to fill the pores that are bigger than the critical sized pore. As grain growth can be stagnant in the coarse grained sample with faceted grains (See S3L-16.), liquid filling of other intact pores is not possible for a long period of sintering time. In contrast, for the fine-grained sample, liquid can fill only small pores at the beginning because of a small liquid meniscus radius. As the liquid meniscus radius can increase with abnormal grain growth (AGG) in the fine-grained sample, pore filling can occur continuously with AGG.

2L-13. When pore filling occurs, the effective volume of liquid in the bulk decreases by the amount of liquid that filled the pore. (Pore filling can be considered as suction of liquid from a dense solid-liquid two phase bulk material.) Because of a reduction of the liquid volume fraction in the bulk, the capillary pressure of liquid increases (more negative) and the grains in the bulk tend to become more anhedral. This grain shape accommodation is achieved mostly by grain growth. Meanwhile, around the liquid pocket that is formed, surrounding grains grow towards the liquid pocket center, leading to microstructural homogenization. Sample shrinkage must occur with grain shape accommodation and microstructural homogenization. As there are many pores in a liquid phase sintering sample, pore filling, grain shape accommodation, and microstructural homogenization do not occur separately, but concomitantly throughout the sample. The variation of grain shape during densification must be negligible in real compacts.

Cf: Kang SJL, et al., *J. Am. Ceram. Soc.*, 74, 425-27 (1991)

The driving force (pressure) for sample shrinkage can be expressed as the variation of the total interfacial energy with respect to the variation of the total volume, $-P = dE/dV_t$.

Cf: Fig. 3.13 in the book “Sintering”.

2L-14. In solid state sintering, the number of small pores is large because all the pores shrink continuously with the transport of atoms from the grain boundary to pore surface. When grain growth, in particular abnormal grain growth, takes place, many small pores can be entrapped within grains.

In liquid phase sintering, small pores are easily eliminated by liquid filling of pores. (Pore filling occurs in temporal sequence: small pores earlier and large pores later.) Entrapment of small pores hardly occurs unless there are insoluble gases in the pore. As a consequence, it is expected that the number of pores is smaller and the average size of pores larger in LPSed sample than those in SSSed sample, if the relative densities and the average grain sizes of both samples are the same.

2L-15. The situation is similar to sintering of a powder compact with a very large pore. Considerable grain growth takes place in three agglomerates before liquid filling of the large pore in the center. Meanwhile, the neck between agglomerates will increase with filling of liquid at the neck and growth of grains into the liquid at the neck. After liquid filling of the large pore, growth of surrounding grains towards the liquid pocket center will take place, leading to microstructural homogenization. With an increasing liquid volume fraction, the kinetics of densification will increase. If the dihedral angle is zero degrees and the liquid volume fraction is large, there can be viscous flow of the solid/liquid mixture into the large pore at the early stage of sintering.

Cf: Kang SJL, et al., *Powder Metall.*, 27, 97-100 (1984).

2L-16. In SSS, the application of external gas pressure is an additional sintering pressure to the capillary pressure of pores in a sample with isolated pores. Atom transport kinetics from the grain boundary to pore surface increases. The order of external gas pressure in gas pressure sintering is, in general, the same as that of capillary pressure. The atom transport kinetics from the grain boundary to pore surface and hence the densification kinetics increases, but the contribution of external pressure is simply relative to capillary pressure.

In LPS, external gas pressure accelerates the wetting of the pore surface and the flow of liquid into pores, and hence can instantaneously increase densification and further promote the wetting of other intact pore surfaces. In LPS, mass flow of liquid leads to densification, while only diffusional atom transport induces densification in SSS. A quantitative analysis of the effect of external gas pressure can be found in a reference. (Lee SM, Kang SJL, *Z. Metallkd.*, 96, 141-47 (2005).)

2L-17. Inhomogeneous mixing of two elemental powders can cause locally enhanced densification during heating, generating pores, and the formation of large natural pores at the sites of agglomerates of low melting point particles after melting. The presence of large pores in a liquid phase sintering compact increases the densification time considerably. According to the pore filling theory, the time period necessary for full densification is, as a first approximation, linearly proportional to the cube of the maximum pore size in the case of diffusion-controlled grain growth.

2L-18. SSS: Densification (shape accommodation of grains for densification) is achieved only by atom transport from the grain boundary to the pore surface.

LPS: Shape accommodation of grains, which is essential for densification, can easily be achieved by grain growth via atom transport through a liquid matrix at the early stage of LPS, unlike the case of SSS. Grain shape accommodation by contact

flattening is inconsiderable. (Contact flattening can be valid only at the early stage LPS and only in samples with a dihedral angle of 0 degrees, but is insignificant in general.) Densification during LPS occurs mostly by liquid filling of pores (pore filling) as a result of grain growth.

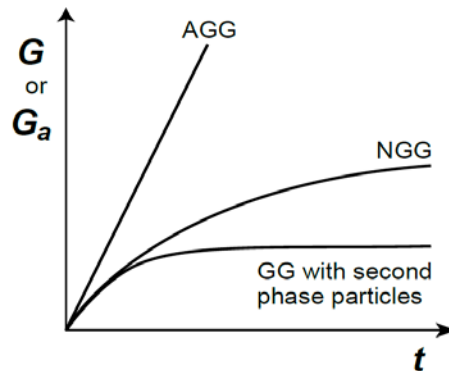
Cf: - Lee SM, Kang SJL, *Z. Metallkd.*, 92, 669-74 (2001).

- Kang SJL, "Liquid phase sintering: Fundamentals" in "*Encyclopedia of Materials: Technical Ceramics and Glasses*," A. Leriche and F. Cambier (eds), Elsevier (2020).

PART III. Grain Growth and Microstructural Evolution

III-1. Solid state sintering

3-1. An explanation can easily be made by considering with Eqs (6.1) – (6.3), Eq. (6.12), and Eqs (9.2) and (9.3) in the book “Sintering”. In NGG, $G \propto t^{1/2}$. In AGG, $G_a \propto t$. In GG with second phase particles, as sintering proceeds, a limiting grain size is exhibited due to the Smith-Zener drag of particles. The variation of grain size with respect to sintering time can be drawn as given in Fig. S3-1 for the three different cases. In this figure, the initial grain size is assumed to be negligible.



<Fig. S3-1>

3-2. $D^2 - D_0^2 = A \cdot \exp(-Q/RT)t$. Insertion of the given data gives $A = 1.00 \times 10^8$ and $Q = 246.6$ kJ. The answer is $19.8 \mu\text{m}$.

3-3. Two single crystalline particles: Increase in contact (grain boundary) area between the two particles until the dihedral condition is satisfied at the neck. This conclusion is for an idealized system with identical particles.

Single-/poly-crystalline particles: Growth of the single-crystalline particle into the polycrystalline particle takes place. The increase in the neck area between the two original particles will occur only via surface diffusion and will be slower than that of two single crystalline particles, where grain boundary and lattice diffusion can also be operative for neck growth. When the single crystal particle scavenges all the grains in the polycrystalline particle, the two particles become a single crystal with a neck. When the particle is annealed for a long time, the neck size increases with atom transport from the spherical surface and eventually becomes a spherical single crystal.

3-4. D_b^\perp : the diffusion coefficient of slowly moving species.

For an M_aX_b compound, if $D_M^\perp \gg D_X^\perp$, $D_b^\perp = (D_X^\perp)^\perp/b$. (See Fig. 13.1 in the book “Sintering”).

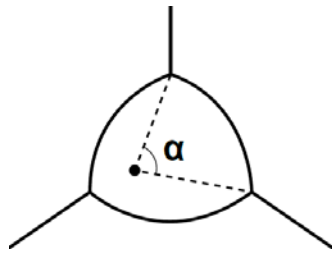
V_m : the molar volume of the compound.

3-5. Diffusional flow of gas across a side of wall (a boundary) $\propto (\gamma_b/R)R \cdot \alpha = \gamma_b \cdot \alpha$, where R is the radius of curvature of the wall (boundary) and α the angle of the wall (Fig. S3-5).

$$\Sigma \alpha_i = 2\pi - (n/3)\pi = \{(6-n)/3\}\pi, \text{ where } n \text{ is the number of walls.}$$

Change in the content of gas due to diffusion = mobility $\times \gamma_b \Sigma \alpha_i$

$$\therefore dA/dt = (\pi M \gamma_b / 3)(n-6)$$

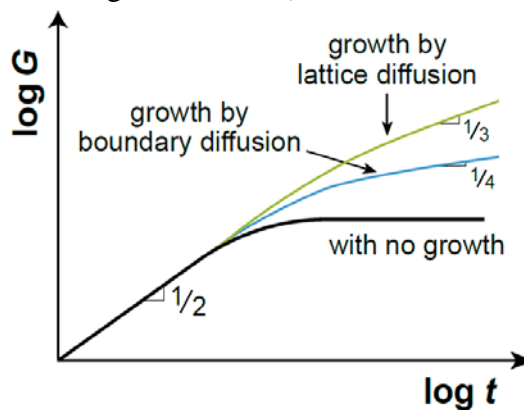


<Fig. S3-5>

3-6. For the derivation of the original equation, it is assumed that all the second phase particles that are attached to the boundary exhibit the maximum drag force. In reality, however, the particles that are attached to but located in front of the moving boundary do not impede the migration but can facilitate (assist) the migration. The particle that is attached to the moving boundary but located behind it exerts a drag force from nearly zero to the maximum drag force of $\pi r \gamma_b$. As there are particles that impede or otherwise assist the boundary migration, the original equation overestimates the drag effect. The functional dependence on particle volume and particle size, however, is correct.

Cf: Manohar PA, et al., *ISIJ Inter.*, 38, 913-24 (1998).

3-7. According to Eq. (6.12) in the book “Sintering”, there is a limiting grain size in a sample that contains second phase particles. As the particle size increases, the limiting grain size increases in proportion. (See Eq. (6.13).) For the growth of second phase particles by lattice and grain boundary diffusion, their size is proportional to $t^{1/3}$ and $t^{1/4}$, respectively. (Consider Ostwald ripening of second phase particles and the scaling law. Also refer to: Martin JW and Doherty RD, *Stability of Microstructure in Metallic Systems*, Cambridge University Press, Cambridge, 236, 1976.)



<Fig. S3-7>

3-8. – Second-phase particles that are uniformly distributed in a matrix suppress grain growth. This effect can be beneficial for densification because the suppression of grain growth reduces pore coalescence and possible pore entrapment within grains. This conclusion should be correct under the assumption that the densification is not affected by the second-phase particles. Few experimental and theoretical studies have been carried out for the effect of small second phase particles on densification, in particular final densification, in contrast to their effect on grain growth, which is well known as the Smith-Zener effect. Apparently, diffusion distance for densification should increase for boundary diffusion and may be unaffected for lattice diffusion. The kinetics of atom detachment from the boundary between grains and particles, and the kinetics of atom

diffusion along the boundary must be different from those in a sample without second phase particles

- For samples with large second phase particles or platelets, it is well documented that overall densification is retarded by the second phase particles.

Cf: Kang SJL, *Sintering: Densification, Grain growth and Microstructure*, Elsevier Butterworth-Heinemann (2005).

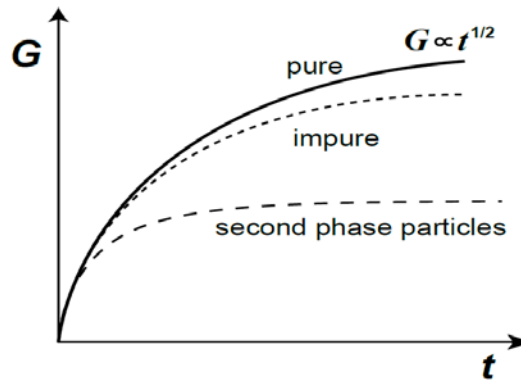
3-9. Elastic strain energy can be expressed as Eq. (7-5), if the solute atom is a hard sphere. Insertion of the data into Eq. (7-5) gives 1.146×10^{-19} Nm(J) per Ca atom and 6.9×10^4 J/mol. The degree of segregation can be estimated by using Eq. (7.7). At 1700 K, for example, the ratio of the Ca to Mg at the boundary is ~ 130 times that in the bulk. This value, however, would be overestimated because of the strain energy caused by the solute segregation at the boundary and the elasticity of atoms.

3-10. Consider a reaction of the solute atom in the lattice (I_l) and the host atom at the boundary (H_b) to make the solute atom at the boundary (I_b) and the host atom in the lattice (H_l). The concentrations are expressed as C , $(1-C_b)$, C_b , and $(1-C)$, respectively. Using the mass action law, one can write the following equation.

$$C_b(1-C) = C(1-C_b)\exp(-\Delta E/RT).$$

Arranging this equation, one can obtain the solute concentration equation at the boundary.

3-11. Grain growth in the pure sample follows the normal grain growth law (parabolic law). Grain growth in the impure sample can follow the normal grain growth law at the beginning with a high driving force, but later deviates from it due to the solute drag effect. Grain growth in the sample with second phase particles deviates from the ideal law from the beginning and later stops.



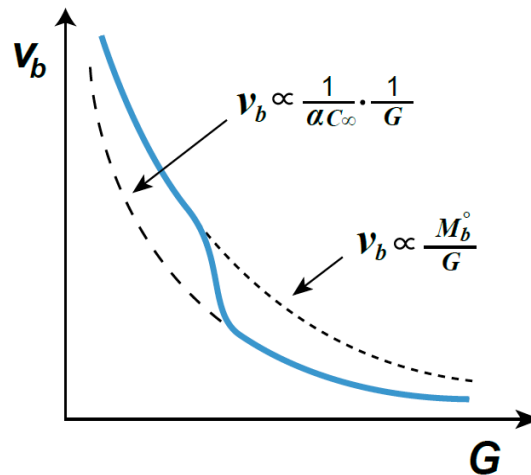
<Fig. S3-11>

3-12. $v_b = M_b F_b \propto M_b / G$. $v_b G = \text{const.}$

For small grains with a high driving force for boundary migration, the drag of solute atoms segregated at the boundary should be insignificant and the boundary velocity can be similar to that of the pure boundary. In this case, the boundary mobility M_b would be the intrinsic mobility of the boundary. As the grain size increases, the driving force for boundary migration decreases and solutes can segregate significantly, and a pronounced drag effect will appear.

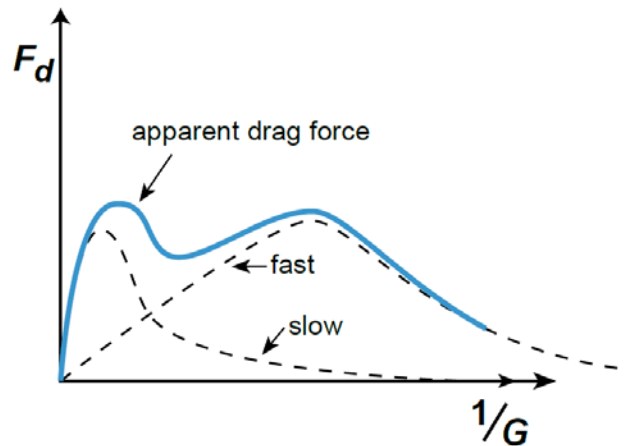
As the driving force for boundary migration is inversely proportional to grain size, the boundary velocity is also inversely proportional to grain size. The effect of grain size on boundary velocity can be drawn schematically, as in Fig. S3-12.

Note that there is a transition in the boundary migration velocity.



<Fig. S3-12>

3-13. The solute drag force varies with the boundary velocity, which is inversely proportional to the grain size ($v_b \propto M_b/G$). When we plot F_d vs $1/G$, the figure will be similar to Fig. 7.1 in the book “Sintering”. As there are two kinds of solutes with low and high drift velocity, two separate curves of drag force will be present, as shown in Fig. S3-13.



<Fig. S3-13>

3-14. (a) Temperature dependence of grain boundary segregation:

From Eq. (7.3)

$$\frac{X_B^b}{1 - X_B^b} = \frac{X_B}{X_A} \exp\left(\frac{-\Delta E}{kT}\right)$$

Taking logarithms,

$$\ln\left(\frac{X_B^b}{1 - X_B^b}\right) \propto \frac{1}{T}$$

\therefore Solute segregation is reduced with a temperature increase, as schematically shown in Fig. S3-14(a).

(b) Grain boundary velocity with temperature:

For a pure material, the grain boundary velocity is proportional to the boundary mobility, as

$$v_b = M_b^0 F_b \propto \exp(-Q_m / RT).$$

Taking logarithms,

$$\ln v_b \propto 1/T$$

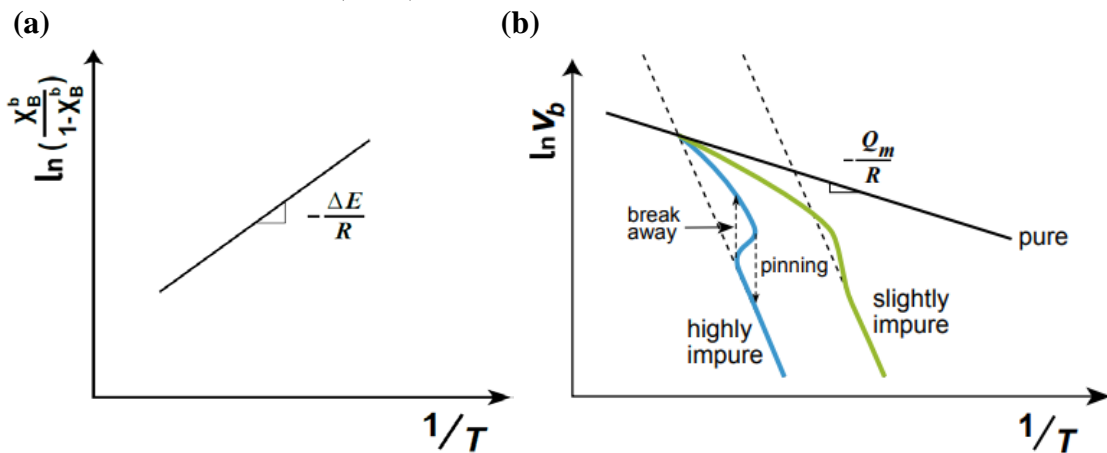
For an impure material, solute segregation decreases and solute drag reduces as temperature increases. With a low impurity level the impurity drag decreases continuously with an increase of temperature because of the reduction in solute segregation and the increase in boundary mobility with higher temperature.

The impurity drag effect is higher in a sample with a high impurity level than in a sample with a low impurity level. However, with increasing temperature, breakaway of the grain boundary from the segregated solutes can occur. These dependences of grain boundary velocity on temperature ($\ln v_b$ versus $1/T$) for various materials are shown in Fig. S3-14(b). In the impurity drag regime, the relationship between the boundary velocity and the driving force can be expressed as:

$$v_b = \frac{F}{\frac{1}{M_b^0} + \frac{\alpha C_\infty}{1 + \beta^2 v_b^2}} \approx \frac{F}{\frac{1}{M_b^0} + \alpha C_\infty}$$

The slopes in the figure are related to the apparent activation energies for boundary migration. Here, Q_m is the activation energy for diffusion of atoms across the boundary in pure material. If the mobility of a pure boundary is much larger than that of an impure boundary, the activation energy for boundary migration is that for diffusion of impurity atoms across the boundary.

Cf: Luecke K, Stuewe HP, "On the theory of grain boundary motion", in *Recovery and Recrystallization of Metals*, L. Himmel (ed.), Gordon and Breach, New York, 171-210 (1963).



<Fig. S3-14>

3-15. Most likely no. In a sample that exhibits intensive AGG, the size of the matrix grains is practically unchanged during AGG. According to the analysis by Cahn, Luecke and Stuewe, all the boundaries migrate under any driving force, which can cause deviation of GG behavior from normal and grain growth occurs continuously. Under the mechanism of solute drag, some large grains can form, but a few exceptionally large grains are unlikely to form. The solute drag mechanism cannot properly explain grain growth stagnation, which is commonly observed in systems with incubated AGG, and repetitive grain growth behavior, which was recently observed with an increased temperature or annealing time. (Cf: Jung SH, Kang SJL, *Acta Mater.* 69, 283-91 (2014); Kang SJL, et al., *Cearm. Int.*, 50, 37441-48 (2024).) Moreover, the solute drag mechanism does not provide an explanation as to why AGG occurs only in some specific

systems and not in other solute-segregated systems. The variation in grain growth behavior with respect to solute concentration, where AGG is observed for a certain range of solute concentration and apparently normal grain growth (NGG) for a concentration above and below the range, can also not be explained by the solute drag mechanism. (Cf: An SM, Kang SJL, *Acta Mater.*, 59, 1964-73 (2011).)

3-16.

$$F_b^t = F_b^o + F_b^d = \frac{v_b}{M_b^o} + \frac{\alpha C_\infty v_b}{1 + \beta^2 v_b^2} \approx \left(\frac{1}{M_b^o} + \alpha C_\infty \right) v_b$$

$$\therefore M_b = \left(\frac{1}{1 + \alpha C_\infty M_b^o} \right) M_b^o$$

For a high M_b^o ($M_b^o \gg M_b$), M_b is $1/\alpha C_\infty$ and can be expressed as $\frac{D_b^\perp}{RT} \frac{1}{C - C_\infty} \frac{V_m}{\omega}$ for the McLean model. Here D_b^\perp is the diffusion coefficient of the impurity across the boundary and has a different value from that in pure material, C_∞ the impurity concentration in the bulk, C the impurity concentration at the boundary, and ω the grain boundary thickness.

3-17. The polycrystal with a 99.8% purity has a higher activation energy. Diffusion of impurities and that of host atoms across the boundary can govern the kinetics of the boundary migration in the sample with 99.8% and 99.999% purity, respectively. The activation energy in the sample with 99.8% purity should be the sum of the migration enthalpy of solute atoms across the boundary and the segregation enthalpy of solute atoms, as explained below.

In the sample with 99.8% purity at a low temperature,

$$v_b \cong \frac{1}{\alpha C_\infty} F_b \approx \frac{D_b^\perp}{RT} \cdot \frac{1}{(C - C_\infty)} \frac{V_m}{\omega} F_b \propto \frac{D_b^\perp}{C - C_\infty}$$

$$\frac{X_B^b}{X_A^b} = \frac{X_B}{X_A} \exp\left(-\frac{\Delta g}{kT}\right), \quad X_B^b = \frac{X_B}{X_A} X_A^b \exp\left(-\frac{\Delta g}{kT}\right)$$

$$X_B^b - X_B = \frac{X_B}{X_A} X_A^b \left[\exp\left(-\frac{\Delta g}{kT}\right) - \frac{X_A}{X_A^b} \right]$$

$$\approx X_B \exp\left(-\frac{\Delta g}{kT}\right) \propto \exp\left(-\frac{\Delta h_{seg}}{kT}\right)$$

$$\frac{1}{C - C_\infty} \propto \exp\left(\frac{\Delta H_{seg}}{RT}\right), \quad \Delta H_{seg} < 0$$

$$\therefore v_b \propto \exp\left(\frac{\Delta H_{seg} - \Delta H_m}{RT}\right)$$

3-18. (a) The pore number $\propto 1/G^2$.

(b) The drag force \propto (drag per pore) \div (boundary area) $\propto G \times 1/G^2 = 1/G$

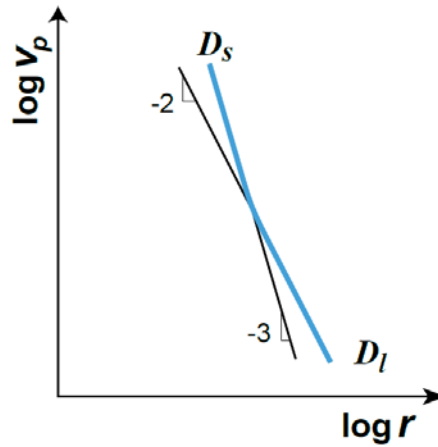
Note the condition, $r \propto G$.

3-19. The mobility of a pore that moves via surface diffusion $M_b^S \propto 1/r^4$

The mobility of a pore that moves via lattice diffusion $M_b^l \propto 1/r^3$

As $F_b \propto r$, $v_p^S \propto 1/r^3$ and $v_p^l \propto 1/r^2$.

If the migration of a pore is governed by lattice diffusion, the migration can be governed by surface diffusion with decreasing pore size, as schematically shown in Fig. S3-19 of a $\log v_b$ vs. $\log r$ plot.

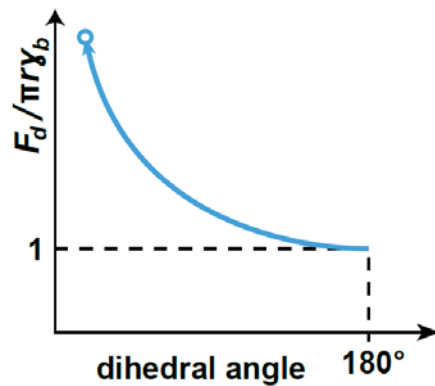


<Fig. S3-19>

3-20. (a) $\pi r \gamma_b$.

(b) The circumference of a pore increases as the dihedral angle decreases. As a result, the drag force will increase with a decreasing dihedral angle, as schematically shown in Fig. S3-20.

(c) With a decreasing dihedral angle, the pore migration rate will decrease as a result of an increased drag force. It may be worth to note that the peak steady-state velocity, which corresponds to the maximum velocity of pores before pore/boundary separation, was calculated to increase with decreasing dihedral angle (C. H. Hsueh, et al. *Acta Metall.*, 30, 1269-79 (1982).) For a constant driving force, the pore velocity should decrease with a reduction of the dihedral angle.



<Fig. S3-20>

3-21.

$$v_P = M_P F_P = \frac{D_g p \Omega^2}{2\pi r^3 (kT)^2} \cdot \pi r \gamma_b \propto \frac{D_g}{r^2}$$

$$D_g = \frac{2}{3} \left\{ \left(\frac{RT}{\pi} \right)^3 \frac{1}{M} \right\}^{1/2} (d^2 P_T N_A)^{-1} \propto \frac{1}{P_T}$$

where M is the molar mass, d the atom diameter, P_T the gas pressure in the pore, and N_A Avogadro's number.

$$\therefore v_P \propto \frac{1}{r^2} \cdot \frac{1}{P_T} = \frac{1}{r^2} \frac{r}{2\gamma} \propto \frac{1}{r}$$

3-22. Assume that the number ratio of two different sized pores with radius r_1 and r_2 is 1 to N.

Then, $r_1 = N^{1/3} r_2$.

$$F_p^d(r_1) = \pi r_1 \gamma \quad F_p^d(r_2) = \pi r_2 \gamma = \pi N^{-1/3} r_1 \gamma$$

$$\therefore v(r_1) = M_p(r_1) F_b^d(r_1) \propto 1/r_1, \quad v(r_2) = M_p(r_2) F_b^d(r_2) \propto N^{1/3}/r_1.$$

$$v(r_1)/v(r_2) = N^{-1/3}.$$

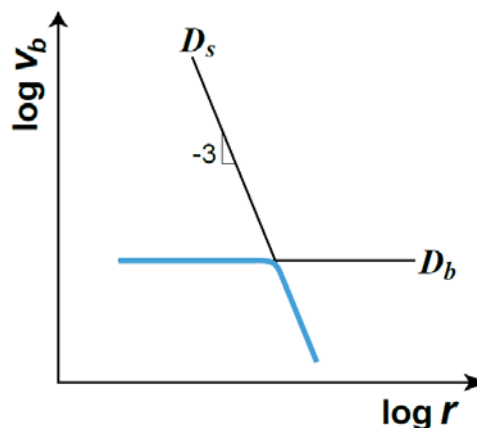
3-23. As the rate equation of pore migration by gas diffusion includes the vapor pressure of the material, the activation energy of grain growth is the activation energy (enthalpy) of vaporization (sublimation) of the material.

3-24. When the boundary migration is governed by boundary diffusion across the boundary,

$$v_b = v_p \propto M_b F_b \propto F_b = \propto 1/G = \text{const.} \neq f(r)$$

When the boundary migration is governed by the movement of pores via surface diffusion,

$$v_b = v_p^{SD} \propto 1/r^3.$$



<Fig. S3-24>

3-25. (a) To enhance densification and suppress grain growth, in particular AGG. To enhance densification rate relative to grain growth rate, $(d\rho/dt)/(dG/dt)$.

(b) - Application of external pressure, such as hot pressing, hot isostatic pressing, and gas pressure sintering, for enhancing densification.

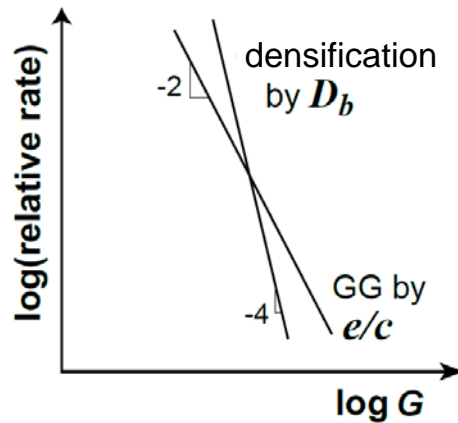
- Modification of thermal cycle, such as fast firing and two step sintering, for suppressing grain growth

- Application of electric field, such as spark plasma sintering with external pressure and flash sintering, for enhancing densification and suppressing grain growth.

- Change in boundary structure by adding dopants and changing atmosphere, which can suppress grain growth, in particular AGG.

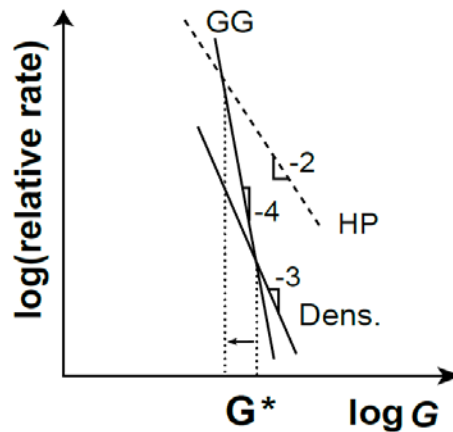
Cf: Kang SJL, *Materials*, 13 (16) 3578 (2020).

3-26. Comparison of the dependence of relative rates on grain size can give an answer. As Fig. S3-26 shows, the compact with fine particles will exhibit less grain growth than that of the compact with coarse particles.



<Fig. S3-26>

3-27. The production cost of fine powder is usually higher than that of coarse powder. Fine powder has, in general, higher sinterability than coarse powder. The optimum size can be determined from a plot of $\log(\text{relative densification and grain growth rate})$ versus $\log(\text{grain size})$, as in Figure S3-27 (Fig. 11.4(a) in the book “Sintering”). The optimum size is related to G^* . If the particle size is too small, grain growth dominates and the advantage of using fine powder can be marginal. If the particle size is too large, it takes too much time to obtain a fully dense material. In hot pressing the relative densification rate increases while the relative grain growth rate is, in principle, unchanged. The slope of the $\log(\text{relative densification rate})$ versus $\log(\text{grain size})$ plot for hot pressing is -2 . G^* decreases in hot pressing and the optimum size also decreases



<Fig. S3-27>

3-28. - This map is for the case at final stage sintering of densification by lattice diffusion and grain growth by surface diffusion. The number of pores per grain is assumed to be constant. This condition gives a result that the drag force of pores per unit area of grain boundary decreases with growth of grains for an invariable size of pores and pore separation can occur. It is uncertain if this consequence is reasonable.

- Increases of lattice diffusion and grain boundary diffusion, and a decrease of surface diffusion increase densification and decrease grain growth. To reduce the pore/boundary separation region, however, surface diffusion should be enhanced. A conflicting requirement vis-à-vis surface diffusion for densification and pore/boundary separation.

- 3-29. (a) As temperature increases, lattice diffusion relative to surface diffusion increases. As a result, growth of grains at T_2 is reduced compared with that at T_1 for the same relative density. The trajectory at T_2 is lower than that at T_1 .
- (b) The minimum grain size G^* for pore/boundary separation is expressed as Eq. (11.18) in the book “Sintering”. If the activation energy for diffusion of atoms across the boundary is larger than that for surface diffusion, G^* decreases with increasing temperature, and *vice versa*.
- (c) From Eqs (11.19) and (11.20), the critical size G^* , which is different from that in (b), is proportional to D_s/D_l . Therefore, G^* decreases with increasing temperature.

3-30. Densification by grain boundary diffusion

$$\frac{1}{\rho} \frac{d\rho}{dt} \propto \frac{D_b \delta_b \gamma_s V_m}{RTG^4 \rho} \quad (11.21)$$

Grain growth by surface diffusion

$$\frac{1}{G} \frac{dG}{dt} \propto \frac{D_s \delta_s \gamma_b V_m}{RTG^4 (1-\rho)^{4/3}} \quad (11.20)$$

- (a) This is the case described in Section 11.4.2.

From Eqs (11.20) and (11.21),

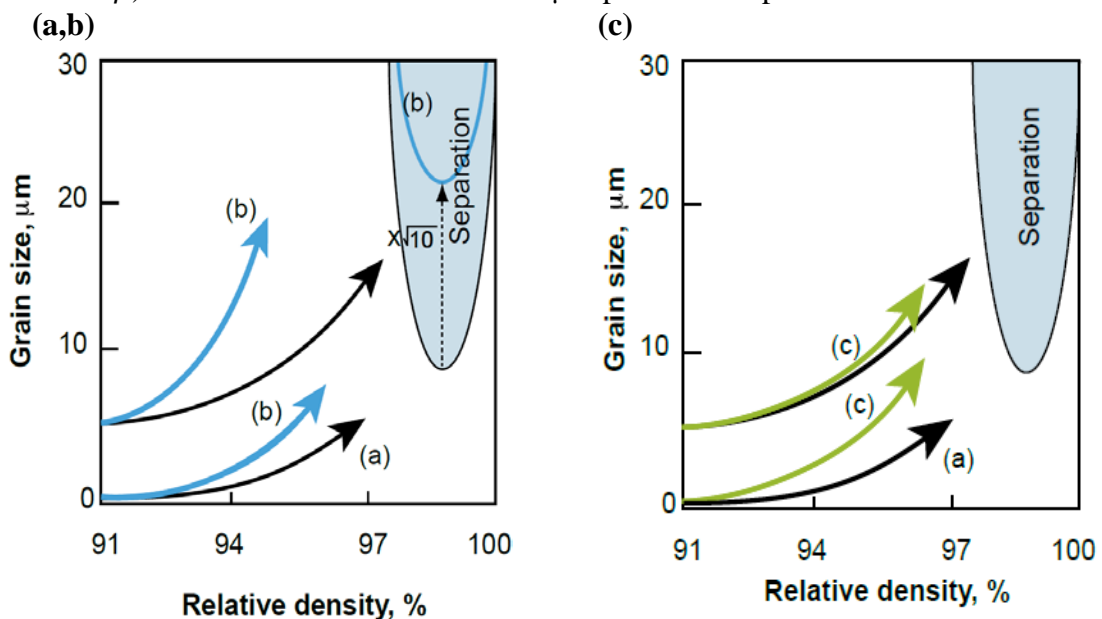
$$\frac{dG}{d\rho} \propto \frac{D_s \delta_s \gamma_b}{D_b \delta_b \gamma_s (1-\rho)^{4/3}} G \propto G$$

The sintering trajectory of a 0.5 μm powder compact is schematically illustrated in Fig. S3-30. Note that the slope of the trajectory is proportional to G and the ratio of relative growth rate to relative densification rate is independent of G .

- (b) Assuming other parameters are unchanged with D_s enhancement, the minimum grain size of the separation region increases by $\sqrt{10}$ times. (Consider an equation for the critical grain size, which has a similar form to that of Eq. (11.18).)

The slope of the microstructural development trajectories increases ten fold (Eqs (11.20) and (11.21)), as shown in Fig. S3-30.

- (c) This is the case described in Section 11.4.1. From Eqs (11.19) and (11.20), $dG/d\rho$ is independent of grain size. Assuming that the densification rate is lower than that in (a), the trajectories can be drawn as in Fig. S3-30. Note that the shapes (slopes at a fixed ρ) of the two curves for 5 and 0.5 μm powder compacts are the same.



<Fig. S3-30>

3-31. (a) For a system with densification by lattice diffusion and grain growth by surface diffusion,

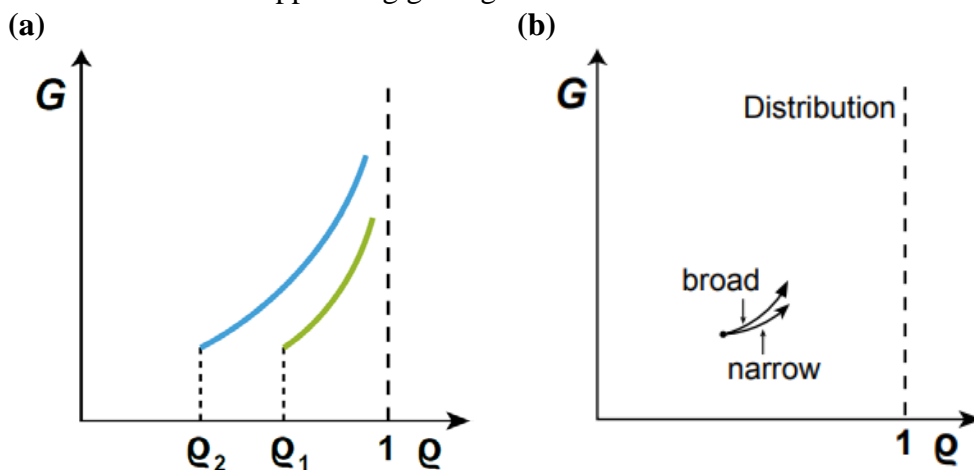
$$\frac{1}{\rho} \frac{d\rho}{dt} \propto \frac{D_l(1-\rho)^{1/3}}{G^3\rho} \quad \text{and} \quad \frac{1}{G} \frac{dG}{dt} \propto \frac{D_s}{G^4(1-\rho)^{4/3}}$$

$$\therefore \frac{dG}{d\rho} \propto \frac{D_s}{D_l} \frac{1}{(1-\rho)^{5/3}}$$

For $\rho_1 > \rho_2$, $(dG/d\rho)_1 > (dG/d\rho)_2$.

The schematic figure in Fig. S3-31(a) shows the G - ρ trajectories of the two kinds of samples. Note that $dG/d\rho$ is independent of G , but dependent on ρ .

(b) With broadening of the pore size distribution, the drag force of pores should decrease and hence grain growth will increase. (Note the same porosity.) The overall densification, however, should decrease. (Consider the cases of pores of constant size and a mixture of two different sizes. The densification rate is proportional to the product of capillary pressure and surface area of pores. The drag force is proportional to the pore size.) The slope of G vs. ρ trajectory of the sample with a broad pore size distribution is expected to be steeper than that of the sample with a narrow pore size distribution, as schematically shown in S3-31(b). In this regard, it would be beneficial to prepare compacts with a narrow size distribution of pores for enhancing densification while suppressing grain growth.

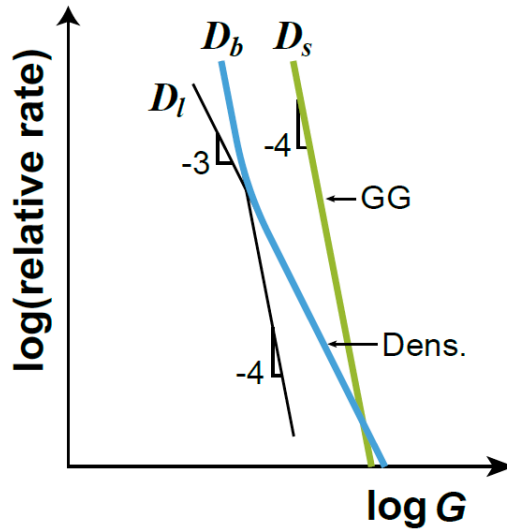


<Fig. S3-31>

3-32. From Eqs. (11.19) and (11.21), $(1/\rho)(d\rho/dt) \propto G^{-3}$ and G^{-4} for densification by lattice and grain boundary diffusion, respectively.

From Eq. (11.20), $(1/G)(dG/dt) \propto G^{-4}$ for grain growth governed by the movement of pores via surface diffusion. Fig. S3-32 delineates the variation of relative rates with respect to grain size

3-33. The dependence of densification on grain size is different from that of grain growth on grain size. (See Fig. 11.7 in the book “Sintering”.) \therefore Herring’s scaling law is not applicable.



<Fig. S3-32>

3-34. (a) The activation energy can be obtained from a plot of $\ln D$ vs. $1/T$.

(b) As the activation energy for lattice diffusion is larger than that of surface diffusion, the effect of lattice diffusion relative to that of surface diffusion increases with increasing temperature. Fast heating and sintering at a temperature higher than the conventional sintering temperature are thus beneficial for minimizing grain growth and enhancing densification. (This argument is also valid for a system where densification occurs by lattice diffusion and grain growth by the diffusion of atoms across the boundary. Thermodynamic basis of fast firing.)

$$D_l \propto \exp(-Q_l/RT) \quad D_s \propto \exp(-Q_s/RT) \quad Q_l > Q_s$$

$$D_l/D_s \propto \exp\{-(Q_l-Q_s)/RT\}$$

\therefore As T increases, D_l/D_s increases. Fast firing is beneficial.

3-35. From the densification and grain growth equations,

$$\frac{d\rho}{dG} = \left(\frac{733D_b\delta_b\gamma_s}{110D_s\delta_s\gamma_b} \right) \frac{(1-\rho)^{\frac{4}{3}}}{G}$$

$$\frac{1}{(1-\rho)^{\frac{4}{3}}} d\rho = A \cdot \frac{1}{G} dG,$$

where $A = \frac{733D_b\delta_b\gamma_s}{110D_s\delta_s\gamma_b}$.

Initial condition: $\rho = 0.9$, $G = 1.0 \times 10^{-6}$.

$$\int_{0.9}^{\rho} (1-\rho)^{-\frac{4}{3}} d\rho = A \cdot \int_{10^{-6}}^G \frac{1}{G} dG,$$

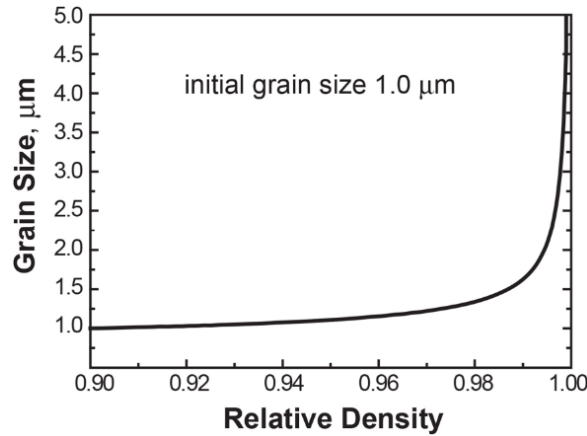
$$3(1-\rho)^{\frac{1}{3}} - 3(0.1)^{\frac{1}{3}} = A \cdot \ln\left(\frac{G}{10^{-6}}\right).$$

At 1500 °C, $A = 15.34$.

$$\therefore G = 10^{-6} \cdot \exp\left[\frac{1}{15.34} \left\{ 3(1-\rho)^{\frac{1}{3}} - 6.52 \right\}\right]$$

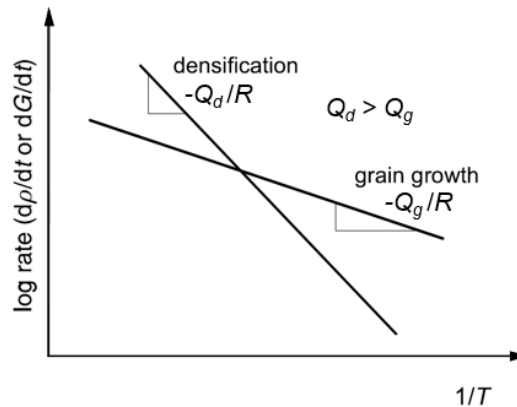
The density versus grain size trajectory is then as given in Figure S3-35.

The derived equation is valid under the assumption that the grain growth is governed by surface diffusion. This assumption, however, may not be justified at the very final stage of densification, where grain growth should be governed by the boundary mobility itself (boundary control region). In reality, the grain size at full densification has a finite value, in contrast to an infinite size predicted by the equation.



<Fig. S3-35>

3-36. The difference in activation energy between those of densification and grain growth. For systems where the activation energy for densification is larger than that of grain growth, which is common, fast firing and sintering at high temperature are beneficial for densification while suppressing grain growth. (See Fig. S3-36.) (Note that there is a typo in Fig. 11.9 in the book “Sintering”. The slope should have a negative sign.)



<Fig. S3-36>

- 3-37. (a) Fabrication of sintered compacts with different grain sizes may not be a big problem if one can prepare a compact with fine grains. (Refer to the solutions of 2-48 (S2-48) and 3-41 (S3-41).) Conventional sintering and long-time annealing can allow the fabrication of compacts with coarse grains.
 (b) and (c) Use of appropriate polymer spheres can be a solution.
- 3-38. (i) In a powder mixture with a high volume fraction of A, powder B, which exhibits high sinterability, is expected to act as a bonding material of powder A. Therefore, densification can be enhanced with decreasing particle size of powder B.
 (ii) In a powder mixture with a high volume fraction of powder B, powder A can act as impeding particles against densification. With a reduction of particle size of powder

A, the impeding effect is expected to increase and densification will be reduced. The relative size of powder A and powder B might give a different conclusion (See S3-8.).

3-39. Consider a system with $Q_d > Q_g$, which appears to be valid for most of the sintering systems.

In slow heating and at low temperature, grain growth relative to densification is more significant than that at high temperature. The driving force for densification reduces with grain growth. However, the time for densification is extended.

In fast heating, although the time period for densification is reduced, higher driving force for densification is maintained than that in the sample with slow heating because of less grain growth than in the sample with slow heating.

Therefore, the observed phenomenon can be an incidental result.

Cf: Morgan CS, Tennery VJ, "Magnesium enhancement of sintering of alumina," in "Sintering Processes," Mater. Sci. Res. Vol. 13, G. C. Kuczynski (ed.), Plenum Press, N.Y., 427-36 (1980).

3-40. In the techniques with an external field, the heating rate is much faster than that in the conventional sintering, and sometimes, overshooting can occur. Recent studies reported that the major mechanism of the unconventional sintering techniques with an external field is "Joule heating" with a very high rate. It appears that the fast firing mechanism is valid as the major mechanism in those techniques.

Cf: - Bordia RK, et al., *J. Am. Ceram. Soc.*, 100, 2314-52 (2017).

- Ji W, et al., *J. Eur. Ceram. Soc.*, 37, 2547-51 (2017).

3-41. (i) Use of fine powder with a narrow grain size distribution. The material cost increases.
(ii) Increase of green density by use of high pressure compaction. There is a limitation to the maximum green density that is possible.

(iii) Application of external pressure and/or an external field, such as in hot pressing, microwave sintering, spark plasma sintering and flash sintering. In most cases, the cost of equipment increases.

(iv) Modification of the thermal cycle, such as in fast firing and two-step sintering. These two techniques are known to be effective in suppressing grain growth.

(v) Use of additives. Its applicability is limited because the additives may affect the material properties.

(vi) Modification of sintering atmosphere.

(vii) Addition of second phase particles or a liquid. Properties of the final product can be degraded.

Cf: Kang SJL, *Materials*, 13 (16) 3578 (2020).

3-42. Physically, boundary migration is the result of thermal jumping of atoms across the boundary and sitting (attachment) of the transported atoms on the surface of a growing grain. The two processes can be considered to be diffusion and interface reaction of atoms, respectively. This concept is in accord with that for the transport of atoms from a source to a sink.

Rough boundary: There are numerous defects on the surface of a growing grain and no energy barrier is present for the attachment of atoms. The kinetics is governed by diffusion (thermal jumping across the boundary) of atoms and is proportional to the driving force for boundary migration.

Faceted (flat) boundary: The atomic structure on a faceted boundary is ordered with few surface defects. The migration mechanism of a faceted boundary was observed to be similar to that of a solid/liquid interface in the growth of a faceted crystal, where the interface reaction and diffusion governs the kinetics under low and high driving force, respectively. The migration rate of a faceted boundary was also observed to be insignificant under a driving force below a critical value and linearly proportional to the driving force above a critical value. For migration of a faceted boundary, the mixed control mechanism, either interface reaction or diffusion, appears to be valid.

Cf: - Merkle KI, Thompson LJ, *Mater. Lett.*, 48, 188-93 (2001).

- Wei J, et al., *Nature Mater.*, 20, 951-55 (2021).

- Kang SJL, et al., "Interface Structure-Dependent Grain Growth Behavior in Polycrystals" Chapter 12 in "*Microstructural Design of Advanced Engineering Materials*," D. Molodov (ed), Wiley-VCH, 299-322 (2013).

- An SM, et al., *Acta Mater.*, 60, 4531-39 (2012).

- 3-43. Because the migration mechanism can change with respect to the driving force. For a driving force smaller than a critical value, attachment of atoms, i.e. interface reaction, on the surface of a growing grain is the controlling step of boundary migration. The migration rate is insignificant for the region of low driving force while it is linearly proportional to the driving force larger than the critical value, a result of diffusion control. The mixed control mechanism, either diffusion or interface reaction, is valid for boundary migration

Cf: - An SM, et al., *Acta Mater.*, 60, 4531-39 (2012).

- Kang SJL, et al., *J. Am. Ceram. Soc.*, 98, 347-60 (2015).

- Kang SJL, et al., *J. Ceram Soc. Jpn.*, 124, 1159-65 (2016).

- 3-44. According to the mixed control mechanism of boundary migration, the migration rate of a faceted grain boundary is not linearly proportional to the driving force. The boundary migration rate is negligible for the driving force below a critical value and linearly proportional to the driving force above the critical value. As the driving force for boundary migration is inversely proportional to the average grain size, some large grains in the fine powder compact can have driving forces larger than the critical value and grow rapidly while others remain almost unchanged, resulting in the formation of abnormal grains (AGG) in the fine powder compact. On the other hand, in the coarse powder compact, no grain can have a driving force larger than the critical value and no grain can grow appreciably, and a unimodal grain size distribution is shown.

Cf: Kang SJL, et al., *J. Am. Ceram. Soc.*, 98, 347-60 (2015); *J. Ceram Soc. Jpn.*, 124, 1159-65 (2016); *J. Am. Ceram. Soc.*, 92, 1464-71 (2009)

- 3-45. Experimental results show that there is a critical driving force for appreciable migration of a faceted boundary and its migration rate is non-linear with respect to the driving force, similar to the case of the growth of a faceted crystal in a matrix (An SM, et al., *Acta Mater.*, 60, 4531-39 (2012)). As the migration rate of each boundary is governed by the driving force for its migration relative to the critical driving force, the growth (shrinkage) of each grain in a sample must be governed by the driving force for its growth (or shrinkage) relative to the critical driving force for appreciable boundary migration. The overall grain growth behavior in a sample with numerous grains is therefore determined by the relative value between the driving force for the growth of the largest grain in the sample, Δg_{\max} , and the critical driving force, Δg_c . (A coupling effect of Δg_c and Δg_{\max}

(the mixed mechanism principle of grain growth and microstructural evolution, which is the same as that for two-phase systems).) (See 3L-13.) Fig. S3-45 depicts schematically the mixed mechanism principle of grain growth (microstructural evolution). The predicted grain growth behavior at the time of observation is as follows:

- Normal grain growth (NGG) for $\Delta g_c = 0$
- Pseudo-normal NGG (PNGG) for $0 < \Delta g_c \ll \Delta g_{max}$
- Abnormal grain growth (AGG) for $\Delta g_c \leq \Delta g_{max}$
- Stagnant grain growth (SGG) for $\Delta g_c \gg \Delta g_{max}$

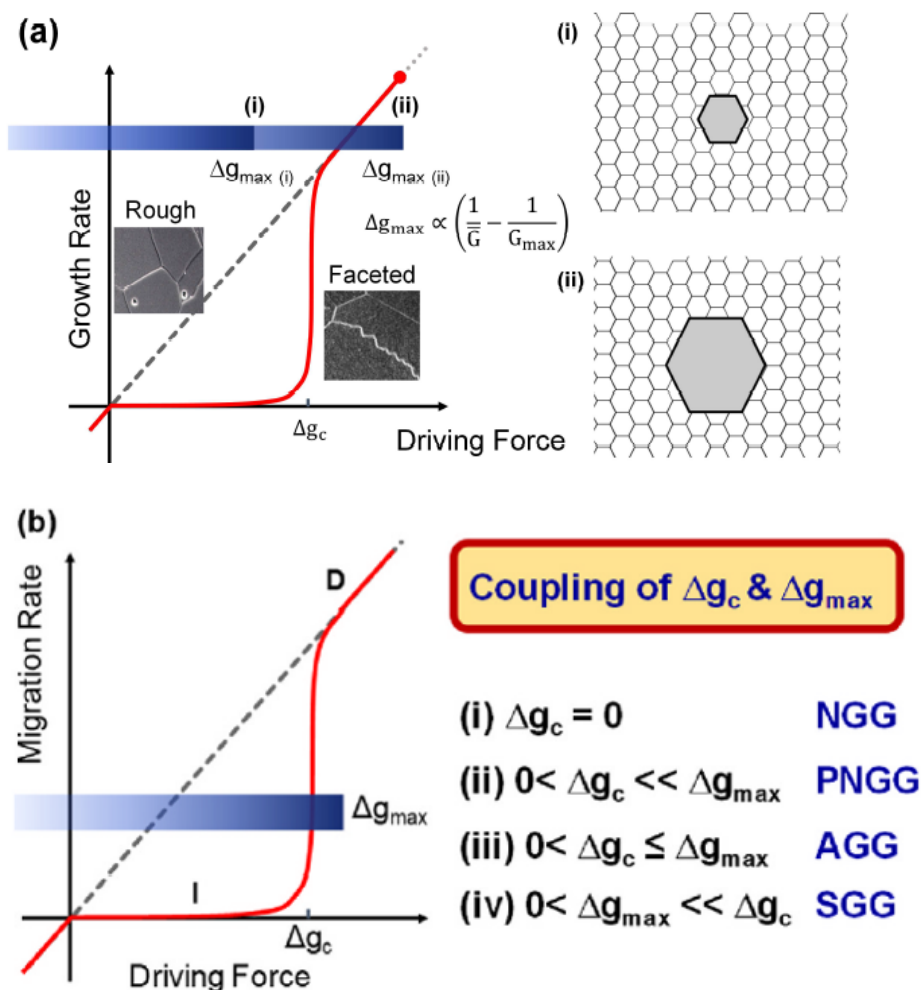
With regard to the mixed mechanism principle of grain growth (microstructural evolution) a few attempts have been made to calculate grain growth governed seemingly by interface reaction-control (Chen K, et al., *Acta Mater.*, 167, 241-47 (2019)) or by mixed control of boundary migration (Hu J, et al., *J. Materiomics* 7, 1007-13 (2021)). Further studies on the calculation and simulation of grain growth by the mixed control of boundary migration seem to be appropriate and desirable. (Cf: Kang SJL, Fisher JG, *Open Ceramics*, 16, 100484 (2023).)

Note that grain growth behavior changes with increased sintering time at a constant temperature because Δg_{max} changes (in general, decreases) with grain growth.

Cf: - Kang SJL, et al., *J. Am. Ceram. Soc.*, 92, 1464-71 (2009).

- An SM, et al., *Acta Mater.*, 60, 4531-39 (2012).

- Kang SJL, et al., *J. Ceram Soc. Jpn.*, 124, 1159-65 (2016).



<Fig. S3-45>

Fig. S3-45. (a) Schematic representation of the mixed control mechanism of grain growth and microstructural evolution. Maximum driving force Δg_{\max} for the largest grain of size G_{\max} depends on the average grain size \bar{G} and the grain size distribution in the sample, while critical driving force Δg_c depends on boundary structure. The horizontal blue bar represents the range of values for driving force Δg . (i) and (ii) represent microstructures with values of Δg_{\max} smaller and larger than Δg_c respectively. (b) Various types of grain growth behavior, such as normal (NGG), pseudo-normal (PNGG), abnormal (AGG) and stagnant (SGG), are possible depending on the relative values of Δg_{\max} and Δg_c at the time of observation (Kang SJL, et al., *J. Ceram. Soc. Jpn.*, 124, 1159-65 (2016); Kang SJL, et al., *Ceram. Int.*, 50, 39441-48 (2024)).

3-46. According to the mixed mechanism principle of microstructural evolution, There can be two groups of strategies with regard to the critical driving force for appreciable boundary migration, Δg_c , and the maximum driving force for the growth of the largest grain in the sample, Δg_{\max} .

Δg_c : (i) Make the boundary more faceted to increase Δg_c above Δg_{\max} . No grain can grow appreciably. Essentially stagnant grain growth (SGG) will exhibit.

(ii) Make the boundary rough to decrease Δg_c far below Δg_{\max} . Normal (fairly normal) grain growth will take place.

Δg_{\max} : (i) Use of a coarse powder to reduce Δg_{\max} below Δg_c . Essentially SGG will exhibit.

(ii) Prepare a powder with a narrow size distribution to reduce Δg_{\max} below Δg_c .

Cf: - Kang SJL, et al., *J. Ceram. Soc. Jpn.*, 124, 1159-65 (2016).

- Fisher JG, Kang SJL, *J. Am. Ceram. Soc.*, 102, 717-35 (2019).

3-47. (a) The driving force $\Delta g \propto (1/r - 1/R) \propto 1/r \propto 1/G$, where R is the effective radius of the single crystal, r that of polycrystal grains, and G the average grain size in the polycrystal. See Fig. S3-47(a).

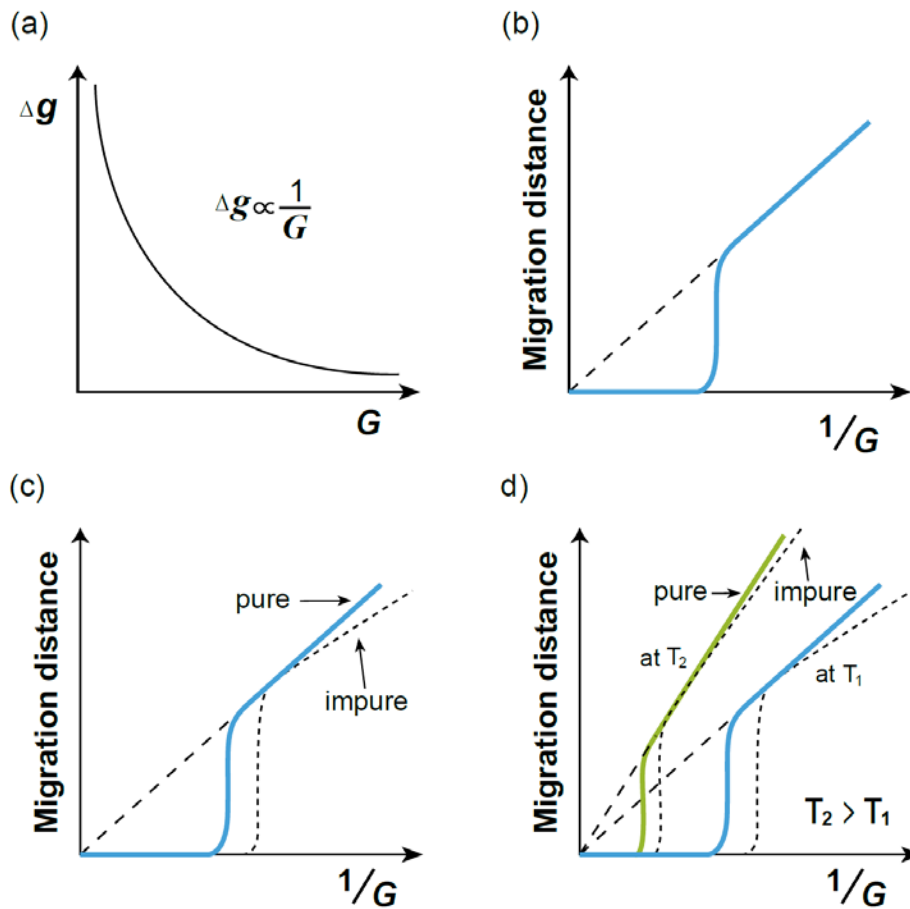
(b) Below a critical driving force (larger than a critical grain size), there is essentially no migration. Above it (smaller than a critical size), the migration distance is linearly proportional to the driving force, which is inversely proportional to the average grain size in polycrystals, as shown in Fig. S3-47(b).

(c) and (d) For low driving force, solute drag effect is significant. As the solute drag reduces the driving force for boundary migration, the critical driving force for an impure polycrystal can be larger than that for a pure polycrystal. For high driving force, the solute drag effect can be insignificant and the migration distance can be similar to that of a pure sample. As the migration distance increases under a very high driving force, however, solutes can considerably segregate at the migrating boundary and the migration distance will be reduced compared with that in the pure sample, as shown in Fig. S3-47(c).

At a higher temperature, the migration distance increases compared with that at a low temperature. The effect of solute segregation is reduced at a higher temperature and the deviation from the linearity of the migration distance for an impure sample should be less than that in a pure material, as shown in Fig. S3-47(d).

Cf: - An SM, et al., *Acta Mater.*, 60, 4531-39 (2012).

- Kang SJL, et al., *J. Am. Ceram. Soc.*, 98, 347-60 (2015).



<Fig. S3-47>

3-48. (a) - Make the boundary faceted. As there is a critical driving force for the migration of a faceted boundary, it is critical to keep the boundary faceted for suppressing grain growth in the polycrystal. If grain growth occurs in the polycrystal, the driving force for the growth of a single crystal seed decreases and its growth stops when the driving force becomes smaller than a critical value.

- Prepare a polycrystal sample with an appropriate grain size. If the grain size is too small, the possibility of the appearance of abnormal grain growth in the polycrystal increases during annealing of the bilayer sample. (See Prob. 3-46.)

Cf: Kang SJL, et al., *J. Am. Ceram. Soc.*, 98, 347-60 (2015).

(b) With the formation and thickening of a liquid film, the growth kinetics will decrease if the crystal growth is governed by diffusion of atoms across the film. (Appreciable growth of a single crystal means that the growth is governed by diffusion control.) If the growth is governed by the interface reaction at the surface, which is unlikely, however, the kinetics will be essentially unchanged.

Cf: Choi SY, et al., *Acta Mater.*, 52, 3721-26 (2004).

3-49. At low temperature, where the critical driving force Δg_c for appreciable boundary migration can be larger than the maximum driving force Δg_{max} for growth of the largest grain in the compact, none of the grains grow appreciably, showing SGG. As temperature increases, Δg_c decreases and can become smaller than Δg_{max} . Then, AGG takes place. When AGG is completed with further increase in temperature, Δg_{max} decreases considerably and can be smaller than Δg_c at the increased temperature. Grain growth is

then stagnant (secondary SGG). Further increase in temperature reduces Δg_c further and it can be lower than the reduced Δg_{max} . AGG then takes place again, showing secondary AGG. Such repetitive grain growth behavior with temperature increase can exhibit as a result of reduction of Δg_c and reduction of Δg_{max} with the completion of primary AGG. Depending on the variation of the relative value between Δg_c and Δg_{max} , different grain growth behavior exhibits with an increased temperature.

Cf: - Jung SH, Kang SJL, *Acta Mater.*, 69, 283-91 (2014).

- Kang SJL, et al., *Ceram. Int.*, 50, 37441-48 (2024).

3-50. According to the analyses of particle drag and impurity drag of boundaries, the effects of second phase particles and impurities at the boundary are expressed as a reduction of the driving force for boundary migration. Therefore, Δg_{max} decreases with the presence of particles and impurities. As the grain growth behavior is governed by the relative value of Δg_{max} and Δg_c in the mixed mechanism principle of microstructural evolution, the presence of second phase particles and impurities at the boundary can change grain growth behavior and their effects should appear in terms of the variation of Δg_{max} for a given Δg_c . When a liquid film is present at the boundary, the activation energy for diffusion of atoms and the diffusion distance change. As the driving force for boundary migration and the boundary energy anisotropy were assumed to be invariable, Δg_{max} does not change with the presence of a liquid film; grain growth behavior is not expected to change (Cf: S3L-15(a)).

The boundary energy and its anisotropy can, in fact, vary with impurity segregation and film formation at the boundary, unlike the assumption of this problem. Those variations affect Δg_c and also Δg_{max} , though not significantly. Considering the variation of Δg_c together with Δg_{max} and their relative value, the effects of impurities, second phase particles and liquid films on grain growth behavior can be understood.

Cf: - Kang SJL, et al., *J. Am. Ceram. Soc.*, 98, 347-60 (2015)

- Kang SJL, Fisher JG, *Open Ceramics*, 16, 100484 (2023).

Note added in proof: for all solutions in this part, except those from S3-42 to S3-50, grain growth is assumed to be governed solely by diffusion of atoms. (Here, the word diffusion means the thermal jumping and position change of atoms across the boundary, following the conventional understanding.)

III-2. Liquid phase sintering

3L-1. - The basic assumption of LSW theory is a constant mobility of the solid/liquid interface and, as a result, uniform precipitation of material on the interface. This assumption is valid only for a system where diffusion of atoms governs the kinetics of grain growth. In this respect, Wagner's interface reaction model is for a system where the diffusion distance is constant, and therefore it does not describe the interface reaction kinetics but rather the diffusion kinetics with a fixed diffusion distance. (Note that the kinetic equation of Wagner's interface reaction takes the same functional form as that of grain growth in a solid state.).

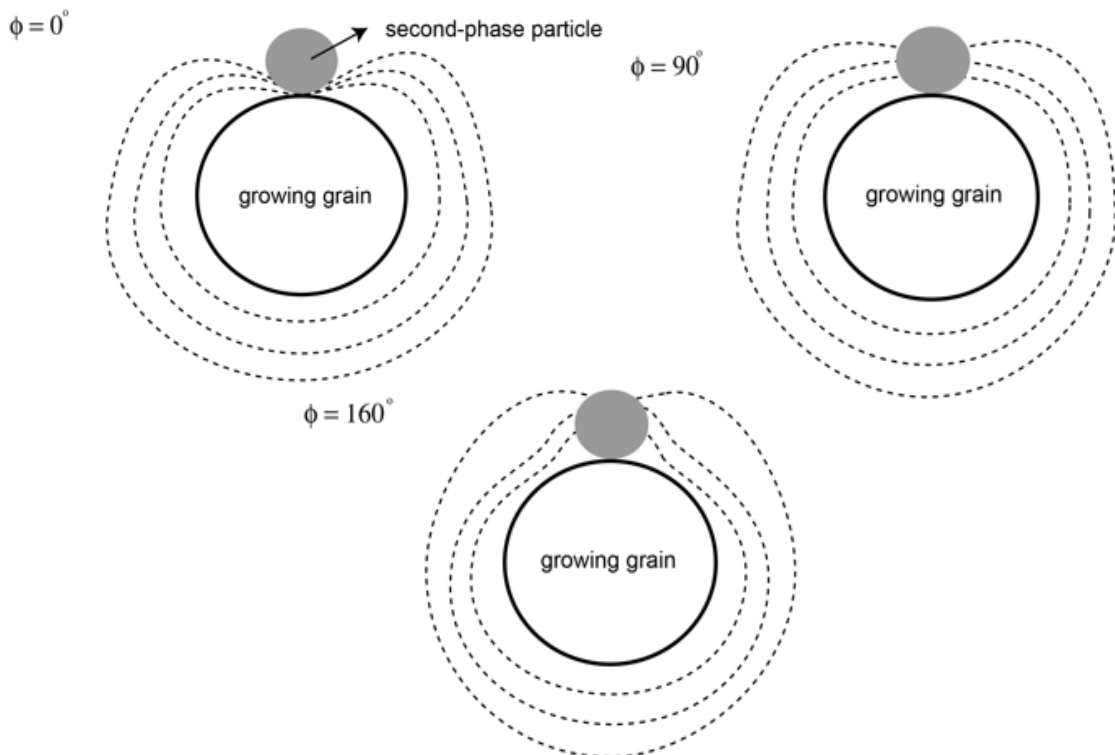
- Another assumption is that the particles are infinitely dispersed. (The volume fraction of solid is assumed to be zero.) As a result, the amount of solute in the matrix is invariable with grain growth, unlike in real systems, where the solute amount in the

matrix decreases, though not significantly, with grain growth. With an increase in the volume fraction of solid, the kinetics also increases, but the functional form of the kinetic equation is the same.

- The kinetic equation of LSW is expressed as $a^3 - a_0^3 = kt$ for diffusion control. Another important result is that there is a stationary (invariable) relative size distribution of grains (grain size relative to average sized grain) starting from any grain size distribution.

3L-2. Dihedral angle $\phi = 0^\circ$: material deposition is suppressed in the contact region, as schematically shown in Fig. S3L-2.

Dihedral angle $\phi = 160^\circ$: material deposition is enhanced in the contact region.



<Fig. S3L-2>

3L-3. (i) Liquid will first flow from the sample with a large grain size (sample A) to that with a very small grain size (sample B) until the liquid pressure in both samples becomes the same. (The liquid pressure in sample A is higher than that in sample B.) The volume of flown liquid will not be large.

(ii) Slight shape accommodation of grains in sample A and slight rounding of grains in sample B during grain growth.

(iii) Faster growth of grains in sample A near the bonded region than in bulk.

(iv) Long-time annealing results in a uniform microstructure.

3L-4 - Immediately after the contact, liquid will flow from the α -liquid compact to the β -liquid compact. (See Fig. 3-13 in the book “Sintering” and consider the pressure in the liquid.)

- With a change of the liquid volume fraction in two different compacts, the growth kinetics of α and β grains can, though not significantly, be enhanced and reduced,

respectively. With growth of grains, a limited liquid flow can occur from the α -liquid compact to the β -liquid compact to maintain a hydrostatic pressure in the liquid.

3L-5. Dissolution/precipitation: diffusion of atoms through a liquid governs the kinetics. The kinetics is proportional to the driving force and dependent on the diffusion distance. Evaporation/condensation: deposition of atoms on the surface governs the kinetics. This mechanism is similar to the diffusion control mechanism with a constant diffusion distance. Therefore, the kinetics is independent of the distance of atom transport.

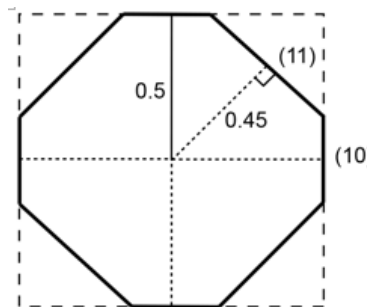
3L-6. - Measure sintering time to obtain the same grain size at different temperatures. As $G^n - G_0^n = kt \propto \exp(-Q/RT)t$, $t \propto \exp(Q/RT)$. From the slope of a plot of $\ln t$ vs. $1/T$, Q can be obtained. In this treatment, all other parameters, including the liquid volume fraction, are assumed to be constant with respect to temperature.

- The limiting step of grain growth in a liquid matrix is the transport of atoms across the matrix. The boundary between grains cannot move without atom transport through the matrix because the dihedral angle condition is imposed at the triple junction of the grain boundary and the solid/liquid interface.

3L-7. At equilibrium $\frac{2\gamma_i}{h_i} = \text{constant}$ (Wulff constant, Eq. (15.26) in the book "Sintering").

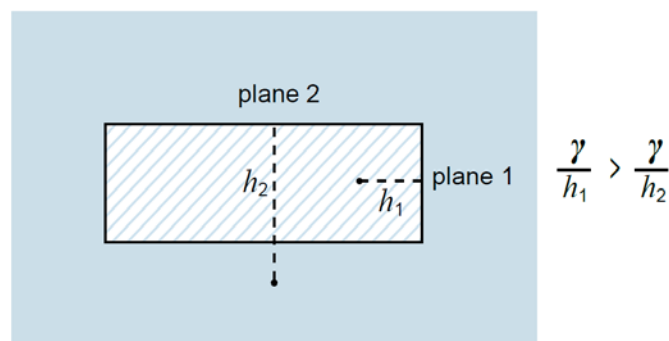
$$\therefore \gamma_i \propto h_i$$

The equilibrium shape of this crystal is as shown in Figure S3L-7.



<Fig. S3L-7>

3L-8. The local capillary pressure on plane i of the rectangular cuboid-shaped crystal can be expressed as $2\gamma/h_i$, as explained in Fig. S3L-8. (The effective size of the crystal for each plane is different.) Therefore, the capillary pressure on a small plane is higher than that on a large plane. Atoms on the small plane dissolve and precipitate on the large plane until the shape becomes an equilibrium shape, that is, a regular cube.



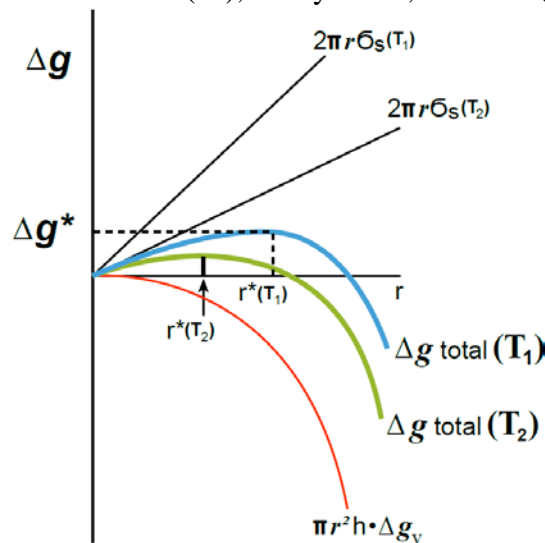
<Fig. S3L-8>

3L-9. (a) $\Delta g = \pi r^2 h \cdot \Delta g_v + 2\pi r \cdot \sigma_s$, where Δg_v is the difference in volumetric free energy between the solid and the liquid (the driving force for precipitation) and σ_s the free energy for step generation (step free energy). From $d(\Delta g)/dr = 0$, the critical driving force for nucleation $\Delta g^* = \pi \sigma_s^2 / h \Delta g_v$.

The variation of Δg can be drawn schematically as in Fig. S3L-9.

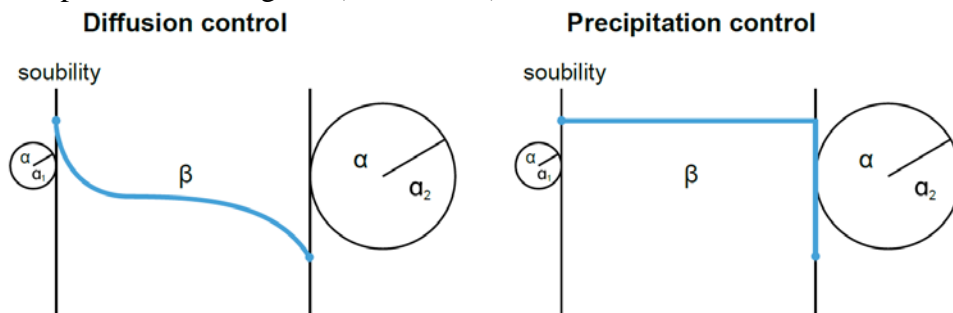
(b) As temperature increases from T_1 to T_2 , σ_s decreases. As a result, the critical driving force Δg^* and the critical radius of nucleus r^* decrease, as schematically shown in Fig. S3L-9.

Cf: Kang SJL, et al., "Interface Structure-Dependent Grain Growth Behavior in Polycrystals" Chapter 12 in "Microstructural Design of Advanced Engineering Materials," D. Molodov (ed), Wiley-VCH, 299-322 (2013).



<Fig. S3L-9>

3L-10. In the case of diffusion-controlled growth, the concentration of solute in front of each particle corresponds with its solubility, high for small particle and low for large particle. In the case of precipitation-controlled growth, as the precipitation is the limiting step for growth of the large particle, the concentration in the liquid is the solubility of the small particle, as schematically shown in Fig. S3L-10. For precipitation control, the grain shape should be angular (Cf: S3L-12).



<Fig. S3L-10>

3L-11. For growth of a faceted crystal, there is an energy barrier for atom attachment and the presence of defects on the surface is necessary for its growth if the driving force is not large enough for stable attachment of atoms on the surface. Surface defects, such as screw dislocations, may initially be present on the surface or form via nucleation of a stable island layer. Under these conditions, the growth of the crystal occurs via lateral

spreading of atoms at the edge of the defects or the nucleus (2-dimensional nucleation and growth). If the driving force is large enough for stable attachment of atoms, diffusion of atoms through the matrix governs the growth of the crystal. Even for such a case, as the surface energy anisotropy is large, the apparent shape of the growing crystal can be well faceted.

In dissolution of a faceted crystal, each corner of the crystal acts as a dissolution source without an energy barrier and the dissolution of a grain can occur over multilayers. As a result, the shape of small dissolving grains may be less faceted (sometimes rounded).

Cf: - Han JH, et al., *Acta Metall.*, 37, 2705-708 (1989).

- Moon H, et al., *Acta Mater.*, 49, 1293-99 (2001).

3L-12. The difference in grain growth mode is the result of growth behavior of individual grains.

According to the crystal growth theory, the growth rate of a spherical grain is linearly proportional to its driving force and that of a faceted grain is non-linear with respect to its driving force. For a faceted grain, its growth is negligible for a driving force smaller than a critical value, where the attachment (interface reaction) of atoms on the surface is the controlling step for the growth of the crystal. For a driving force larger than the critical value, the governing step is the diffusion of atoms to the growing crystal; the growth rate is linearly proportional to the driving force. In a liquid phase sintering compact with numerous grains, each grain has its own driving force for growth or dissolution with respect to a critical sized grain, which neither grows nor shrinks.

The sample that exhibits NGG is a system with rounded grains, which follows the LSW theory. The sample that exhibits AGG is a system with faceted grains. When the driving forces of some large grains are larger than a critical value, these grains will grow in proportion to their driving force and become large abnormal grains. Other grains that have driving forces smaller than the critical driving force essentially do not grow, forming matrix grains together with the dissolving grains.

Cf: Kang SJL, et al., "Interface Structure-Dependent Grain Growth Behavior in Polycrystals" Chapter 12 in "Microstructural Design of Advanced Engineering Materials," pp. 299-322, D. Molodov (ed), Wiley-VCH (2013).

3L-13. According to crystal growth theory, the growth rate of a grain in a liquid matrix can be represented schematically by the dashed line and the curve shown in Fig. S3L-13 (Jung YI, et al., *J. Mater. Res.*, 24, 2949-59 (2009)) depending on the shape of the grain, either spherical or (partially) faceted. The critical driving force Δg_c for appreciable growth is related to the transition of the growth mechanism between interface reaction control and diffusion control (the mixed control mechanism). The critical driving force is dependent on the step free energy of the solid/liquid interface, and qualitatively on the shape of grains for a given system, zero for spherical grains and non-zero for (partially) faceted grains. The dissolution rate, however, is linearly proportional to the driving force for dissolution as there is no energy barrier for detaching an atom from the corner of the faceted grain and multilayer dissolution can also occur.

In a liquid phase sintering sample with numerous grains, each grain has its own driving force for growth or dissolution. There is a range of driving forces and the maximum driving force for growth Δg_{\max} is for the largest grain in the sample (see Fig. S3-45).

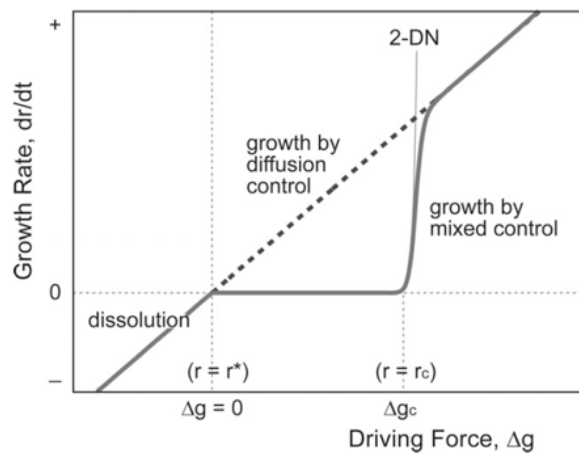
Grain growth behavior in a liquid matrix is then governed by a coupling effect of Δg_c and Δg_{\max} (the mixed mechanism principle of grain growth and microstructural evolution). Variation of microstructure with respect to time or other thermodynamic parameters can be described by estimating the growth or dissolution rate of individual

grains from a calculation of the critical sized grain, which is neither growing nor shrinking, using a mass conservation equation (the mixed mechanism theory of grain growth (Jung YI, et al., *J. Mater. Res.*, 24, 2949-59 (2009)). The mixed mechanism principle and theory of grain growth (microstructural evolution) predicts various types of grain growth behavior during sintering. The predicted grain growth behavior at the time of observation is as follows:

- Normal grain growth (NGG) for $\Delta g_c = 0$
- Pseudo-normal NGG (PNGG) for $0 < \Delta g_c \ll \Delta g_{\max}$
- Abnormal grain growth (AGG) for $\Delta g_c \leq \Delta g_{\max}$
- Stagnant grain growth (SGG) for $\Delta g_c \gg \Delta g_{\max}$

Note that grain growth behavior changes with increased sintering time at a constant temperature because Δg_{\max} changes with grain growth. In general, Δg_{\max} is expected to decrease with overall grain growth because driving force for growth is inversely proportional to mean grain size. In the case of SGG and typical AGG, however, Δg_{\max} increases with sintering time.

Cf: Jung YI, et al., *J. Mater. Res.*, 24, 2949-59 (2009).



<Fig.S3L-13>

- 3L-14. (a) One can determine the critical grain size by using a mass conservation equation.
 (b) Yes. With a change in step free energy, the critical driving force as well as the growth kinetics change. As a result, the critical grain size also changes.
 (c) With an increase of the step free energy from zero, the growth behavior will change from normal and pseudo-normal to abnormal and stagnant. (Refer to the Mixed Mechanism Principle of Microstructural Evolution, S3L-13)

Cf: Jung YI, et al., *J. Mater. Res.*, 24, 2949-59 (2009).

- 3L-15. (a) As Δg_{\max} is slightly larger than Δg_c , AGG will take place during sintering. With an increasing volume fraction of liquid, however, the difference in growth rate between grains with larger and smaller driving forces than Δg_c is reduced. As a result, AGG behavior will be less intensive in a sample with a high liquid volume fraction than that with a low liquid volume fraction. (See Fig. 15-10 in the book "Sintering".)
 (b) As temperature increases, Δg_c decreases and can become smaller than Δg_{\max} . The grains that have driving forces larger than Δg_c then will grow appreciably, forming abnormal grains. AGG will thus take place.

Cf: - Park CW, Yoon DY, *J. Am. Ceram. Soc.*, 85, 1585-93 (2002)

- Jung YI, et al., *J. Mater. Res.*, 24, 2949-59 (2009)

3L-16. (a) The growth rate of a faceted grain, like a WC grain, is non-linear with respect to the driving force for its growth, as schematically shown in Figure 15.9 in the book “Sintering”. With a reduction of particle size, Δg_{\max} increases and can become larger than Δg_c . For a sample where Δg_{\max} is larger than Δg_c , the condition for AGG, large grains that have driving forces larger than Δg_c can grow rapidly, thereby forming abnormally large grains.

(b) - An increase of Δg_c above Δg_{\max} (increase of step free energy) by decreasing temperature or adding dopants. Stagnant grain growth is predicted to occur. This can be the case of VC addition to WC-Co.

- A decrease of Δg_{\max} below Δg_c by increasing the initial powder size or modifying (reducing) the particle size distribution. SGG is expected to occur.

- Introduction of surface defects by, such as, severe ball milling. Defect-assisted growth can lessen AGG behavior.

Cf: Fisher JG, Kang SJL, *J. Am. Ceram. Soc.*, 102, 717-35 (2019).

3L-17. The maximum driving force for the growth of the largest grain in a sample is governed by the average grain size and size distribution. In this regard, the retardation of AGG by two-step LPS is expected to be related to a reduction of the maximum driving force after the first-step sintering in a short period of time, compared with the maximum driving force at the beginning of conventional LPS. The reduction of the maximum driving force would be possible because of a difference in the growth kinetics of individual grains between the first-step sintering and the conventional sintering, and hence in the relative grain size distribution.

Cf: - Chen IW and Wang XH, *Nature*, 404, 168-71 (2000).

- Yang DY, et al., *J. Am. Ceram. Soc.*, 94, 1019-24 (2011).

3L-18. (a) Difference in solid/liquid interfacial energy anisotropy. High for faceted grains and low (zero) for rounded grains.

(b) Diffusion control in growth of rounded grains. Mixed (diffusion or interface reaction) control in growth of faceted grains.

(c) At the beginning, as Δg_{\max} is much larger than Δg_c , grain growth behavior will be quite normal (pseudo-normal). When most small grains disappear with the growth of many (abnormal) grains, Δg_{\max} is reduced considerably. If the reduced Δg_{\max} is slightly larger than Δg_c , AGG will take place. If the reduced Δg_{\max} is smaller than Δg_c , SGG will appear. During long-time annealing, the sample that exhibited AGG will exhibit SGG with the completion of AGG. On the other hand, the sample that exhibited SGG can exhibit AGG. During extended annealing of the sample with SGG, the grain size distribution broadens and Δg_{\max} can become larger than Δg_c . This case represents incubated AGG, which we sometimes observe in many faceted systems.

Cf: Jung YI, et al., *J. Mater. Res.*, 24, 2949-59 (2009).

3L-19. According to the mixed mechanism principle of microstructural evolution, grain growth behavior is governed by the relative value between the critical driving force for appreciable migration of the solid/liquid interface, Δg_c , and the maximum driving force for the growth of the largest grain in the sample, Δg_{\max} . Rounded grains with $\Delta g_c=0$ always exhibit normal growth behavior following the LSW theory. Faceted grains with $\Delta g_c \neq 0$ exhibit different types of growth behavior depending on the relative value of

Δg_c and Δg_{max} . (See S3L-13.) The difference in growth behavior of the two different types of grains, faceted and rounded, in the same liquid matrix shows that the equilibrium shape of grains governs the grain growth behavior in a liquid matrix, normal for rounded grains and non-normal for faceted grains.

Cf: Yoon BK, et al., *Acta Mater.*, 53, 4677-85 (2005).

3L-20. Ball milling introduces defects on the surface of a powder. Surface defect-assisted grain growth can then take place. The surface defects reduce the critical driving force for appreciable growth of grains and the growth rate of grains smaller than the critical size is not insignificant, unlike the case of 2D-nucleation and growth. The tendency of AGG is reduced. Ball milling can reduce the particle size. This effect, however, can enhance AGG, in contrast to the observation. (It was reported that ball milling essentially does not reduce the particle size in carbide systems.)

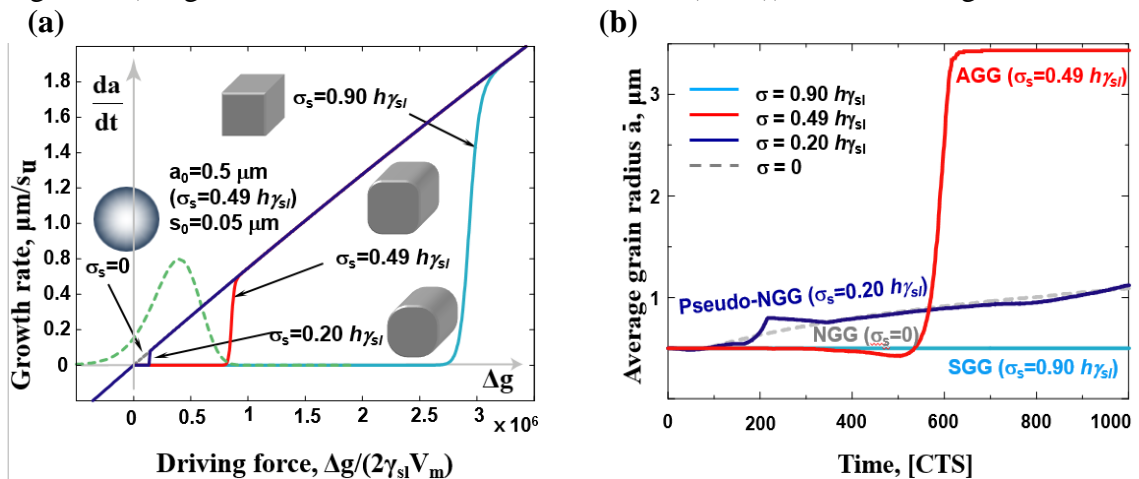
Cf: Yang DY, et al., *J. Ceram. Soc. Jpn.*, 120, 467-72 (2012)

3L-21. (i) For $\Delta g_{max} < \Delta g_c$, the growth of a faceted grain with few surface defects can occur only by 2-D nucleation and growth; its rate is insignificant (essentially negligible). In such a system, SGG behavior will be exhibited. On the other hand, for grains with surface defects, defect-assisted growth, the rate of which is not negligible, can take place. Grain growth, though its rate is low, will take place. When the sample that exhibits SGG is annealed for long time, AGG can take place (incubated AGG) because a small number of grains may eventually grow large enough to have driving forces larger than Δg_c .

(ii) For $\Delta g_{max} > \Delta g_c$, in a system with few surface defects, the grains having driving forces larger than Δg_c grow in proportion to their driving force, which results in the formation of abnormal grains. In a system with surface defects, as the grains with driving forces smaller than Δg_c can also grow, though not significantly, the observed AGG behavior will be lessened compared with that in a system with few surface defects. After the completion of AGG at the expense of all matrix grains, the grain growth behavior will be stagnant with a unimodal grain size distribution.

(iii) For $\Delta g_{max} \gg \Delta g_c$, the grain growth behavior will be quite normal, as many grains grow in proportion to their driving force. (Refer to Fig. S3L-21.)

For the above different modes of grain growth, their kinetics and resultant microstructural evolution can be calculated using the mixed mechanism theory of grain growth (Jung YI, et al., *J. Mater. Res.*, 24, 2949-59 (2009)), such as in Fig. S3L-21.



<Fig. S3L-21>

Fig. S3L-21. (a) Variation of growth rate of a grain with respect to the driving force normalized to $2\gamma_{sl}V_m$ for various critical driving forces Δg_c , which are dependent on the surface energy anisotropy (macroscopically the grain shape), i.e. the step free energy σ_s of facets. Schematic equilibrium shapes of a grain for different step free energies are shown. The dashed green curve shows the frequency plot of grains in a system with $\sigma_s = 0.49 h\gamma_{sl}$, where the average grain radius is $0.5\mu\text{m}$ and the standard deviation is $0.05\mu\text{m}$. (b) Variation of the average radius of grains with calculation time steps for systems shown in (a). For the calculation, the data used in a paper by Jung et al. (*J. Mater. Res.*, 24, 2947-59 (2009)). Here, h is the step height. (Kang SJL, "Sintering" (Chap. 6) in "*Ceramics Science and Technology*," R. Riedel and I.W. Chen (eds), Weinheim: Wiley-VCH Verlag & Co. KGaA, 141-69 (2012).)

- 3L-22. (a) A well-faceted cube. As temperature decreases, surface energy anisotropy increases.
 (b) The growth mechanism of spherical grains is diffusion of atoms through the matrix. The growth mechanism of faceted grains is either diffusion through the matrix or reaction (stable sitting) of atoms at the solid/liquid interface for a driving force larger or smaller, respectively, than the critical driving force for appreciable growth of grains (mixed control mechanism)
 For spherical grains, the LSW cubic law is valid. For faceted grains, a simple equation cannot describe their kinetics. It is, however, possible to theoretically predict the variation of the average grain size and grain size distribution with respect to the annealing time (Y.-I. Jung, et al., *J. Mater. Res.*, 24, 2949-59 (2009)).
 (c) The growth of facets governs the overall growth of partially faceted grains. Therefore, the interface reaction mechanism for grains with $\Delta g_{\text{max}} < \Delta g_c$ and the diffusion mechanism for grains with $\Delta g_{\text{max}} > \Delta g_c$ are valid.
 As the critical driving force changes with surface energy anisotropy, grain growth behavior also changes with the fraction of round-edged area. (Refer to Fig. S3L-21)

3L-23. SSS: Grain growth has long been understood to be governed by the migration of grain boundaries, though a few studies^{1,2} suggested that the movement of triple lines and quadruple points can govern the boundary migration, in particular, in materials with nano-scaled grains. It can be concluded that, in general, boundary migration of which the driving force is the capillary energy difference between two adjacent grains governs the grain growth kinetics in a solid state.

Rf: 1. Streitenberger P, Zoellner D., *Acta Mater.*, 59, 4235-43 (2011) / *Acta Mater.*, 78, 114-24 (2014)

2. Dong Y, Chen IW, *J. Am. Ceram. Soc.*, 101, 1857-69 (2018)

LPS: For a sample with a nonzero dihedral angle between grains, boundary migration is limited to the migration of the junctions between two adjacent grains because of the dihedral angle condition. The material transport through a liquid matrix between adjacent growing and shrinking grains induces migration of the junction. Therefore, the material transport through the matrix and the resultant junction movement governs the boundary migration and the grain growth kinetics, unlike the case of SSS. This junction-controlled boundary migration in LPS is physically similar to the triple line-controlled boundary migration in SSS. If the dihedral angle is zero degrees and a liquid film is present between grains, material transfer across the liquid film between grains must govern the grain growth kinetics, similar to the case of SSS.

PART IV. Supplementary Subjects

IV-1. Sintering of ionic compounds

4I-1. The free energy increase ΔG by the formation of n Frenkel defects in one mole of a crystal is expressed as

$$\Delta G = n\Delta g_F - T\Delta S_c$$

where Δg_F is the formation energy of a Frenkel defect pair and ΔS_c the increase in configurational entropy of the crystal.

$$\Delta S_c = k \ln \left\{ \frac{N_A!}{(N_A - n_i)! n_i!} \right\} \left\{ \frac{N_A!}{(N_A - n_v)! n_v!} \right\}$$

where n_i is the number of interstitial atoms and n_v the number of vacancies.

Using Stirling's approximation ($\ln N! = N \ln N - N$ for $N \gg 1$) and the relation $n_i = n_v = n$,

$$\Delta S_c \approx 2k \{ N_A \ln N_A - (N_A - n) \ln (N_A - n) - n \ln n \} \text{ and}$$

$$\Delta G = n\Delta g_F - 2kT \left\{ N_A \ln \left(\frac{N_A}{N_A - n} \right) + n \ln \left(\frac{N_A - n}{n} \right) \right\}$$

Use of the equilibrium condition ($(\partial \Delta G / \partial n)_{T,P} = 0$) and the approximation

$$N_A - n \approx N_A$$

give the expression

$$\frac{n_v}{N_A} = \exp \left(- \frac{\Delta g_F}{2kT} \right).$$

4I-2.

$$\begin{aligned} O_O^X &\rightleftharpoons \frac{1}{2} O_2(g) + V_O^{\cdot\cdot} + 2e' \\ \frac{p_{O_2}^{1/2} [V_O^{\cdot\cdot}] n^2}{[O_O^X]} &= K_g \quad [V_O^{\cdot\cdot}] = \frac{1}{2} n \\ p_{O_2}^{1/2} \cdot \frac{1}{2} n^3 &= K_g \\ p_{O_2} &= \frac{4K_g^2}{n^6}, \quad n = p_{O_2}^{-1/6} \cdot (4K_g^2)^{1/6} \\ \text{If } n &\ll N_C \\ \frac{n}{N_C} &= \exp \left(\frac{E_F - E_C}{kT} \right) \\ kT \ln \frac{n}{N_C} &= E_F - E_C \end{aligned}$$

In terms of p_{O_2} ,

$$E_F = E_C + kT \ln \frac{n}{N_C} = E_C - \frac{kT}{6} \ln p_{O_2} - kT \ln N_C + \frac{1}{6} kT \ln (4K_g^2)$$

In terms of $[V_O^{\cdot\cdot}]$,

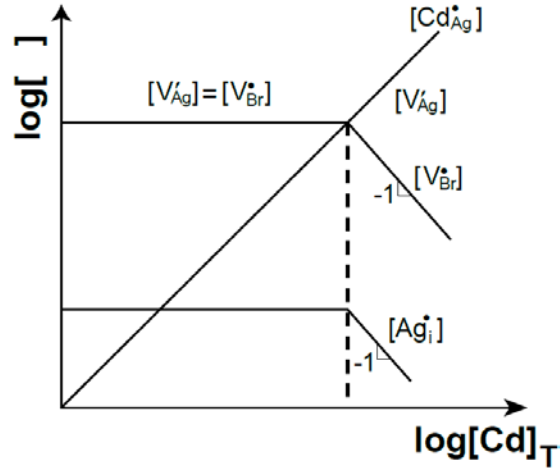
$$\begin{aligned} n &\cong 2[V_O^{\cdot\cdot}] \\ E_C - E_F &= kT \ln \frac{N_C}{n} = kT \ln \frac{N_C}{2[V_O^{\cdot\cdot}]} \end{aligned}$$

$$E_F = E_C - kT \ln \frac{N_C}{2[V_O^{\bullet}]}$$

4I-3. Intrinsic:

$$\begin{aligned} \text{null} &\rightleftharpoons V_{Ag}' + V_{Br}^{\bullet} & K_S &= [V_{Ag}'] [V_{Br}^{\bullet}] \\ Ag_{Ag}^X &\rightleftharpoons V_{Ag}' + Ag_i & K_F &= [V_{Ag}'] [Ag_i] \end{aligned}$$

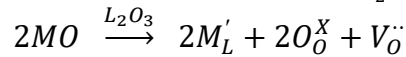
Extrinsic:



<Fig. S4I-3>

4I-4.

$$\begin{aligned} \text{null} &\rightleftharpoons 2V_L''' + 3V_O^{\bullet} : [V_L''']^2 [V_O^{\bullet}]^3 = K_S \\ L_L^X &\rightleftharpoons L_i^{\bullet} + V_L''' : [L_i^{\bullet}] [V_L'''] = K_F \\ \text{null} &\rightleftharpoons e' + h^{\bullet} : np = K_i \\ \frac{3}{2} O_2 &\rightleftharpoons 3O_O^X + 2V_L''' + 6h^{\bullet} : \frac{[V_L''']^2 p^6}{p_{O_2}^{3/2}} = K_g \end{aligned}$$

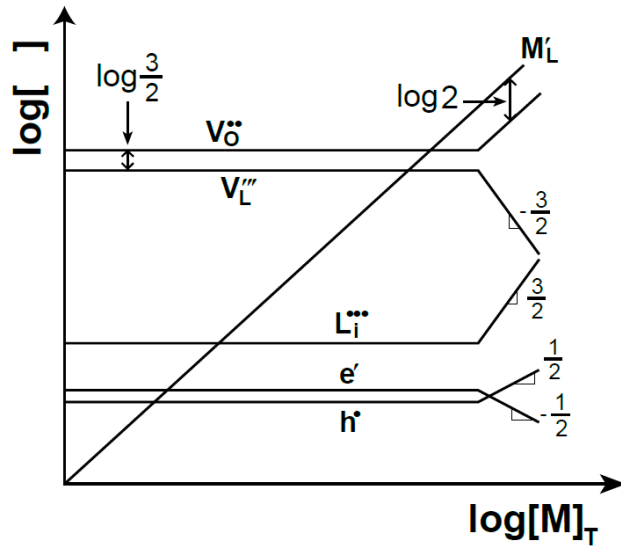


Intrinsic:

$$2[V_O^{\bullet}] = 3[V_L''']$$

Extrinsic:

$$\begin{aligned} [M_L'] &= 2[V_O^{\bullet}] \\ 2\log[V_L'''] + 3\log[V_O^{\bullet}] &= \text{const} \\ \log[V_L'''] &\propto -\frac{3}{2}\log[V_O^{\bullet}] \\ \log[L_i^{\bullet}] + \log[V_L'''] &= \text{const} \\ \log[L_i^{\bullet}] &\propto -\log[V_L'''] \\ 3[V_L'''] + n &= 2[V_O^{\bullet}] + 3[L_i^{\bullet}] + p \\ 2\log[V_L'''] + 6\log p &= \text{const} \\ \log p &\propto -\frac{1}{3}\log[V_L'''] \end{aligned}$$



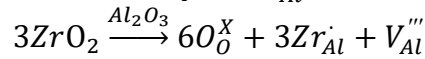
<Fig. S4I-4>

4I-5.

$$\begin{aligned}
 null &\rightleftharpoons 2[V_{Al}'''] + 3[V_O^{\bullet\bullet}] & K_s &= [V_{Al}''']^2 [V_O^{\bullet\bullet}]^3 & 3 \log[V_O^{\bullet\bullet}] + 2 \log[V_{Al}'''] &= const \\
 Al_{Al} &\rightleftharpoons Al_i^{\bullet\bullet} + V_{Al}''' & K_F &= [Al_i^{\bullet\bullet}] [V_{Al}'''] & \log[Al_i^{\bullet\bullet}] + \log[V_{Al}'''] &= const \\
 null &\rightleftharpoons e' + h' & & & K_i &= np
 \end{aligned}$$

$$\frac{3}{2} O_2 \rightleftharpoons 3O_O^X + 2V_{Al}''' + 6h' \quad K_g = \frac{[V_{Al}''']^2 p^6}{p_{O_2}^{3/2}} \quad 2 \log[V_{Al}'''] + 6 \log p = const$$

$$[Zr]_T = [Zr_{Al}^{\bullet}]$$

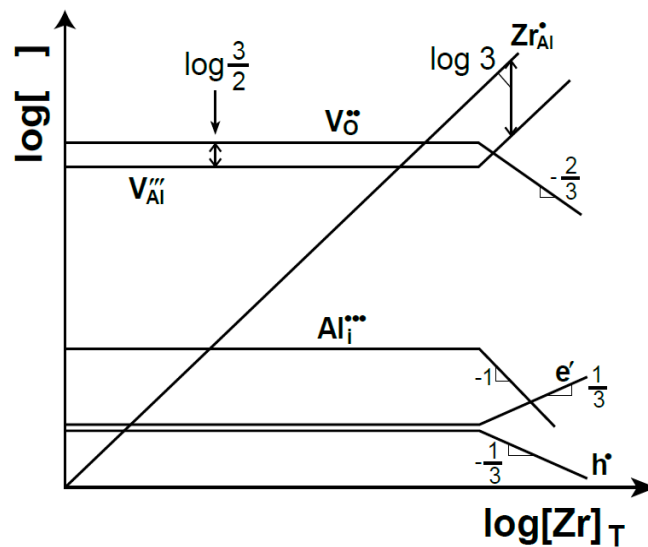


Intrinsic :

$$2 [V_O^{\bullet\bullet}] = 3 [V_{Al}'''] \quad \log[V_O^{\bullet\bullet}] = \log[V_{Al}'''] + \log \frac{3}{2}$$

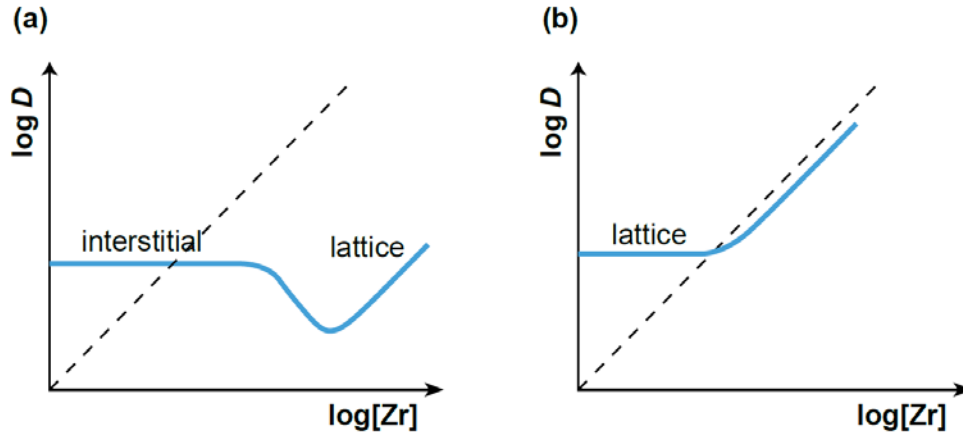
Extrinsic :

$$[V_{Al}'''] = \frac{1}{3} [Zr_{Al}^{\bullet}] \quad \log[V_{Al}'''] = \log[Zr_{Al}^{\bullet}] - \log 3$$



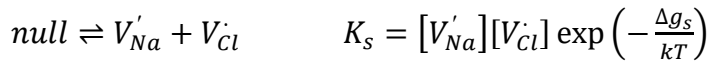
<Fig. S4I-5>

4I-6. For $Q_i \ll Q_l$, where Q_i and Q_l are, respectively, the activation energies for interstitial and lattice diffusion, Al diffusion can be governed by interstitial diffusion until the concentration of the interstitial Al atoms is considerably decreased. When the concentration of Al vacancies increases considerably in the extrinsic region, Al diffusion can be governed by the lattice diffusion, as schematically shown in Fig. S4I-6(a). For $Q_i \gg Q_l$, Al diffusion is always governed by lattice diffusion, as in Fig. S4I-6(b).

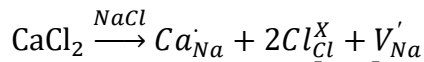


<Fig. S4I-6>

4I-7. Intrinsic:

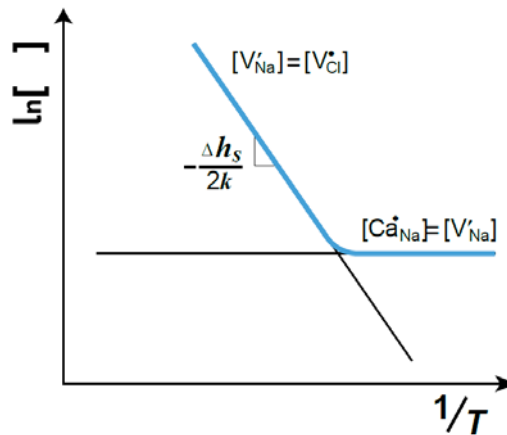


Extrinsic:



For an extrinsic region $[Ca'_{Na}] = [V'_{Na}]$.

As temperature increases, $[V'_{Na}]$ and $[V_{Cl}]$ increase following the Schottky defect equation. In Fig. S4I-7, Δh_s is the formation enthalpy of a Schottky pair.



<Fig. S4I-7>

4I-8. (a) In this case, Eqs. (12.14) and (12.5) hold for the dissolution of L_2O_3 in MO and the Schottky defect formation, respectively.

For the intrinsic region at high temperature

$$\begin{aligned} [V_{O^{\bullet\bullet}}] &= [V_{M^{\prime\prime}}] \\ [L]_{total} &= [L_M^{\bullet}] \end{aligned}$$

For the extrinsic region at low temperature

$$[L]_{total} = [L_M^\bullet] \approx 2[V_M''] = \text{constant}$$

Therefore, the plot is as presented in Figure S4I-8(a).

Here, Δh_s is the formation enthalpy of a Schottky pair.

Note that $[V_M''] [V_O^{\bullet\bullet}] = K_s = K_{s_0} \exp\left(-\frac{\Delta h_s}{kT}\right)$

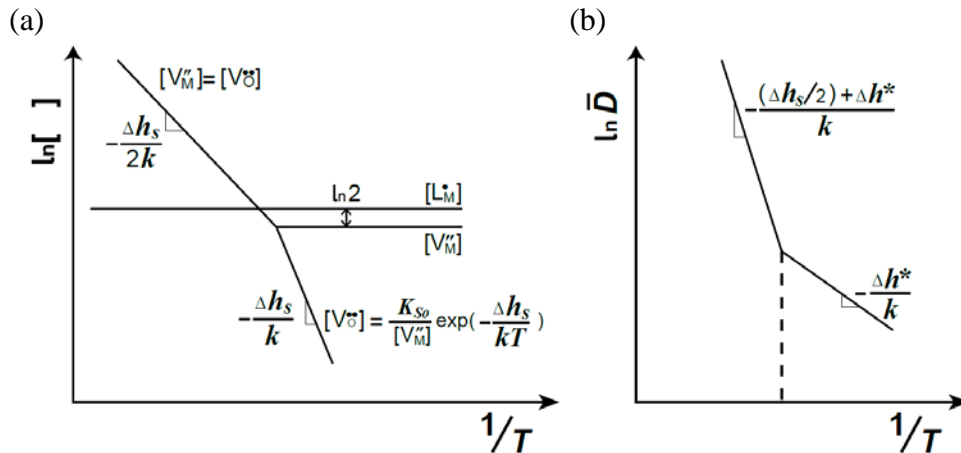
(b)

$$\bar{D} \approx D_M = \alpha \lambda^2 \nu [V_M''] \exp\left(-\frac{\Delta g^*}{kT}\right).$$

For the intrinsic region, $\bar{D} \propto \exp\left(-\frac{\Delta h_s}{2kT}\right) \cdot \exp\left(-\frac{\Delta h^*}{kT}\right).$

For the extrinsic region, $\bar{D} \propto \exp\left(-\frac{\Delta h^*}{kT}\right).$

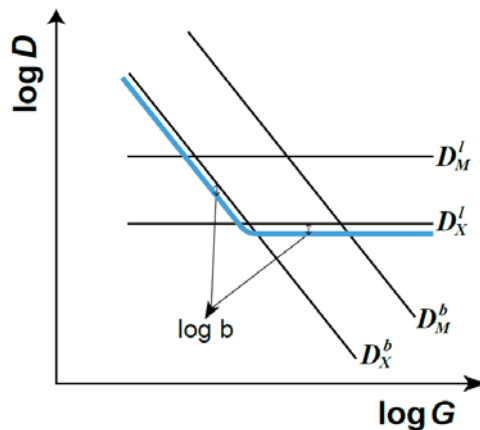
Here, α is the geometrical factor, λ the jump distance, ν the vibrational frequency, Δg^* the activation energy for migration, and Δh^* the enthalpy of migration (see reference 17 in Part V of the book "Sintering"). The plot is as presented in Figure S4I-8(b).



<Fig. S4I-8>

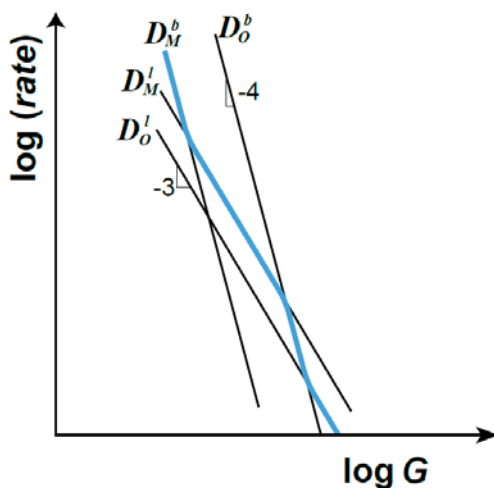
4I-9. (a) The effective diffusion coefficient is expressed as Eq. (13.8) ($\bar{D} = \frac{D_M D_X}{b D_M + a D_X}$)

(b) The variation of the effective diffusion coefficient is as shown in Fig. S4I-9.



<Fig. S4I-9>

4I-10. As the densification rate is proportional to G^{-3} and G^{-4} for lattice and boundary diffusion, respectively, the slope is -3 and -4 in a $\log(\text{rate})$ vs. $\log G$ plot. As the slowly moving species through its fastest path governs the kinetics, the apparent variation of the densification rate will be as presented by the thick blue line in Fig. S4I-10.

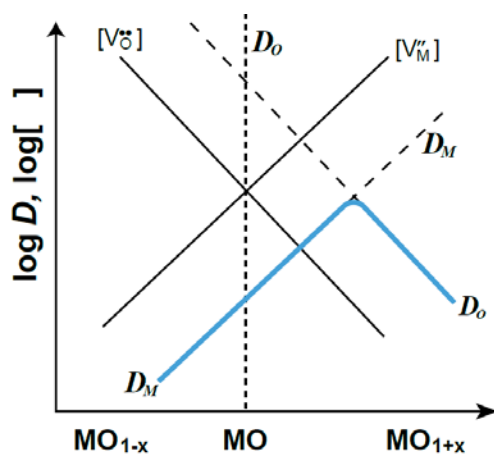


<Fig. S4I-10>

4I-11. (a) $K_S = [V_O^{\bullet\bullet}][V_M^{\prime\prime}] = \text{const}$

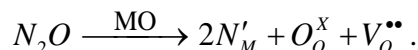
(b) $\bar{D} = \frac{D_M D_O}{D_M + D_O}$

$V_m = V_{MO}$



<Fig. S4I-11>

4I-12. Since $D_M = 100D_O$, an increase in the concentration of oxygen vacancies must improve the densification. The addition of acceptor dopants, such as N_2O , creates oxygen vacancies in MO:



The concentration of oxygen vacancies must be 100 times that of metal vacancies to maximize the densification.

Since $K_S = 10^{-10}$, the optimum anion and cation vacancies are

$$[V_O^{\bullet\bullet}] = 10^{-4} \quad \text{and} \quad [V_M^{\prime\prime}] = 10^{-6}.$$

\therefore The addition of acceptor dopant N_2O by 10^{-4} mole will maximize the densification.

Cf: Fig. 13.3 in the book "Sintering".

4I-13. The sketches are shown in Figs 13.5 and 13.6 in the book “Sintering”.

4I-14. See the solution of 3-16 (S3-16).

$$\begin{aligned}
 F_b^t &= v_b \left(\frac{1}{M_b^0} + \frac{\alpha C_\infty}{1 + \beta^2 v_b^2} \right) \approx \frac{\alpha C_\infty}{1 + \beta^2 v_b^2} v_b \\
 v_b &= \frac{1 + \beta^2 v_b^2}{\alpha C_\infty} F_b^t \approx \frac{1}{\alpha C_\infty} F_b^t \\
 &\approx \left[\frac{D_b^\perp}{RT} \cdot \frac{1}{(C - C_\infty)} \frac{V_m}{\omega} \right] F_b^t \\
 \therefore M_b &= \frac{D_b^\perp}{RT} \cdot \frac{1}{(C - C_\infty)} \frac{V_m}{\omega}
 \end{aligned}$$

Here D_b^\perp is the diffusion coefficient of the impurity across the boundary, C_∞ the impurity concentration in the bulk, C the impurity concentration at the boundary, and ω the grain boundary thickness.

IV-2. Diffusion induced interface migration

4D-1. When solute atoms diffuse along the grain boundary, thin diffusional layers form at both sides of the two neighboring grains and coherency strain energies are stored in the diffusional layers. The coherency strain energies stored in the diffusional layers are different from each other because of the difference in the crystallographic plane of the surfaces between the two adjacent grains. The atoms in the layer with a high strain energy should tend to jump across the grain boundary and join the layer with a low strain energy. Therefore, the direction of DIGM is from the grain with a low strain energy to that with a high strain energy.

4D-2. Driving force for DIGM initiation: The difference in the coherency strain energy stored in the thin diffusional layers on the surfaces of two adjacent grains.

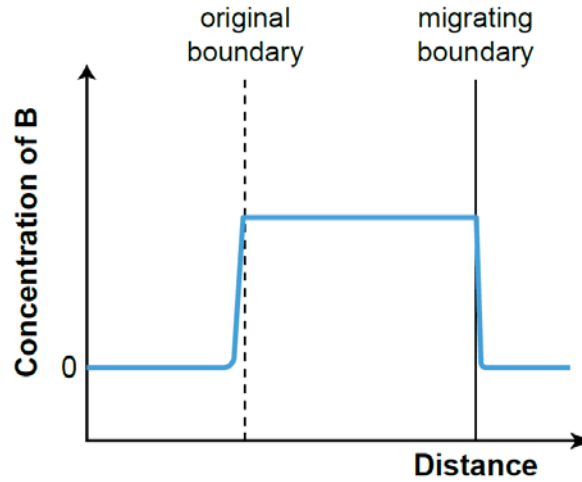
Driving force for DIGM: The coherency strain energy at the surface of the shrinking grain. The strain energy caused by the dislocations generated in the thick migration region is insignificant compared to the coherency strain energy in a thin diffusional layer on the receding grain.

4D-3. At low temperature, followed by grain boundary diffusion, lattice diffusion of solute atoms occurs. The concentration of solute from the grain boundary will take a form of an error function with a surface concentration to be the solubility limit at the annealing temperature. At low temperature, the solubility of B in A is, in general, low and the lattice diffusion as well as boundary mobility are inconsiderable; diffusion induced grain-boundary migration (DIGM) can hardly occur.

At medium temperature, DIGM can occur forming a solid solution layer with many dislocations in the migrated region. The layer thickness increases in proportion to annealing time. The concentration profile of B is as shown in Fig. S4D-3. Note that there is a mistake of the concentration profile near the original boundary in Fig. 8.2 in the book “Sintering”.

At high temperature, DIGM does not occur and only lattice diffusion occurs with a much higher rate than that at low temperature. With an increased temperature, the value of D_l/v_b , where D_l is the lattice diffusivity and v_b the boundary velocity, increases because

the activation energy of D_l is larger than that of D_b^\perp . As a result, at high temperature, coherency breaking can occur at the beginning of lattice diffusion and DIGM does not occur.



<Fig. S4D-3>

4D-4. When LFM occurs in a liquid phase sintering body, some of the migrating films bulge out because of anchoring of the boundary junction possibly due to the dihedral angle condition, if the boundary is not completely wetted. The capillary energy of the migrated region increases with migration. When the capillary energy of the migrating region is balanced with the energy on the surface layer of the receding grain, which is the sum of the coherency strain energy and the capillary energy on the layer (a negative value), migration stops. Therefore, migration reversal will occur when $(4/r) \gamma_{sl} V_m =$ the coherency strain energy per mole.

Cf: Baik YJ, Yoon DN, *Acta Metall.*, 33, 1911-17 (1990).

4D-5. (a) $\sigma_{31} = \sigma_{32} = \sigma_{33} = 0$ (plane stress condition)

(b) $E_c = E(I) - E(II)$

$E(I)$: Elastic strain energy in $\langle x \rangle \langle y \rangle \langle z \rangle$ direction

$E(II)$: Relaxation energy in $\langle x \rangle$ direction perpendicular to the layer

- Calculation of $E(I)$

$$\sigma_{il} = C_{ijkl} \varepsilon_{kl}$$

For a simple cubic system

$$C_{ijkl} = \begin{pmatrix} C_{1111} & C_{1122} & C_{1122} \\ C_{1122} & C_{1111} & C_{1122} \\ C_{1122} & C_{1122} & C_{1111} \end{pmatrix}$$

$$\varepsilon_{11} = \varepsilon_{22} = \varepsilon_{33} \neq 0 \quad \text{and} \quad \varepsilon_{ij} (i \neq j) = 0$$

$$\sigma_{11} = C_{1111} \varepsilon_{11} + C_{1122} \varepsilon_{22} + C_{1133} \varepsilon_{33}$$

$$= \varepsilon_{11} [C_{1111} + 2C_{1122}]$$

$$\sigma_{22} = \varepsilon_{11} [C_{1111} + 2C_{1122}]$$

$$\sigma_{33} = \varepsilon_{11} [C_{1111} + 2C_{1122}]$$

$$\begin{aligned}
\therefore E(\text{I}) &= \frac{1}{2} \sigma_{ij} \varepsilon_{ij} = \frac{1}{2} [\sigma_{11} \varepsilon_{11} + \sigma_{22} \varepsilon_{22} + \sigma_{33} \varepsilon_{33}] \\
&= \frac{1}{2} \varepsilon_{11} [\sigma_{11} + \sigma_{22} + \sigma_{33}] \\
&= 3\varepsilon_{11}^2 \left[C_{1122} + \frac{C_{1111}}{2} \right]
\end{aligned}$$

- Calculation of $E(\text{II})$

$$\text{Stress relaxed: } \sigma_{i'j'} = l_{i'} l_{j'} \sigma_{ij}$$

$$\text{Strain relaxed: } \varepsilon_{i'j'} = l_{i'} l_{j'} \varepsilon_{ij}$$

$$\sigma_{2'2'} = \sigma_{3'3'} = \sigma_{2'3'} = \sigma_{3'2'} = 0$$

Released energy $E(\text{II})$

$$= \frac{1}{2} \sigma_{k'l'} \varepsilon_{k'l'} = \frac{1}{2} (\sigma_{1'1'} \varepsilon_{1'1'} + 2\sigma_{1'2'} \varepsilon_{1'2'} + 2\sigma_{1'3'} \varepsilon_{1'3'})$$

$$\therefore Ec = E(\text{I}) - E(\text{II})$$

$$= 3\varepsilon_{11}^2 \left(C_{1122} + \frac{C_{1111}}{2} \right) - \frac{1}{2} (\sigma_{1'1'} \varepsilon_{1'1'} + 2\sigma_{1'2'} \varepsilon_{1'2'} + 2\sigma_{1'3'} \varepsilon_{1'3'})$$

Cf: Lee HY, Kang SJL, Z. *Metallkde*, 85, 426-31 (1994).

4D-6. Consider first a coherent layer with no dislocations. In this case, the strain ε is expressed as $\varepsilon = \frac{a^\alpha - a^\beta}{a^\beta}$. This strain is related to the number of lattice planes per unit length.

$$\begin{aligned}
\frac{1}{a^\alpha} &= \frac{1}{a^\beta (1 + \varepsilon)} \\
a^\alpha &= a^\beta (1 + \varepsilon), & a^\alpha / a^\beta &= 1 + \varepsilon \\
\varepsilon &= \frac{a^\alpha}{a^\beta} - 1 = \frac{a^\alpha - a^\beta}{a^\beta}
\end{aligned}$$

In the case of a partially coherent layer with dislocations,

$$\begin{aligned}
\frac{1}{a^\alpha} + \frac{1}{d} &= \frac{1}{a^\beta (1 + \varepsilon)} \\
a^\beta \left(\frac{1}{a^\alpha} + \frac{1}{d} \right) &= \frac{1}{1 + \varepsilon} \\
\varepsilon &= \frac{1}{a^\beta \left(\frac{1}{a^\alpha} + \frac{1}{d} \right)} - 1 = \frac{1 - a^\beta \left(\frac{d + a^\alpha}{a^\alpha d} \right)}{a^\beta \left(\frac{d + a^\alpha}{a^\alpha d} \right)} \\
&= \frac{a^\alpha \left(\frac{d}{d + a^\alpha} \right) - a^\beta}{a^\beta}
\end{aligned}$$

4D-7. (a) Migration of the boundary from $(\bar{2}110)$ crystal with a low coherency strain energy to (1000) crystal with a high strain energy.

(b) The migration velocity of the boundary between $(0001)/(01\bar{1}0)$ with a high coherency strain energy is faster than that between $(0\bar{1}12)/(01\bar{1}0)$ with a low coherency strain energy if the mobility of the boundaries is the same.

- 4D-8. (a) Distribution of second phase spinel particles mostly at grain boundaries of corundum grains.
 (b) Diffusion Induced Grain boundary Migration (DIGM) can occur with the dissolution of spinel particles.
 Cf: Lee HY, et al., *J. Am. Ceram. Soc.*, 79, 1659-63 (1996).
- 4D-9. In discontinuous precipitation/dissolution (DP/DD), the migration of grain boundary (interface between the mother phase(s) and the product phase(s)) occurs with depletion/supply of solute atoms transported along grain boundary. The major driving force of DP/DD is the strain energy stored in a thin diffusional layer formed on the receding grain, as in the case of DIGM. Physically, DP/DD appears to be the same phenomenon as that of DIGM. The system of interest with regard to solute source/sink appears to be characterized by the difference between the two phenomena: internal for DP/DD and mostly external for DIGM.
 Cf: - Lee KR, et al., *Acta Metall.*, 35, 2145-50 (1987).
 - Baik YJ, Yoon DN, *Acta Metall.*, 33, 1911-17 (1990).
 - Lee HY, et al., *J. Am. Ceram. Soc.*, 79, 1659-63 (1996).
- 4D-10. When a few grains are chemically unstable, DIGM can occur from their boundary towards the other grains, becoming large abnormal grains. A few examples can be found in BaTiO₃, Al₂O₃ and SiAlON systems.
 Cf: - Lee HY, et al., *Interface Science*, 8, 223-29 (2000)
 - Lee SH, et al., *J. Eur. Ceram. Soc.*, 22, 317-21 (2002).
- 4D-11. When bulk diffusion of solutes into a grain induces high strain energy in the grain, new grains with orientations different from that of the parent grain can form within it. This phenomenon is called diffusion induced recrystallization (DIR). The process of DIR was observed to occur with the formation of many misfit dislocations within a new solid-solution, rearrangement and polygonization of dislocations to form low grain boundaries, and formation of high angle grain boundaries. This DIR process is similar to that of recrystallization of a plastically deformed material.
 Cf: - Lee HY, Kang SJL, *Acta Mater.*, 38, 1307-12 (1990)
 - K.-W. Chae et al., *Acta Mater.*, 44, 1793-99 (1996)
 - Y.-K. Paek, et al., *J. Eur. Ceram. Soc.*, 24, 613-18 (2004)
- 4D-12. The driving force of DIGM is usually larger than that of normal grain growth (Cf: Lee HY, et al., *Interface Science*, 8, 223-29, (2000) or Fig 8.9.) and can be much larger than the critical driving force for appreciable boundary migration of a faceted boundary. This understanding gives an expectation of a similar degree of DIGM for the two different types of boundaries. The mobility of a faceted boundary, however, can vary considerably with the crystallographic orientation. (Cf: An SM, et al., *Acta Mater.*, 60, 4531-39 (2012).) Therefore, the DIGM rate can vary from boundary to boundary in a sample with faceted boundaries. It seems, however, that the overall degree of DIGM in the sample with faceted boundary would be similar to that in the sample with rough boundary.

SUBJECT INDEX

Basis of Sintering Science

Capillarity, Capillary pressure 1-4, 1-15
Dihedral angle (groove angle) and boundary energy 1-20, 1-21, 1-22, 1-27, 1-28
Driving force of sintering (thermodynamic and kinetic) 1-1, 2-20, 2-23, 2-26
Elastic strain energy and surface energy 1-11, 1-12
Entrapped gases and gas pressure 1-5, 1-6, 1-7, 1-8, 1-9
(Equilibrium) shape of pores or grains 1-16, 1-17, 1-18, 1-19,
Liquid film formation and microstructure 1-29
Microstructure of two phase systems 1-30, 1-31
Second phase particles/pores and their location 1-23, 1-24
Surface energy and surface tension 1-2, 1-3, 1-10
Vapor pressure 1-13, 1-14
Wetting angle and microstructure 1-25, 1-26

Bonding and Densification

Solid State Sintering

Dedensification, pore opening 2-37, 2-41, 2-42
Effect of entrapped gases 2-37, 2-38, 2-39, 2-40
Effect of external (gas) pressure 2-19, 2-21, 2-22, 2-34, 2-44
Effect of grain boundary structure 2-46
Effect of grain growth 2-27, 2-28, 2-36
Effect of particle size 2-11, 2-31, 2-32, 3-38
Effect of sintering time 2-30, 2-35
Effect of temperature 2-31, 2-34
Pore entrapment and densification limit 2-18, 2-19, 2-37
Scaling law (Herring's) 2-12, 2-13, 2-14, 2-15
Sintering diagram 2-25
Sintering kinetics 2-5, 2-6, 2-8, 2-9, 2-10
Sintering mechanisms 2-1, 2-2, 2-3, 2-4, 2-7, 2-16, 2-17, 2-18, 2-20, 2-24, 2-29, 2-33, 2-43,
2-44, 2L-9, 2L-18
Sintering techniques 2-45, 2-48
Stability of pores 2-47

Liquid Phase Sintering

Capillary and compressive force between particles 2L-1, 2L-2
Contact flattening model and theory 2L-4, 2L-6
Effect of external gas pressure 2L-16
Effect of grain growth 2L-11, 2L-12
Effect of particle size 2L-8, 2L-12
Effect of wetting and dihedral angle 2L-7
Microstructure of liquid phase sintered samples 2L-3, 2L-6, 2L-14, 2L-15, 2L-17
Pore filling model and theory 2L-4, 2L-5, 2L-6
Sintering mechanisms 2L-9, 2L-10, 2L-13, 2L-18

Grain Growth and Microstructural Evolution

Solid State Sintering

Boundary migration and grain growth, mixed control mechanism of 3-42, 3-43, 3-44, 3-46, 3-47, 3-48

Effect of impurity/solute segregation on boundary migration 3-12, 3-13, 3-14, 3-16

Effect of impurity/solute segregation on grain growth 3-11, 3-15, 3-17

Effect of particles/pores (Smith-Zener drag) 3-6, 3-7, 3-8, 3-11, 3-18

Effect of thermal cycle, fast firing 3-34, 3-36, 3-39

Grain growth, kinetics and microstructure 3-1, 3-2, 3-3, 3-4, 3-5, 3L-23

Grain growth and microstructural evolution, (mixed mechanism) principle of 3-45, 3-49, 3-50

Impurity/solute segregation 3-9, 3-10, 3-14

Microstructure development 3-26, 3-27, 3-28, 3-29, 3-30, 3-31, 3-32, 3-33, 3-35

Pore migration and grain growth 3-19, 3-20, 3-21, 3-22, 3-23, 3-24

Pore/boundary separation 3-25, 3-29, 3-30

Sintering processes 3-37, 3-41, 3-46, 3-48

Unconventional sintering techniques 3-40

Liquid Phase Sintering

Calculation of grain growth 3L-13, 3L-14

Crystal/grain growth, mechanisms of 3L-9, 3L-10, 3L-12, 3L-22, 3L-23

(Equilibrium) shape of crystals/grains 3L-7, 3L-8, 3L-11

Lifshitz-Slyozov-Wagner (LSW) theory (*see* Ostwald ripening)

Microstructural variation during liquid phase sintering 3L-2, 3L-3, 3L-4

Grain growth and microstructural evolution, (mixed mechanism) principle/theory of 3L-13, 3L-14, 3L-15, 3L-18, 3L-19, 3L-20, 3L-21

Ostwald ripening 3L-1, 3L-5, 3L-6, 3L-15

Sintering processes 3L-16, 3L-17

Supplementary Subjects

Sintering of Ionic Compounds

Boundary segregation/migration 4I-13, 4I-14

Defect formation 4I-1, 4I-2, 4I-3, 4I-4, 4I-5, 4I-7, 4I-8, 4I-11

Densification 4I-10, 4I-12

Diffusion 4I-6, 4I-8, 4I-9, 4I-11, 4I-12

Diffusion Induced Interface Migration

Coherency strain and energy 4D-5, 4D-6

Diffusion induced recrystallization 4D-11

Discontinuous precipitation/dissolution 4D-9

Driving force for DIGM 4D-1, 4D-2, 4D-4

Effect of boundary structure/orientation 4D-7, 4D-12

Microstructural evolution 4D-3, 4D-8, 4D-10

Korea Advanced Institute of Science and Technology
Yuseong-gu, Daehak-ro 291,
Daejeon 34141, Republic of Korea

ISBN 979-1192990-19-4 (95570)

비매품/무료

95570



9 791192 990194

ISBN 979-11-92990-19-4 (PDF)

